THE ABRAHAM-MINKOWSKI CONTROVERSY AND HE-MCKELLAR-WILKENS PHASE

THE ABRAHAM-MINKOWSKI CONTROVERSY AND HE-MCKELLAR-WILKENS PHASE

By

NIKOLA K. MILADINOVIC, B.Sc., M.Sc.

A Thesis
Submitted to the School of Graduate Studies
in Partial Fulfilment of the Requirements
for the Degree
Doctor of Philosophy

McMaster University

DOCTOR OF PHILOSOPHY (2016) McMaster University
(Physics) Hamilton, Ontario

TITLE:	The Abraham-Minkowski Controversy and He-McKellar-Wilkens Phase
AUTHOR:	Nikola K. Miladinovic, B.Sc., University of Toronto (2009), M.Sc., McMaster University (2011)
THESIS ADVISER:	Dr. Duncan O'Dell
NUMER OF PAGES:	xvi , 144

Abstract

This thesis investigates the long-standing Abraham-Minkowski controversy concerning the momentum of light inside a dielectric medium. A revealing connection to the optical He-McKellar-Wilkens (HMW) phase is found upon studying the Langrangian describing the classical laser-atom interaction. This connection is further highlighted by moving into a semi-classical model in which the phase arises as a result of the transformation between the Abraham and Minkowski Hamiltonians. The HMW along with the Aharonov-Casher phases are found to be both dynamic and geometric depending on the representation. It is shown that an optical version of the HMW phase is acquired by a dipole moving in a laser beam, and I propose several interferometric schemes in order to observe the optical HMW effect. Finally, by moving into a cavity system, it is possible to account for the back action of the atoms on the light which changes the electromagnetic mode structure. This increase in model sophistication grants an alternative vantage from which to interpret the Abraham-Minkowski problem.

Acknowledgements

I would first and foremost like to thank my supervisor, Duncan O'Dell, for his support and guidance over the last 6! years. Thanks to my office mates Jesse and Faiyaz for making me realize how weird and dark humans really are when you get to know them. A big thank you to my two best Hamilton brothers Ray and Rory for reminding me that I'll never get that nature publication. And to my friends and family back home including the PVC - you guys have been good to me, and I'm grateful for that. Finally, I wouldn't be here without the wisdom and input I have received from Arjun, Chris Lam, and Betty. Thank you all!

I dedicated this thesis to Arjun, Betty, and of course Chris Lam. You have inspired a generation of winners and thinkers. You have opened your arms and embraced the pursuit of wonder and joy. You have brought tremendous happiness to a young soul looking for purpose.
I thank thee.

Preface

This Thesis began as an investigation into the form of the electromagnetic momentum inside a dielectric. Two competing expressions for the form of the momentum were proposed by Abraham and Minkowski over 100 years ago, and yet still the debate continues. I should mention at the outset of my thesis that it is no longer a question of which representation is correct - they are both correct given the right context. The question I wanted to answer was - in what situation is the Minkowski or the Abraham expression appropriate? This thesis is an attempt to answer this question, and to shed new light on a centuries old problem. While researching the A-M problem, it became obvious that there was a deep connection between the two forms of the momentum and the geometric phase known as the He-McKellar-Wilkens phase. Although it is likely that other researchers have understood this connection, in all our searching, we did not find this connection mentioned in the literature. It began to dawn on us that with this deep connection, we could effectively study the A-B momentum by looking into the HMW phase. Our research direction began to shift towards fully understanding the HMW phase and how it would be possible to observe it in an optical system. Chapter 3 of this thesis highlights the progress we have made in this enterprise. As a late addition to this thesis, I decided to include earlier work I had done on the Abraham-Minkowski problem in cavity systems. The work was incomplete, however, upon returning to the problem I was able to fill in some of the major holes that had plagued the project - largely due to having a fuller understanding of the problem. I hope that the work presented in this thesis will be of some small use to people interested in studying electromagnetic momentum in a medium. Most of all, I hope that the experimental proposals inspire experimentalists to undertake this calling!

"My advice is, don't touch it with a ten foot pole! The literature is indeed conflicting; also opaque, ambiguous, unclear, and---much of it---incompetent."

-- David Griffiths

Contents

List of Figures

Chapter 1

Introduction

1.1 The Abraham-Minkowski momentum

There has been a recent resurgence of interest in understanding the electromagnetic momentum density in a dielectric medium [1, 2, 3, 4, 5, 6, 7, 8, 9, 10, 11, 12, 13, 14, 15, 16, 17, 18, 19, 20, 21, 22]. Two different forms of the momentum density were proposed by Minkowski and Abraham over 100 years ago [23, 24]. Minkowski argued that the momentum density of an electromagnetic field in matter be of the form

$$\mathbf{S}_{\text{Min}} = \mathbf{D} \times \mathbf{B}, \tag{1.1}$$

while Abraham held

$$\mathbf{S}_{\text{Abr}} = \frac{1}{c^2}\mathbf{E} \times \mathbf{H}. \tag{1.2}$$

The Abraham-Minkowski dilemma can be recast in terms of the photon momentum traveling through a dielectric medium. The Abraham photon momentum is $\mathbf{p}_{\text{Abr}} \approx \hbar\omega_a/cn$ while the Minkowski photon momentum is $\mathbf{p}_{\text{Min}} \approx$

$\hbar\omega_a n/c$, where n is refractive index of the material. It is hard to believe that such a glaring difference has not been sorted out yet, but after 100 years, the debate still continues. Part of the difficulty in answering this lies in the fact that experiments have been preformed which claim to support both forms. Consider the following two gedanken experiments. In the first experiment suggested by Balazs [25] and further clarified by Barnett and Loudon [2], a photon travels through a block of transparent material 1.1.

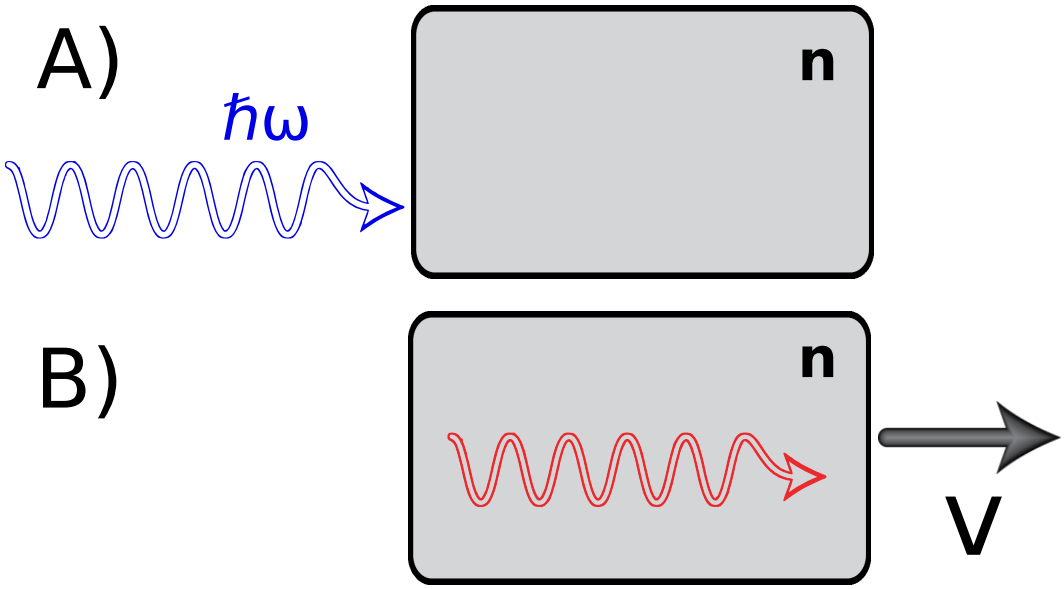

Figure 1.1: A thought experiment which supports the Abraham representation of the photon momentum. In (A) a photon travels towards a stationary dielectric block of refractive index n. In (B) we assume the photon is completely transmitted with no reflection. The velocity of the photon is reduced as it travels through the dielectric material to c/n. By invoking a conservation of mass-energy argument, it's easy to show that the momentum of the photon inside the material should be the Abraham momentum $\hbar\omega/cn$.

The total energy of the system before the photon enters the medium is $E_{\text{total}} = \hbar\omega + Mc^2$, where M is the mass of the block. While traveling through the block, the photon speed slows down to c/n and therefore would take a time $t = Ln/c$ to traverse it, where L is the length of the block. Upon exiting, the

photon will have traveled a shorter distance than it would have had it traveled in free space. This difference in distance is $L(n-1)$. By the principle of uniform motion of the center of mass-energy [26], the block must be displaced by some distance Δz in the direction of propagation of the photon. The uniform motion of the center of mass-energy requires that

$$L(n-1)\hbar\omega = \Delta z M c^2. \tag{1.3}$$

If we then assume that the momentum acquired by the block came from the momentum lost by the photon, we obtain

$$p_{\text{block}} = M\frac{\Delta z}{Ln/c}. \tag{1.4}$$

Solving for Δz in Eq. (1.3) and plugging this into Eq. (1.4) yields

$$p_{\text{block}} = \left(1 - \frac{1}{n}\right)\frac{\hbar\omega}{c}. \tag{1.5}$$

By conservation of momentum, we know the total momentum is given simply by the initial momentum of the system

$$p_{\text{total}} = \frac{\hbar\omega}{c}. \tag{1.6}$$

We then set this equal to the final total momentum $p_{\text{block}} + p_{\text{photon}}$, and solve for the final photon momentum inside the block

$$p_{\text{photon}} = \frac{\hbar\omega}{cn} = p_{\text{Abr}}. \tag{1.7}$$

This leaves us with the Abraham momentum.

For the second gedanken experiment we again follow the work of [2]. Here we consider an atom of mass m with a transition frequency of ω_a traveling through a medium with an index of refraction n, at velocity v. Let us also assume that the atom is moving away from a light source emitting at an angular frequency ω.

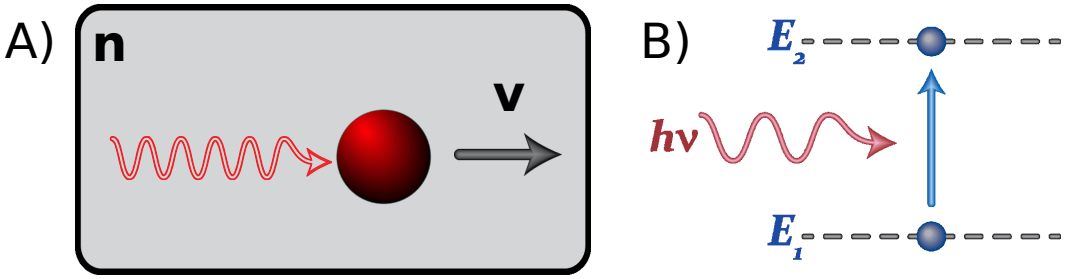

Figure 1.2: A thought experiment which supports the Minkowski representation of the photon momentum. In (A) a photon of optical frequency ω interacts with an atom of mass m and transition frequency ω_a, which is traveling with a velocity $\mathbf{v}$ through a dielectric of refractive index n. In (B) the atom can only absorb the photons if the transition frequency matches the laser frequency in the atom's frame of reference. Since the atom is moving with velocity $\mathbf{v}$, the atom sees the laser frequency shifted to $\omega^{'} = \omega(1 - nv/c)$. Through conservation of energy and momentum, one finds that the photon momentum must be the Minkowski momentum $\hbar\omega n/c$.

The atom can absorb a photon if the Doppler shifted frequency matches the transition frequency of the atom. In this case we require

$$\omega_a = \omega(1 - \frac{nv}{c}). \tag{1.8}$$

By conservation of energy and momentum, in the laboratory frame, we

then have

$$\frac{1}{2}mv_{\text{final}}^2 + \hbar\omega_a = \frac{1}{2}mv_{\text{initial}}^2 + \hbar\omega \tag{1.9}$$

$$mv_{\text{final}} = mv_{\text{initial}} + p_{\text{photon}} \tag{1.10}$$

Combining these two equations with Eq. (1.8) and solving for the photon momentum yields $p_{\text{photon}} = \hbar\omega n/c$, which is none other than the Minkowski momentum! So what exactly is going on here? How can both answers be correct?

This thesis is an attempt to explain this paradox and to better understand the work done by others on the subject.

The importance of unraveling this mystery goes beyond gedanken experiments. Knowledge of the momentum of light in a medium is of importance in interferometry using electromagnetic waves to manipulate atoms. Experiments involving high precision measurements of the photon recoil momentum are used, for example, to determine the fine structure constant [27, 28, 29]. The first experiment designed to measure the momentum of light in a refracting medium was preformed by Jones and Richards at the University of Aberdeen in 1954 [30]. By shining light from a tungsten lamp off of a mirrors submerged in various liquids, they hoped to measure the momentum of light in a medium. These mirrors were suspended by wires and tethered at each end by gold alloy torsion fibers. By subjecting the mirrors to asymmetric intensities of light, they were able to measure the torque on the mirrors, and hence the momentum transferred by the light. By switching between different liquids, they were able to conclude that the momentum transferred scaled with

the refractive indices of the different media in accordance to the Minkowski representation. The next significant experiment was conducted by Ashkin and Dziedzic in 1973 [31]. The experiment consisted of a glass cell containing air and water. By shining a laser through the water/air interface, the radiation pressure would cause the surface to either bulge in or out depending on the form of the photon momentum. If the Minkowski momentum was correct, then the surface would be expected to bulge in, while the opposite would be seen if the Abraham representation was correct. By studying the emerging laser beam profile, they were able to determine that surface of the water bulged outward as predicted by the Minkowski momentum. In 1977, an experiment by Walker and Walker [32] built off of earlier work by James [33] in order to prove the existence of the Abraham force (see Chapter 2) which is responsible for the difference between the two momenta. Using a disc of barium titante suspended on a torsion fiber, they were able to measure the torque due to time varying electric and magnetic fields. In doing so, they were able to confirm the existence of the Abraham force. Also in 1977, Jones and Leslie [34] repeated the experiment first performed by Jones and Richards with improved technology. They implemented a laser and superior mirrors to obtain a final result with a standard deviation of only 0.05%. They were able to confirm the Minkowski momentum, however, they later concluded that both forms can be interpreted as being correct if one assumed the Abraham momentum included a mechanical momentum component from the material itself. In 2005, David Pritchard's group at MIT set out to determine whether atoms in a rubidium BEC, subjected to an optical pulse, recoiled in accordance to Minkowski's or Abraham's prediction [35]. Figure (1.3) shows the experiment in which a standing wave pulse is applied to a BEC cloud of rubidium atoms. The mo-

mentum kick out-couples a small fraction of atoms which evolve at a different rate from the other atoms. After a short delay, a second pulse recombines the atoms and their interference is observed. This two-pulse Ramsey interferometer revealed a momentum kick in accordance with the Minkowski form of the momentum of light $\mathbf{p}_{\text{Min}} = \hbar\omega n/c$. On the other hand, Peng and Leonhardt's

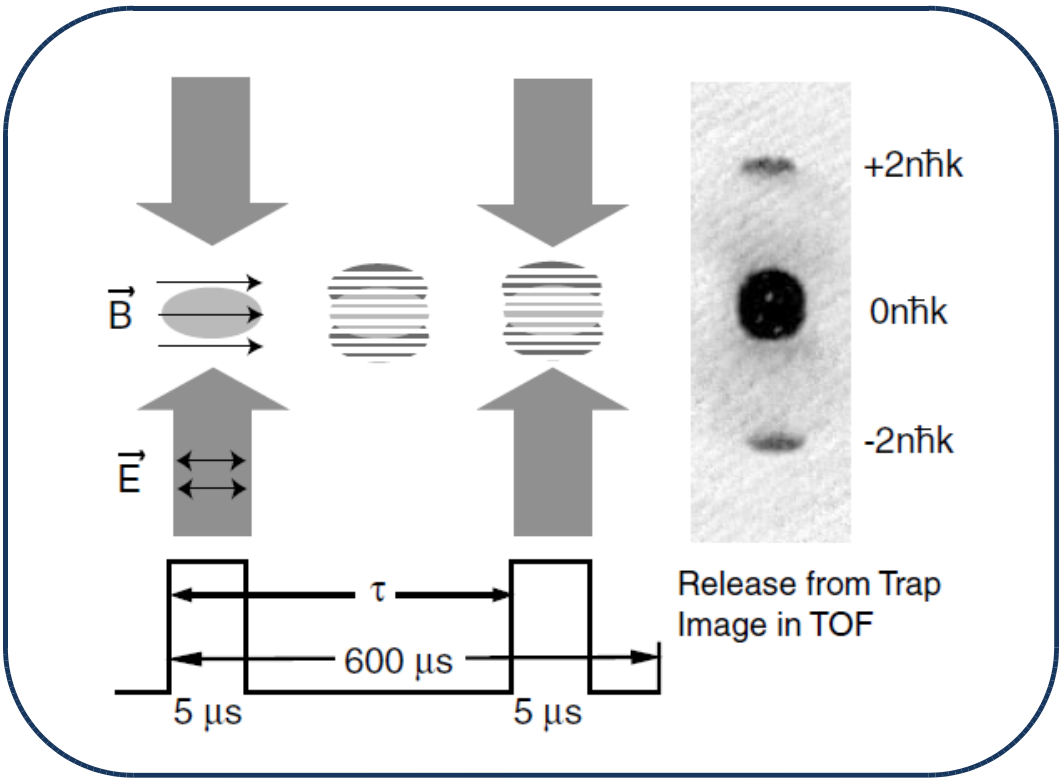

Figure 1.3: An experiment performed by the Pritchard and Ketterle group at MIT in which they attempt to measure the momentum of light in a medium. A standing wave pulse is applied to a rubidium BEC which outcouples a portion of the atoms from the zero momentum state into the $2\hbar k$ momentum state. These atoms are allowed to evolve in this seperate state for 600 ms before being recombined with the original zero momentum batch. The interference pattern is then imaged to determine the momentum kick the atoms received. They conclude that the momentum kick is modified by the presence of the BEC itself, and show that the atoms receive an impulse of $2\hbar kn$ - consistent with Minkowski's prediction. However, as we show in this thesis, this is also consistant with Abraham's prediction.

experiment in 2015 claims to have demonstarted that the momentum of light traveling through a liquid is of the Abraham form $\mathbf{p}_{\text{Abr}} = \hbar\omega/nc$ [36]. Figure (1.4) shows a graphical representation of the experiment in which a laser is shone onto the surface of water. By observing an inward bulge on the surface, they were able to conclude through momentum conservation arguments that the light momentum must be of the Abraham form. Similarly, W. She, J. Yu and R. Feng have claimed to observe the Abraham momentum in their experiment. The setup consisted of a thin silica glass nano-filament which was subjected to a laser pulse. The pulse traveled down the filament and exited out of the free end causing the filament to recoil. This pushing force (rather than a pulling force) on the filament is indicative of the Abraham momentum, and hence they concluded that the momentum of the light inside the filament must be of the Abraham form. It should be noted that this experiment is not without controversy [37]

In his famous review on relativity [38], Pauli pointed out that the Abraham momentum density $\mathbf{g}_A$ gives the same ponderomotive force on a stationary dielectric as the Minkowski momentum density $\mathbf{g}_M$ except for an extra term, which we shall call the Abraham force (also sometimes called the Röntgen force)

$$\mathbf{F}_{\text{A}} = \frac{\partial}{\partial t}(\mathbf{d} \times \mathbf{B}), \tag{1.11}$$

where $\mathbf{d}$ is the electric-dipole moment, and $\mathbf{B}$ is the magnetic field. However, Pauli noted that "Because of the smallness of this term, it is hardly likely that an experiment could be devised for deciding in favour of one or the other of the two approaches". J. P. Gordon has convincingly shown that when the Lorentz force is used to calculate the ponderomotive force on a nondispersive

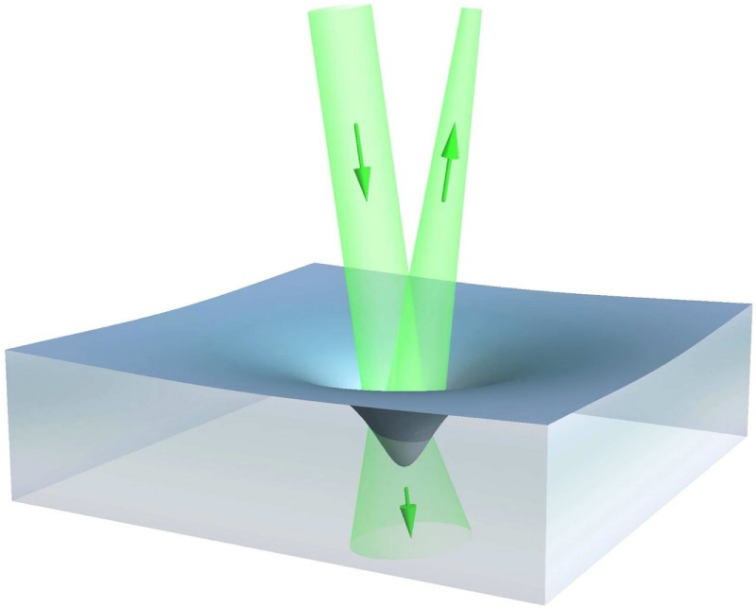

Figure 1.4: An experiment preformed by Ulf Leonhardt and Nan Peng's group on the optical force of light acting on water. By balancing the momentum from the incident, reflected, and transmitted light with the surface tension, they predict that an inward bulge in the liquid would be indicative of the Abraham momentum, while an outward bulge, the Minkowski momentum. Upon shining a laser upon the surface, they observed an inward bulge in the liquid which corroborates the Abraham representation.

dielectric medium the result agrees with the Abraham form [39]. Note: on page 13 of [29] by Cladé et al., they claim that Gordon's paper supports Minkowski, but this is an error. In fact, he clearly states, "In this work we demonstrate for nondispersive dielectric media that Abraham's form ... does indeed represent the true momentum density of electromagnetic fields." The Lorentz force approach allows for a physical interpretation of the origin of the Röntgen term as being due to the Lorentz force on the internal electric current in an oscillating dipole due to the magnetic field. Hinds and Barnett used the Lorentz force approach to study the simplest dielectric of all, a single atom, interacting with a travelling pulse of laser light [1]. The standard optical dipole force

$$F_{\text{dip}} = -\frac{1}{2}\alpha\nabla E^2, \tag{1.12}$$

predicts that an atom will be attracted into a red-detuned pulse. Here $\mathbf{E}$ is the electric field and we have introduced the polarizability α. Hinds and Barnett showed, however, that the extra Abraham force term given in Eq. (1.11) produces a force of twice the magnitude and in the opposite direction to the dipole force so that the atom is *repelled* from the pulse.

It appears that there is now a consensus that both the Abraham and the Minkowski forms can be correct, depending upon exactly what is measured [40, 41]. An important step in resolving the Abraham-Minkowski puzzle was the realization that $\mathbf{p}_{\text{Min}}$ and $\mathbf{p}_{\text{Abr}}$ are the photon momenta associated with the canonical and kinetic momentum of the atoms, respectively. This link appears to have first been established by Loudon, Babiker, Baxter and Lembessis [41]. This allows for a more intuitive understanding of the mechanism responsible for the different responses seen in experiments. In particular, it has been argued

that the Abraham momentum is associated with centre-of-mass motion of a medium, whereas if the medium is capable of diffracting (as cold atoms can), the Minkowski momentum is more relevant because the momentum operator in quantum mechanics is associated with the canonical momentum (however, we shall see in this thesis that this argument due to Barnett [2] has its limitations since we use diffraction to obtain a result in agreement with Abraham). In this thesis we extend this line of investigation by considering the quantum phases acquired by atoms interacting with light. In particular, inside a plane wave laser beam an atom will feel no classical dipole force and yet will acquire a quantum phase due to the Röntgen interaction (it is straightforward to show that in the path-integral formulation of quantum mechanics a term related to that given in Eq. (1.11) leads directly to the HMW phase). This line of inquiry leads us to connect the Abraham momentum density with the so called He-McKellar-Wilkens (HMW) phase.

1.2 The HMW phase

Geometric phases were introduced into quantum mechanics by Michael Berry in 1984 [42], although certain special cases were already known (see [43] for a review). The geometric phase is a measure of the failure of certain variables to return to their original values after cycling around a closed circuit in some parameter space. The simplest example is a tangent vector parallel transported along a circuit on a sphere as shown in Figure (1.5). Parallel transport means that that the tangent vector cannot rotate about the normal vector perpendicular to the surface. It is found upon completing the cycle, that a rotation in the vector's orientation has accumulated during the transport process.

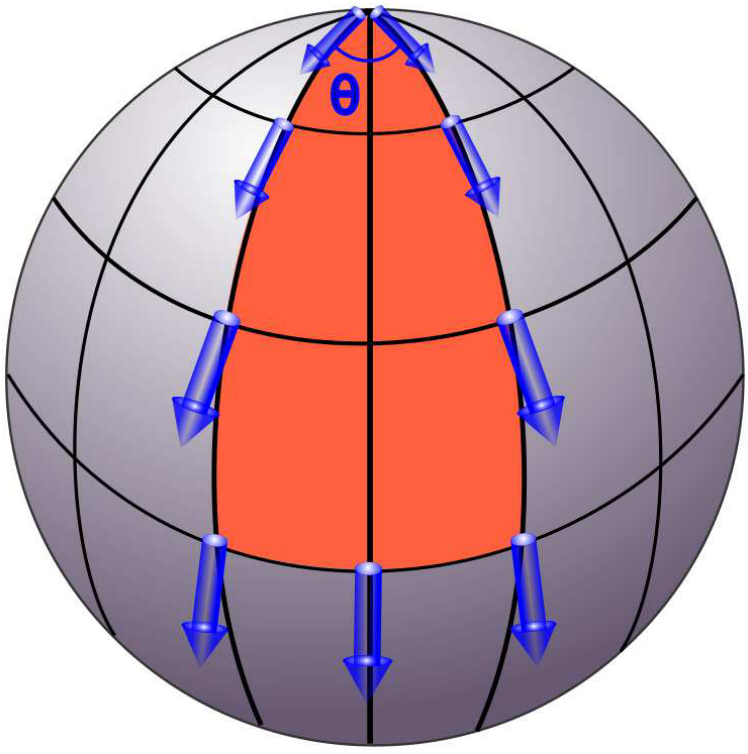

Figure 1.5: Parallel transport of a tangent vector around a circuit on the surface of a sphere is an example of motion that gives rise to a geometric phase shift. In this particular circuit we start and end at the north pole.

Now instead of the tangent vector, suppose we are interested in a two level atom. The Hamiltonian for this atom interacting with light is given by [44]

$$H = \frac{\hat{P}^2}{2M} + V + U, \tag{1.13}$$

where V is any external potential and U is the atom-field coupling operator given, in the basis of the ground and excited state of the atom, by

$$U = \frac{\hbar\Omega}{2}\begin{bmatrix} \cos(\theta) & e^{-i\phi}\sin(\theta) \\ e^{i\phi}\sin(\theta) & -\cos(\theta) \end{bmatrix}. \tag{1.14}$$

Here Ω is the generalized Rabi frequency which characterizes the coupling strength, θ is the mixing angle, and ϕ is the laser phase. The eigenstates for the coupling operator are the dressed state vectors $|\chi_1(r)\rangle, |\chi_2(r)\rangle$

$$|\chi_1\rangle = \begin{bmatrix} \cos(\frac{\theta}{2}) \\ e^{i\phi}\sin(\frac{\theta}{2}) \end{bmatrix}, \tag{1.15}$$

$$|\chi_2\rangle = \begin{bmatrix} -e^{-i\phi}\sin(\frac{\theta}{2}) \\ \cos(\frac{\theta}{2}) \end{bmatrix}. \tag{1.16}$$

We can then write the state of the atom Ψ in terms of the dressed state basis as

$$|\Psi(r,t)\rangle = \psi_1(r,t)\,|\chi_1(r)\rangle + \psi_2(r,t)\,|\chi_2(r)\rangle\,. \tag{1.17}$$

The evolution of this state vector is determined by the Schrödinger equation

$$i\hbar\frac{\partial}{\partial t}\Psi(r,t) = \left(\frac{\hat{P}^2}{2M} + V + U\right)\Psi(r,t), \tag{1.18}$$

Note that the spatial derivative originating from the canonical momentum operator $\hat{P}$ acts not only on the amplitudes ψ_j, but also on the basis vectors $|\chi_j\rangle$. Suppose now we are interested in a situation in which $\psi_2 = 0$. Plugging in Eq. (1.17) into Eq. (1.18) and taking the dot product with $|\chi_1\rangle$ yields

$$i\hbar\frac{\partial}{\partial t}\psi_1 = \left[\frac{\left(\hat{P} - \mathbf{A}\right)^2}{2M} + V + U_1 + \phi(r)\right]\psi_1 \tag{1.19}$$

where $\mathbf{A} = i\hbar\langle\chi_1, \nabla\chi_1\rangle$ behaves like an effective vector potential, $\phi = \frac{\hbar^2}{2M}|\langle\chi_1, \nabla\chi_1\rangle|^2$ is like the scalar potential, and U_1 is the component of the coupling operator along $|\chi_1\rangle$.

What is of interest to us is the appearance of the effective vector potential $\mathbf{A}$ which arises due to the spatial dependence of the basis vectors. In Section 3, we will show that if one calculates the phase the atom in state $|\chi_1\rangle$ acquires traveling along some path Γ, the presence of the vector potential $\mathbf{A}$ gives rise to an extra phase, in addition to the standard dynamic phase, given by

$$e^{\frac{i}{\hbar}\int_\Gamma \mathbf{A}(\mathbf{r})\cdot d\mathbf{r}}. \tag{1.20}$$

This phase only depends on the path, and not on the interaction time - hence the name geometric phase. Dynamic phases on the other hand are induced by potentials (which gives rise to classical forces). As such they are characterized by their dependence on the interaction time, and hence the velocity of the particle in question. Additionally, the dynamic phase is independent of direction of propagation. Geometric phases, on the other hand, are propagation direction dependent, do not depend on the interaction time, and by extension are independent of the particle velocity. These characteristic features will be used

in Section 3 in order to differentiate geometric and dynamic perturbations.

This thesis primarily focuses one such geometric phase which arises in atomic physics - The He-McKellar-Wilkens (HMW) phase. The HMW phase is a topological quantum phase predicted by He and McKellar in 1993 [45] and independently by Wilkens in 1994 [46]. It is one of a family of four such phases that includes the Aharonov-Bohm (AB) [47] and Aharonov-Casher (AC) [48] phases that are all related by electromagnetic dualities [49]. The AB phase arises when a charged particle moves in a region of space where there is a nonzero magnetic vector potential $\mathbf{A}$ and yet the magnetic field $\mathbf{B} = \nabla \times \mathbf{A}$ vanishes, as is the case outside of a solenoid. There is no force acting on the particle and according to classical mechanics the particle is unaffected by the presence of the solenoid. However, in the quantum case the particle's wave function is affected. Any path encircling the solenoid acquires the phase

$$\phi_{\mathrm{AB}} = (q/\hbar) \oint \mathbf{A}(\mathbf{r}) \cdot d\mathbf{r}, \tag{1.21}$$

which can be seen in the interference pattern between paths passing on different sides of the solenoid. The significance of the AB phase is generally taken to be that it can either be viewed as a manifestation of the physical reality of electromagnetic potentials or of the non locality of quantum mechanics [50]. The HMW phase [45, 46]

$$\phi_{\mathrm{HMW}} = \hbar^{-1} \oint [\mathbf{B}(\mathbf{r}) \times \mathbf{d}] \cdot d\mathbf{r}, \tag{1.22}$$

is associated with a neutral quantum particle endowed with an electric dipole moment $\mathbf{d}$ moving in a closed circuit in a static magnetic field of strength $\mathbf{B}$.

Like the AC phase $\phi_{\rm AC} = -(\hbar c^2)^{-1} \oint [\mathbf{E}(\mathbf{r}) \times \boldsymbol{\mu}] \cdot d\mathbf{r}$, where a magnetic moment $\boldsymbol{\mu}$ moves in a static electric field and experiences, to first order in v/c, the motional magnetic field $\mathbf{B}_{\rm mot} = -\mathbf{v} \times \mathbf{E}/c^2$, the electric dipole in the HMW phase experiences a motional electric field $\mathbf{E}_{\rm mot} = \mathbf{v} \times \mathbf{B}$ leading to the Röntgen interaction [46] (note this implies the HMW phase is also a first order effect). In order to obtain a finite HMW (or AC) phase the physical electromagnetic fields should not vanish everywhere on the circuit (unlike in the AB phase) but nevertheless various configurations of the fields and polarization have been proposed [45, 46, 49, 51] where no forces appear to act and yet the phase is finite. Indeed, it has been shown that the HMW phase can be derived by considering the sum of the two AB phases acquired by the two charges forming the dipole [51].

Experimental confirmation of the AB [52, 53, 54, 55] and the AC [56, 57, 58, 59, 60] phases came quite quickly after the theoretical predictions and the experiments have continued to be refined over the years. The HMW phase was only recently detected using an atom interferometer operating in the Mach-Zehnder configuration [61, 62, 63, 64]. These latter experiments took care to establish that the phase was time independent and reversed sign when the direction of travel of the atoms was reversed, which are the hallmarks of a geometric phase (of which topological phases are a particular case) and are in contrast to dynamical phases.

Both the HMW and the AC phases can be derived using the Feynman path integral. The standard integral approach which associates the phase $\frac{1}{\hbar} \int L dt$ with every path if we adopt the standard direct coupling Lagrangian

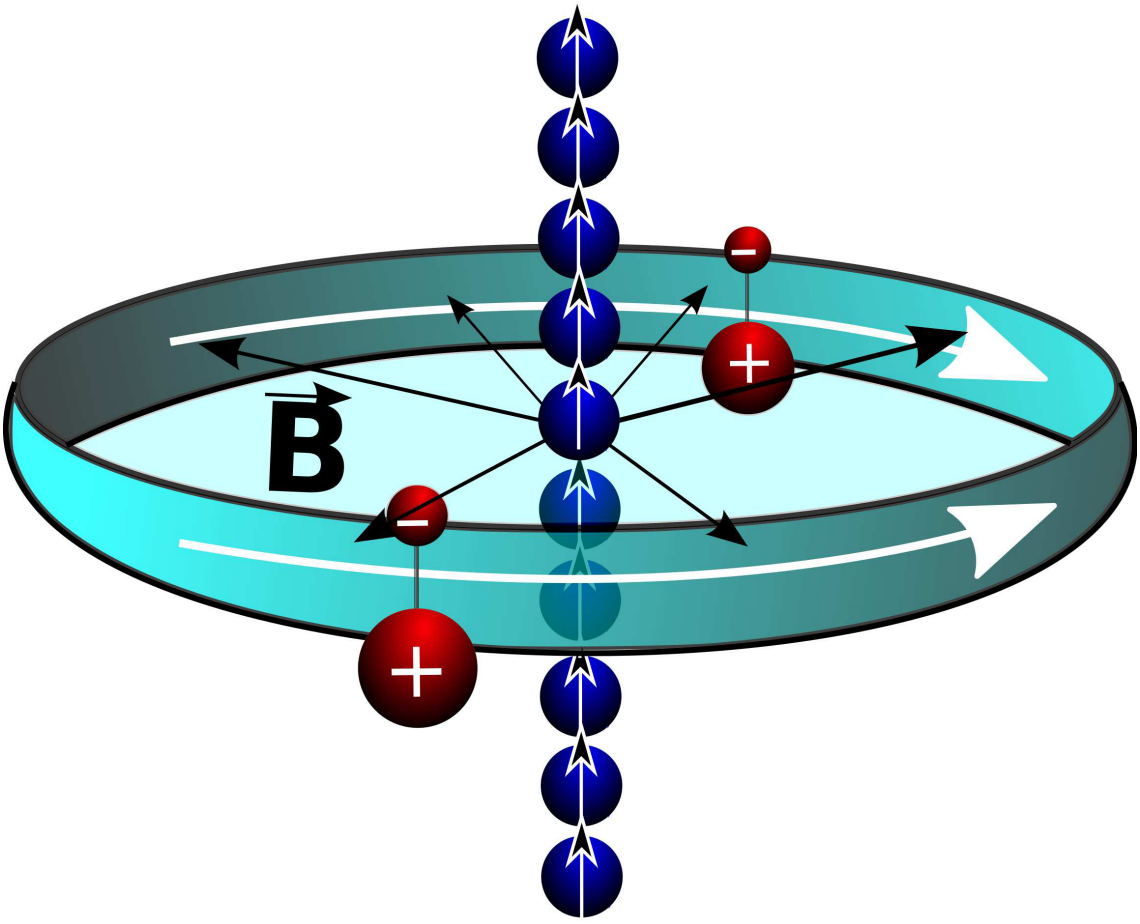

Figure 1.6: An arrangement to observe the HMW phase $\phi_{\text{HMW}} = \hbar^{-1} \oint [\mathbf{B}(\mathbf{r}) \times \mathbf{d}] \cdot d\mathbf{r}$ analogous to the Aharonov-Casher phase with the magnetic dipole of the AC phase case replaced by an electric dipole in the HMW arrangement, and the static radial electric field swapped with a static radial magnetic field. The magnetic field here is created using a line of magnetic monopoles - which is purely a hypothetical arrangement. In this arrangement the radial magnetic field is always perpendicular to the dipole moment $\mathbf{d}$ providing a nonzero HMW phase without any classical forces acting on the atom.

L supplemented by the motional fields is

$$L = \frac{1}{2}mv^2 + \mathbf{d}\cdot(\mathbf{E}+\mathbf{v}\times\mathbf{B}) + \boldsymbol{\mu}\cdot(\mathbf{B}-\mathbf{v}\times\mathbf{E}/c^2), \tag{1.23}$$

where m is the mass of the particle and $\mathbf{E}$ and $\mathbf{B}$ are specified in the laboratory frame. Because we are interested in the optical regime where the $\mathbf{E}$ and $\mathbf{B}$ fields rapidly change sign, whereas μ does not (as we will show in Chapter 3), we shall neglect the third term in Eq. (1.23) because it vanishes when averaged over an optical cycle. The above Lagrangian can be compared to the standard *minimal* coupling Lagrangian for a charged particle

$$L = \frac{1}{2}mv^2 + q\mathbf{v}\cdot\mathbf{A} - q\phi, \tag{1.24}$$

where ϕ is the scalar potential. Comparing terms we can formally associate $\mathbf{B}\times\mathbf{d}$ with $q\mathbf{A}$ and $\mathbf{d}\cdot\mathbf{E}$ with $-q\phi$. In this way the HMW phase given in Eq. (1.22) follows directly from the AB phase given in Eq. (1.21). Apart from the quantum HMW phase, these associations also suggest that we can treat the dipole as an effective charge interacting with the following effective fields

$$\mathbf{B}_{\text{eff}} \equiv \nabla\times\mathbf{A}_{\text{eff}} = \frac{1}{q}\nabla\times(\mathbf{B}\times\mathbf{d}) \tag{1.25}$$

$$\mathbf{E}_{\text{eff}} \equiv -\nabla\phi_{\text{eff}} - \frac{\partial\mathbf{A}_{\text{eff}}}{\partial t} = \frac{1}{q}\left[\nabla(\mathbf{d}\cdot\mathbf{E}) - \frac{\partial}{\partial t}(\mathbf{B}\times\mathbf{d})\right]. \tag{1.26}$$

that account for (classical) electromagnetic forces on the dipole. In the linear response regime $\mathbf{d} = \alpha(\mathbf{E}+\mathbf{v}\times\mathbf{B})$ [51], where α is the polarizability, we can replace the second term in the Lagrangian by $(\alpha/2)(\mathbf{E}+\mathbf{v}\times\mathbf{B})^2$. Following through the calculation we find that to lowest order in v/c we can replace

$\mathbf{B} \times \mathbf{d}$ by $\alpha(\mathbf{B} \times \mathbf{E})$ and $\mathbf{d} \cdot \mathbf{E}$ by $(\alpha/2)E^2$ in the Eqns. (1.25) and (1.26). The terms depending on $\mathbf{B} \times \mathbf{E}$ are proportional to the local Poynting vector $\mathbf{S} = (\mathbf{E} \times \mathbf{B})/\mu_0$ of the optical field. In the plane wave laser beams we shall consider here, the Poynting vector has zero curl and so $\mathbf{B}_{\text{eff}} = 0$. The very interesting case of laser beams with non-zero orbital angular momentum such as Laguerre-Gauss beams that would give $\mathbf{B}_{\text{eff}} \neq 0$ will be considered later in Section 3. We thus find that the force on the dipole in an optical field carrying zero orbital angular momentum is purely due to the effective electric field

$$\mathbf{F} = q\mathbf{E}_{\text{eff}} = \nabla\left(\frac{\alpha}{2}E^2\right) + \alpha\frac{\partial}{\partial t}(\mathbf{E} \times \mathbf{B}). \tag{1.27}$$

The first term is the familiar induced dipole force that depends on the gradient of the intensity [65]. The second term depends on the time-dependence of the Poynting vector. It is zero in static field configurations but gives a contribution, for example, when fields are turned on and off. Unlike the dipole force, it is nonconservative, a feature it shares with magnetic forces in general due to the form of the velocity dependence of the Lagrangian.

1.3 This Thesis

This thesis is organized into 6 sections. In Section 2 I review the classical electromagnetic forces acting on an atom. I show how the dipole and Röntgen forces arise from the Lorentz force acting on the charges of an atom. I then explore the energy-momentum tensor and show how the Abraham and Minkowski tensor representations differ through the Röntgen force.

In Section 3 I introduce the idea of atomic interferometry and review the Feynman path integral approach to calculating phases. I next propose three different experimental arrangements capable of measuring the HMW phase through interferometric means. The first is an atomic Mach-Zehnder interferometer which additionally has an optical beam running along the two arms of the inteferometer. These traveling beams induce an HMW phase in the atoms as they travel along the length of the interferomter which is then measured via interference. The second scheme is a Kapitza-Dirac interferometer which interferes a BEC with itself after splitting it into a coherent superposition of two parts and subjecting each part to an optical field. The two parts acquire HMW phases as a result and interfere with each other when finally recombined. Finally, in the third setup, we consider a BEC in an optical ring trap irradiated by a Laguerre-Gaussian (LG) beam. These LG beams carry angular momentum which is transferred to the atoms when pulsed, thereby rotating the BEC.

In Section 4 I show how two different representation of the direct coupling Hamiltonian give rise to the Abraham or the Minkowski momentum. The HMW and the AC phase arise naturally as a result of the unitary transformation linking the two representations. Surprisingly, in the Abraham represen-

tation the HMW and AC phases appear as dynamic phases.

In Section 5, I approach these questions from the confines of an optical cavity. This allows for a dynamic treatment of the electromagnetic fields. Beginning with a toy model for a double cavity system in which the central mirror is allowed to move, I show that the Abraham momentum arises when one takes into account the back action of the atom on the light. In this case, as the atom moves, the standing wave structure is altered, and hence electromagnetic momentum is transferred. It is this process which is responsible for producing the Abraham momentum.

Finally, in the last section, I give the main conclusions of this thesis and discuss future directions.

Chapter 2

Classical Forces

2.1 Introduction

In this section we focus on the classical forces associated with a neutral particle interacting with an electromagnetic field. We will derive the classical force

$$\mathbf{F} = \alpha \nabla \left(\frac{1}{2} E^2(r,t) \right) + \frac{\partial}{\partial t} \left[\mathbf{d}(r,t) \times \mathbf{B}(r,t) \right], \tag{2.1}$$

and show how the second term, which is often ignored, survives when dealing with pulses. Working out the corresponding Abraham and Minkowski stress-energy tensors allows us to see that the difference between the two is a matter of bookkeeping. We show that the Minkowski stress tensor affiliates the second term in Eq. (2.1) with a mechanical force, while the Abraham stress-tensor groups it with the electromagnetic force. Both formulations turn out to be correct, but answer slightly different questions.

2.2 The Classical Force on an Atom

We begin with the Lorentz force law for a charge q acted on by an electric field $\mathbf{E}$ and a magnetic field $\mathbf{B}$. Let $\mathbf{x}$ be the position of the charge, then

$$\mathbf{F} = q\left(\mathbf{E} + \frac{d\mathbf{x}}{dt} \times \mathbf{B}\right). \tag{2.2}$$

We now wish to calculate the force on a dipole in a nonuniform electromagnetic field. To begin let us write the total force each charge in the dipole experiences,

$$\begin{aligned} m_1\ddot{\mathbf{r}}_1 &= q\left(\mathbf{E}\left(\mathbf{r}_1, t\right) + \dot{\mathbf{r}}_1 \times \mathbf{B}\left(\mathbf{r}_1, t\right)\right) - \nabla \mathbf{U}\left(\mathbf{r}_1, t\right) \quad , \\ m_2\ddot{\mathbf{r}}_2 &= -q\left(\mathbf{E}\left(\mathbf{r}_2, t\right) + \dot{\mathbf{r}}_2 \times \mathbf{B}\left(\mathbf{r}_2, t\right)\right) + \nabla \mathbf{U}\left(\mathbf{r}_2, t\right) \quad . \end{aligned} \tag{2.3}$$

Here $\mathbf{U}$ is the binding potential of the dipole. Making use of the center of mass coordinates

$$\mathbf{R} = \frac{m_1}{m_1 + m_2}\mathbf{r}_1 + \frac{m_2}{m_1 + m_2}\mathbf{r}_2, \tag{2.4}$$

and taking a first order expansion of the fields about the center of mass

$$\begin{aligned} \mathbf{E}\left(\mathbf{r}_1\right) &= \mathbf{E}\left(\mathbf{R}\right) + \left(\mathbf{r}_1 - \mathbf{R}\right) \cdot \nabla \mathbf{E}\left(\mathbf{R}\right) \quad , \\ \mathbf{E}\left(\mathbf{r}_2\right) &= \mathbf{E}\left(\mathbf{R}\right) + \left(\mathbf{r}_2 - \mathbf{R}\right) \cdot \nabla \mathbf{E}\left(\mathbf{R}\right) \quad . \end{aligned} \tag{2.5}$$

A similar expansion applies to the magnetic fields. Substituting the first order expansions into Eq. (2.3), along with the center of mass coordinates, and

adding the two equations together yields

$$\begin{aligned}(m_1+m_2)\,\ddot{\mathbf{R}} &= q\,(\mathbf{r}_1-\mathbf{r}_2)\cdot\nabla\mathbf{E}\,(\mathbf{R})\\ &+q\,(\dot{\mathbf{r}}_1-\dot{\mathbf{r}}_2)\times\mathbf{B}\,(\mathbf{R})+\text{H.O.}\end{aligned} \tag{2.6}$$

The higher order terms are dropped as they are of order $\dot{r}/c$ smaller than the other two terms. We introduce the dipole moment $\mathbf{d} = q(\mathbf{r}_1 - \mathbf{r}_2)$. This allows us to write the dipole force as

$$\begin{aligned}\mathbf{F} &= (\mathbf{d}\cdot\nabla)\,\mathbf{E}+\frac{d\mathbf{d}}{dt}\times\mathbf{B}\\ &= \alpha\left[(\mathbf{E}\cdot\nabla)\,\mathbf{E}+\frac{d\mathbf{E}}{dt}\times\mathbf{B}\right],\end{aligned} \tag{2.7}$$

where α is the polarizability of the atom given by $\mathbf{d} = \alpha\mathbf{E}$. Here we are assuming that the dipole moment follows the external field adiabatically. We then rewrite the full time derivative in terms of the intrinsic time derivative and a comoving derivative $\frac{d}{dt} = \frac{\partial}{\partial t} + \mathbf{v}\cdot\nabla$. The second term is of order v/c smaller than the other terms in the Lorentz force, so we neglect it and simply substitute $\frac{d}{dt} = \frac{\partial}{\partial t}$ into Eq. (2.7).

We now make use of the following vector identity

$$(\mathbf{E}\cdot\nabla)\,\mathbf{E} = \nabla\left(\frac{1}{2}E^2\right)-\mathbf{E}\times(\nabla\times\mathbf{E}), \tag{2.8}$$

and Faraday's law

$$\nabla\times\mathbf{E} = -\frac{\partial\mathbf{B}}{\partial t}, \tag{2.9}$$

which allows us to rearrange Eq. (2.7)

$$\begin{aligned}\mathbf{F} &= \alpha\left[\frac{1}{2}\nabla E^2 - \mathbf{E}\times\left(-\frac{\partial \mathbf{B}}{\partial t}\right) + \frac{\partial \mathbf{E}}{\partial t}\times\mathbf{B}\right] \\ &= \alpha\left[\frac{1}{2}\nabla E^2 + \frac{\partial}{\partial t}\left(\mathbf{E}\times\mathbf{B}\right)\right].\end{aligned} \tag{2.10}$$

In this standard expression [1, 66, 67] many authors emphasize the fact that the second term integrates to zero over an optical cycle. This is certainly true for a plane wave, but is not generally correct. Let's take a closer look at the dipole force by considering a pulsed traveling wave of the form

$$\begin{aligned}\mathbf{E}(r,t) &= \mathcal{E}(\omega t - kz)\cos\left(\omega t - kz\right)\hat{\mathbf{x}}, \\ \mathbf{B}(r,t) &= \mathcal{B}(\omega t - kz)\cos\left(\omega t - kz\right)\hat{\mathbf{y}}.\end{aligned} \tag{2.11}$$

We assume that the envelopes $\mathcal{E}$ and $\mathcal{B}$ vary slowly in time. Plugging this into Eq. (2.10)

$$\begin{aligned}\mathbf{F} &= \alpha\mathcal{E}(\omega t - kz)\frac{\partial}{\partial z}\mathcal{E}(\omega t - kz)\cos^2\left(\omega t - kz\right)\hat{\mathbf{z}} \\ &+ \alpha k\mathcal{E}^2(\omega t - kz)\cos\left(\omega t - kz\right)\sin\left(\omega t - kz\right)\hat{\mathbf{z}} \\ &- \alpha\omega\mathcal{E}(\omega t - kz)\mathcal{B}(\omega t - kz)\cos\left(\omega t - kz\right)\sin\left(\omega t - kz\right)\hat{\mathbf{z}} \\ &+ \alpha\frac{\partial}{\partial t}\left[\mathcal{E}(\omega t - kz)\mathcal{B}(\omega t - kz)\right]\cos^2\left(\omega t - kz\right)\hat{\mathbf{z}}.\end{aligned} \tag{2.12}$$

If we integrate this over an optical cycle, the second and third terms integrate to zero. The time averaged force $\bar{\mathbf{F}}$ is then given by

$$\bar{\mathbf{F}} = \frac{1}{2}\alpha\left[\mathcal{E}(\omega t - kz)\frac{\partial}{\partial z}\mathcal{E}(\omega t - kz) + \frac{\partial}{\partial t}\left(\mathcal{E}(\omega t - kz)\mathcal{B}(\omega t - kz)\right)\right]\hat{\mathbf{z}}. \tag{2.13}$$

The first term in Eq. (2.13) is known as the optical dipole force, while the second term is known as the Abraham force [68] (also called the Röntgen force [69]). Notice that had the amplitudes been constant as in a plane wave, then the second term would vanish. Only when the amplitude is changing does the second term contribute. As was mentioned previously, the Abraham force is usually left out of optical force calculations, however, in the case of a traveling pulse, its contribution is non-negligible. Consider again Eq. (2.13). We can rewrite it as

$$\bar{\mathbf{F}} = \frac{1}{2}\alpha \left[k\mathcal{E}(\omega t - kz)\mathcal{E}'(\omega t - kz) - \frac{2\omega}{c}\mathcal{E}(\omega t - kz)\mathcal{E}'(\omega t - kz) \right] \hat{\mathbf{z}}, \qquad (2.14)$$

where we have made use of the relationship $\mathcal{E} = c\mathcal{B}$. In this representation it is easy to see that the Abraham force is in fact *twice* the magnitude of the optical dipole force, and in the opposite direction [1]! It should be noted however that the momentum transfer is given by $P = \int F dt$. Thus, the Abraham force can only transfer a maximal impulse of $d_0 B_0$ determined by the maximum amplitude (E_0, B_0) of the electromagnetic field. In contrast, the optical dipole term will operate as long as the atoms are acted on by the field (for example, an optical lattice). This is why in most circumstances, the optical dipole force is the dominant effect. Only special cases, such as a pulsed traveling wave, do we observe this extraordinary balance. In the next section we shall show explicitly how the Abraham term allows us to obtain either the Minkowski or the Abraham representation.

Finally, let's look at the decomposition of the dipole force Eq. (2.13) to

better understand the two terms comprising it. How did we arrive at this form for the dipole force? We began with the Lorentz force and determined the total force acting on the center of mass of a dipole configuration by considering the Lorentz force on each of the charges. By doing so we arrived at Eq. (2.7) which contained two components. The first component is the well known force on a dipole due to a nonuniform electric field. The second term is due to the internal dynamics of the atom. Going through the derivation, we see this term is due to the relative motion $\dot{\mathbf{r}}_1 - \dot{\mathbf{r}}_2$ of the charges in the dipole. Interestingly, this is the only term that contributes to the force on a dipole in a transverse plane wave. The i'th component of the dipole force Eq. (2.7) may be written as

$$\mathbf{F}_i = (\mathbf{d} \cdot \nabla)\, \mathbf{E}_i + \left(\frac{d}{dt} \mathbf{d} \times \mathbf{B} \right)_i , \tag{2.15}$$

and for a transverse plane wave, the first term does not contribute, and hence the entire force is contained in the second term.

2.3 Forces in Matter

In this section, we show how the Lorentz force on an atom Eq. (2.10) can be partitioned into bound and free charge forces using Maxwell's equation in matter. We begin with the Lorentz force acting on a linear medium due to an electromagnetic traveling wave of the form $\mathbf{E}(kx-\omega t) = \mathcal{E}(x,t)\cos(kx-\omega t)\hat{\mathbf{z}}$. In this exposition, we will be making use of Maxwell's microscopic equations:

$$\nabla \cdot \mathbf{E} = \frac{\rho}{\epsilon_0} \tag{2.16}$$

$$\nabla \times \mathbf{E} = -\frac{\partial \mathbf{B}}{\partial t} \tag{2.17}$$

$$\nabla \cdot \mathbf{B} = 0 \tag{2.18}$$

$$\nabla \times \mathbf{B} = \mu_0 \mathbf{J} + \mu_0 \epsilon_0 \frac{\partial \mathbf{E}}{\partial t}, \tag{2.19}$$

Maxwell's equations in matter:

$$\nabla \cdot \mathbf{D} = \rho_f \tag{2.20}$$

$$\nabla \times \mathbf{E} = -\frac{\partial \mathbf{B}}{\partial t} \tag{2.21}$$

$$\nabla \cdot \mathbf{B} = 0 \tag{2.22}$$

$$\nabla \times \mathbf{H} = \mathbf{J}_f + \frac{\partial \mathbf{D}}{\partial t}, \tag{2.23}$$

and the auxiliary fields

$$\mathbf{D} = \epsilon_0 \mathbf{E} + \mathbf{P} \tag{2.24}$$

$$\mathbf{H} = \frac{1}{\mu_0}\mathbf{B} - \mathbf{M} \tag{2.25}$$

$$\mathbf{P} = \epsilon_0 \chi_e \mathbf{E} \tag{2.26}$$

$$\mathbf{M} = \chi_m \mathbf{H}, \tag{2.27}$$

where $\mathbf{D}$ is the electric displacement field, $\mathbf{H}$ is the magnetic intensity, $\mathbf{P}$ is the polarization density, and $\mathbf{M}$ is the magnetization density. The microscopic Lorentz force density in the i'th direction is given by [70]

$$\begin{aligned}\mathbf{f}_i &= \rho\mathbf{E}_i + (\mathbf{J}\times\mathbf{B})_i \\ &= (\epsilon_0\nabla\cdot\mathbf{E})\,\mathbf{E}_i + \left(\frac{1}{\mu_0}(\nabla\times\mathbf{B})\times\mathbf{B} - \epsilon_0\frac{\partial\mathbf{E}}{\partial t}\times\mathbf{B}\right)_i .\end{aligned} \tag{2.28}$$

Here we have made use of Maxwell's microscopic equations Eq. (2.19). Using the vector identity $\mathbf{A}\times(\nabla\times\mathbf{A}) = \frac{1}{2}\nabla A^2 - (\mathbf{A}\cdot\nabla)\,\mathbf{A}$, along with Ampère's law we can rewrite this as

$$\begin{aligned}\mathbf{f}_i &= \epsilon_0(\nabla\cdot\mathbf{E})\,\mathbf{E}_i - \frac{1}{2\mu_0}\nabla_i B^2 + \frac{1}{\mu_0}(\mathbf{B}\cdot\nabla)\,\mathbf{B}_i \\ &-\epsilon_0\frac{\partial}{\partial t}(\mathbf{E}\times\mathbf{B})_i - \frac{1}{2}\epsilon_0\nabla_i E^2 + \epsilon_0(\mathbf{E}\cdot\nabla)\,\mathbf{E}_i .\end{aligned} \tag{2.29}$$

For a transverse traveling wave $\mathbf{E}(x,t) = \mathcal{E}(kx-\omega t)\cos(kx-\omega t)\hat{\mathbf{z}}$ and $\mathbf{B}(x,t) = \mathcal{B}(kx-\omega t)\cos(kx-\omega t)\hat{\mathbf{y}}$ the first, third, and last term will drop out since the electromagnetic field doesn't have a longitudinal component. We are therefore left with

$$\mathbf{f}_\mathrm{i} = -\frac{1}{2}\nabla_\mathrm{i}\left(\epsilon_0\mathrm{E}^2 + \frac{1}{\mu_0}\mathrm{B}^2\right) - \epsilon_0\frac{\partial}{\partial\mathrm{t}}(\mathbf{E}\times\mathbf{B})_\mathrm{i}. \tag{2.30}$$

Let's now do the same thing, but instead consider the Lorentz force density $\tilde{\mathbf{f}}$ acting only on the free charges in the material. Following the same procedure used for the microscopic Lorentz force we have

$$\begin{aligned}
\tilde{\mathbf{f}}_i &= \rho_f \mathbf{E}_i + (\mathbf{J_f} \times \mathbf{B})_i \\
&= (\nabla \cdot \mathbf{D})\, \mathbf{E}_i + \left((\nabla \times \mathbf{H}) \times \mathbf{B} - \frac{\partial \mathbf{D}}{\partial t} \times \mathbf{B} \right)_i \\
&= (\nabla \cdot \mathbf{D})\, \mathbf{E}_i - \frac{1}{2} \nabla_i (\mathbf{H} \cdot \mathbf{B}) + (\mathbf{H} \cdot \nabla)\, \mathbf{B}_i \\
&- \frac{\partial}{\partial t} (\mathbf{D} \times \mathbf{B})_i - \frac{1}{2} \nabla_i (\mathbf{D} \cdot \mathbf{E}) + (\mathbf{D} \cdot \nabla)\, \mathbf{E}_i. \qquad (2.31)
\end{aligned}$$

Once again, we drop the first, third, and last term due to the electromagnetic wave being transverse. We then arrive at

$$\tilde{\mathbf{f}}_i = -\frac{1}{2} \nabla_i (\mathbf{D} \cdot \mathbf{E} + \mathbf{H} \cdot \mathbf{B}) - \frac{\partial}{\partial t} (\mathbf{D} \times \mathbf{B})_i . \qquad (2.32)$$

What happens now if we wish to find the Lorentz force density $\check{\mathbf{f}}$ acting on the bound charges?

$$\begin{aligned}
\check{\mathbf{f}}_i &= \rho_b \mathbf{E}_i + (\mathbf{J_b} \times \mathbf{B})_i \\
&= -(\nabla \cdot \mathbf{P})\, \mathbf{E}_i + \left((\nabla \times \mathbf{M}) \times \mathbf{B} + \frac{\partial \mathbf{P}}{\partial t} \times \mathbf{B} \right)_i \\
&= -(\nabla \cdot \mathbf{P})\, \mathbf{E}_i - \frac{1}{2} \nabla_i (\mathbf{M} \cdot \mathbf{B}) + (\mathbf{M} \cdot \nabla)\, \mathbf{B}_i \\
&+ \frac{\partial}{\partial t} (\mathbf{P} \times \mathbf{B})_i + \frac{1}{2} \nabla_i (\mathbf{P} \cdot \mathbf{E}) - (\mathbf{P} \cdot \nabla)\, \mathbf{E}_i. \qquad (2.33)
\end{aligned}$$

Here we have used the relationship $\nabla \cdot \mathbf{P} = -\rho_b$. Dropping the first, third and last terms again yields

$$\check{\mathbf{f}}_i = \frac{1}{2} \nabla_i (\mathbf{P} \cdot \mathbf{E} - \mathbf{M} \cdot \mathbf{B}) + \frac{\partial}{\partial t} (\mathbf{P} \times \mathbf{B})_i . \qquad (2.34)$$

We then see that $\mathbf{f} = \tilde{\mathbf{f}} + \check{\mathbf{f}}$. What does this tell us about the Abraham-

Minkowski momenta? Consider the case in which $M = 0$. The Lorentz force density equations Eq. (2.30), Eq. (2.45), and Eq. (2.34) tell us that the force density due to the electromagnetic momentum carried by the wave is

$$-\epsilon_0 \frac{\partial}{\partial t} (\mathbf{E} \times \mathbf{B})_i = -\frac{\partial}{\partial t} (\mathbf{D} \times \mathbf{B})_i + \frac{\partial}{\partial t} (\mathbf{P} \times \mathbf{B})_i , \tag{2.35}$$

or by integrating over all space and using $\mathbf{P} = \mathbf{d}\delta(\mathbf{r} - \mathbf{r}_{\text{atom}})$ we obtain

$$\frac{\partial}{\partial t} \int \mathbf{S}_{\text{Min}}\, dV - \frac{\partial}{\partial t} \int \mathbf{S}_{\text{Abr}}\, dV = \frac{\partial}{\partial t} (\mathbf{d} \times \mathbf{B}) , \tag{2.36}$$

where

$$\mathbf{S}_{\text{Min}} = \mathbf{D} \times \mathbf{B}, \tag{2.37}$$

is Minkowski's optical momentum density, and

$$\mathbf{S}_{\text{Abr}} = \frac{1}{c^2} \mathbf{E} \times \mathbf{H}, \tag{2.38}$$

is Abraham's optical momentum density. We have arrived at the well known relationship between the Abraham and Minkowski momentum densities [1]

$$\int \mathbf{S}_{\text{Min}}\, dV = \int \mathbf{S}_{\text{Abr}}\, dV + \mathbf{d} \times \mathbf{B}(\mathbf{r}_{\text{atom}}). \tag{2.39}$$

The derivation above gives some insight into the partitioning of electromagnetic momenta into different contributions.

We wish now to understand the relationship between the Abraham/Minkowski momentum, and the energy of the dielectric medium. What is the energy in a dielectric system? We begin by calculating the energy of an electromagnetic

field due to the bound charges.

$$\begin{aligned} \delta W &= \int (\phi\, \delta\rho_{\rm b})\, d^3r = -\int \phi(\nabla\cdot\delta P)\, d^3r \\ &= -\int \nabla\cdot(\phi\, \delta P)\, d^3r + \int (\nabla\phi\cdot\delta P)\, d^3r, \end{aligned} \tag{2.40}$$

where ϕ is the electric potential, $\rho_{\rm b}$ is the bound charge density, and $\mathbf{P}$ is the polarization density. We have made use of the relationship $\rho_{\rm b} = -\nabla\cdot\mathbf{P}$. Using the divergence theorem, the first term in Eq. (2.40) can be written as

$$\int \nabla\cdot(\phi\, \delta P)\, d^3r = \oint \phi\, \delta P\cdot dS. \tag{2.41}$$

If we are integrating over all space, the field at infinity is zero, so this term integrates to zero. Using $\nabla\phi = -\mathbf{E}$ along with $\mathbf{E} = \epsilon\mathbf{E} = \epsilon_0\mathbf{E} + \mathbf{P}$ for a linear dielectric, we obtain

$$\begin{aligned} \delta W &= \int (\nabla\phi\cdot\delta P)\, d^3r = -\int (\mathbf{E}\cdot\delta P)\, d^3r \\ &= \int (\epsilon_0\mathbf{E}\cdot\delta E)\, d^3r - \int (\mathbf{E}\cdot\delta D)\, d^3r \\ &= \int (\epsilon_0\mathbf{E}\cdot\delta E)\, d^3r - \int (\epsilon\mathbf{E}\cdot\delta E)\, d^3r. \end{aligned} \tag{2.42}$$

Then the work done in assembling the bound charges is given by

$$\begin{aligned} W_{\rm bound} &= \int_0^E \delta W = \int_0^E \left[\int (\epsilon_0\mathbf{E}\cdot\delta E)\, d^3r - \int (\epsilon\mathbf{E}\cdot\delta E)\, d^3r\right] \\ &= \frac{1}{2}\epsilon_0 \int E^2\, d^3r - \frac{1}{2}\epsilon \int E^2\, d^3r = -\frac{1}{2}\int \mathbf{P}\cdot\mathbf{E}\, d^3r. \end{aligned} \tag{2.43}$$

The energy is negative since for bound charges, the force between the charges is attractive and hence we lose potential energy as we bring bound charges in

from infinity to form dipolar molecules. Now of course the situation would be reversed if we had started instead with neutral atoms and calculated the work required to separate out the bound charges to create the same polarized configuration. If we had instead begun with neutral atoms, the work required to arrive at the bound charge density ρ_{bound} would be $W = \frac{1}{2}\int \mathbf{P}\cdot\mathbf{E}\, d^3r$. Therefore, the energy W_{bound} required to assemble the bound charges is equal and opposite to the internal potential energy W_{int} present due to the dipoles. We then wish to calculate the total electric energy contained in the system. The electric energy of the system is comprised of three terms: the energy required to assemble the free charges W_{free}, the energy required to assemble the bound charges W_{b}, and the internal potential energy W_{int}. As we have already shown, the bound and internal energies of the system are equal and opposite. This implies that the total energy of the system is simply given by the energy required to assemble the free charges $W_{\text{Total}} = \frac{1}{2}\epsilon\int E^2\, d^3r$. The free charge derivation is similar to the bound case, simply replace the bound charge density with the free charge density and the above result follows [70] . On the other hand, if we are interested only in the energy of the system due to the free and bound charges (i.e not including the internal dipolar energy) then the energy of the system is $W_{\text{free}} + W_{\text{bound}} = \frac{1}{2}\epsilon_0\int E^2\, d^3r$. Returning back to Eq. (2.45) and integrating over all space we see that it may be rewritten as

$$\tilde{\mathbf{F}}_i = -\nabla_i\left(W_{\text{Total}}\right) - \frac{\partial}{\partial t}\left(\int \mathbf{S}_{\text{Min}} d^3r\right)_i . \tag{2.44}$$

Hence the Minkowski momentum describes the electromagnetic momentum associated with the total energy of the dielectric. The Abraham momentum on the other hand arises in Eq. (2.30) and can be written as (again integrating

over space)

$$\mathbf{F}_i = -\nabla_i \left(W_{\text{free}} + W_{\text{bound}}\right) - \frac{\partial}{\partial t}\left(\int \mathbf{S}_{\text{Abr}} d^3r\right)_i . \tag{2.45}$$

Hence the Abraham momentum is shown to only be associated with the energy due to the free and bound charges.

2.4 The Energy-Momentum Tensor

The problem comes down to understanding how to define the electromagnetic energy-momentum tensor in a material. The tensor will have contributing terms from both the electromagnetic field, and also from the material itself. In the following derivation, we assume the medium to be non-magnetic and dispersionless [71].

Let's start where we should start, with Maxwell's equations in matter:

$$\nabla \cdot \mathbf{D} = \rho_f \tag{2.46}$$

$$\nabla \cdot \mathbf{B} = 0 \tag{2.47}$$

$$\nabla \times \mathbf{E} = -\frac{\partial \mathbf{B}}{\partial t} \tag{2.48}$$

$$\nabla \times \mathbf{H} = \mathbf{J}_f + \frac{\partial \mathbf{D}}{\partial t}. \tag{2.49}$$

Here again the electric displacement $\mathbf{D}$ and auxillary magnetic field $\mathbf{H}$ are defined as:

$$\begin{aligned} \mathbf{D} &= \epsilon_0 \mathbf{E} + \mathbf{P}, \\ \mathbf{H} &= \frac{1}{\mu_0}\mathbf{B} - \mathbf{M}. \end{aligned} \tag{2.50}$$

We will also assume the dielectric relationship $\mathbf{D} = \epsilon \mathbf{E}$. We can derive Poynting's theorem by taking the dot product of $\mathbf{E}$ with Eq. (2.49) and $\mathbf{H}$ with Eq. (2.48), then subtracting the two. This yields

$$\mathbf{E} \cdot (\nabla \times \mathbf{H}) - \mathbf{H} \cdot (\nabla \times \mathbf{E}) = \mathbf{E} \cdot \mathbf{J}_f + \mathbf{E} \cdot \frac{\partial \mathbf{D}}{\partial t} + \mathbf{H} \cdot \frac{\partial \mathbf{B}}{\partial t}. \tag{2.51}$$

We then make use of the identity $\mathbf{E} \cdot (\nabla \times \mathbf{H}) - \mathbf{H} \cdot (\nabla \times \mathbf{E}) = -\nabla \cdot (\mathbf{E} \times \mathbf{H})$

which gives us

$$\frac{1}{2}\frac{\partial}{\partial t}\left(\mathbf{E}\cdot\mathbf{D}+\mathbf{B}\cdot\mathbf{H}\right)=-\mathbf{E}\cdot\mathbf{J}_f-\nabla\cdot\left(\mathbf{E}\times\mathbf{H}\right). \tag{2.52}$$

Eq. (2.52) is Poynting's theorem. The term on the left is the rate of change of energy density in the fields, the first term on the right is the rate of work done per unit volume on the charges, and the second term on the right gives the energy flux density. We next derive the force equation for an electromagnetic field on the free charges of a material. The Lorentz force density on free charges is given by

$$\tilde{\mathbf{f}}=\rho_f\mathbf{E}+\mathbf{J}_f\times\mathbf{B}, \tag{2.53}$$

where ρ_f and $\mathbf{J}_f$ are the free charge and free current densities respectively. Substituting in Eq. (2.46) and Eq. (2.49) gives

$$\tilde{\mathbf{f}}=\mathbf{E}\left(\nabla\cdot\mathbf{D}\right)-\mathbf{B}\times\nabla\times\mathbf{H}-\frac{\partial\mathbf{D}}{\partial t}\times\mathbf{B}. \tag{2.54}$$

We can rearrange this and use Eq. (2.48) to get

$$\tilde{\mathbf{f}}=\mathbf{E}\left(\nabla\cdot\mathbf{D}\right)-\mathbf{B}\times\nabla\times\mathbf{H}-\mathbf{D}\times\nabla\times\mathbf{E}-\frac{\partial}{\partial t}\left(\mathbf{D}\times\mathbf{B}\right). \tag{2.55}$$

After some manipulation, we arrive at

$$\tilde{\mathbf{f}}+\frac{\partial}{\partial t}\left[\mathbf{D}\times\mathbf{B}\right]=\nabla\cdot\left(\mathbf{E}\mathbf{D}+\mathbf{H}\mathbf{B}-\frac{1}{2}\mathbf{I}\left(\mathbf{D}\cdot\mathbf{E}+\mathbf{H}\cdot\mathbf{B}\right)\right), \tag{2.56}$$

where I is the unit vector, $\mathbf{EB}$ represents the dyadic product between the electric and magnetic fields defined by $\mathbf{XY}=\mathbf{X}\cdot\mathbf{Y}^T$. We now combine Eq. (2.56) with the Poynting theorem Eq. (2.52) to obtain a four dimensional

expression

$$\frac{\partial \left(T_{\mu\nu}\right)_{\mathrm{Min}}}{\partial x_{\nu}} = f_{\mu}^{\mathrm{M}}. \tag{2.57}$$

Here $f_0^{\mathrm{M}} = -\mathbf{E}\cdot\mathbf{J}_{\mathrm{f}}$ is the rate of work done per unit volume, f_i^{M} is the Lorentz force density in the i'th direction as given by Eq. (2.53), and $T_{\mu\nu}$ is the Minkowski energy-momentum tensor given by

$$\left(T_{\mu\nu}\right)_{\mathrm{Min}} = \begin{pmatrix} \frac{1}{2}\left(\mathbf{E}\cdot\mathbf{D}+\mathbf{B}\cdot\mathbf{H}\right) & \mathbf{E}\times\mathbf{H} \\ \mathbf{D}\times\mathbf{B} & -\mathbf{E}\mathbf{D}-\mathbf{H}\mathbf{B}+\frac{1}{2}\mathbf{I}\left(\mathbf{D}\cdot\mathbf{E}+\mathbf{H}\cdot\mathbf{B}\right) \end{pmatrix} . \tag{2.58}$$

Where

$$T_{00} = \frac{1}{2}\left(\mathbf{E}\cdot\mathbf{D}+\mathbf{B}\cdot\mathbf{H}\right), \tag{2.59}$$

is the energy density

$$T_{0a} = \mathbf{E}\times\mathbf{H}, \tag{2.60}$$

is the energy flux density

$$T_{a0} = \mathbf{D}\times\mathbf{B}, \tag{2.61}$$

is the momentum density

$$T_{ab} = -E_a D_b - B_a H_b + \frac{1}{2}\delta_{ab}\left(\mathbf{E}\cdot\mathbf{D}+\mathbf{B}\cdot\mathbf{H}\right), \tag{2.62}$$

is the Maxwell stress tensor. Here the Greek indices run from $0-3$ while Latin indices run from $1-3$. The stress tensor give the force per unit area acting on a surface. T_{ij} is the force per unit area in the i'th direction acting on a surface oriented in the j'th direction. The force density is the change in mechanical momentum with respect to time. Therefore the Minkowski energy-momentum

tensor gives us an expression which relates the mechanical momentum of a system to the electromagnetic momentum.

Where then does this leave the Abraham representation? Let's go back through the derivation. If we go back to Eq. (2.55) we can see where the Abraham tensor deviates from the Minkowski tensor. Taking Eq. (2.55) and adding $\epsilon_0 (\epsilon_\mathrm{r} - 1) \frac{\partial}{\partial t} \mathbf{E} \times \mathbf{B}$ from both sides gives us

$$\begin{aligned} &\tilde{\mathbf{f}} + \epsilon_0 (\epsilon_\mathrm{r} - 1) \frac{\partial}{\partial t} \mathbf{E} \times \mathbf{B} \\ &= \mathbf{E} (\nabla \cdot \mathbf{D}) - \mathbf{B} \times \nabla \times \mathbf{H} - \mathbf{D} \times \nabla \times \mathbf{E} - \frac{\partial}{\partial t} \frac{\mathbf{E} \times \mathbf{H}}{c^2} \end{aligned} \quad . \tag{2.63}$$

This simple juggling of terms allows us to write the Abraham energy-momentum tensor

$$(T_{\mu\nu})_\mathrm{Abr} = \begin{pmatrix} \frac{1}{2} (\mathbf{E} \cdot \mathbf{D} + \mathbf{B} \cdot \mathbf{H}) & \mathbf{E} \times \mathbf{H} \\ \frac{\mathbf{E} \times \mathbf{H}}{c^2} & -\mathbf{E}\mathbf{D} - \mathbf{H}\mathbf{B} + \frac{1}{2}\mathbf{I} (\mathbf{D} \cdot \mathbf{E} + \mathbf{H} \cdot \mathbf{B}) \end{pmatrix} \quad . \tag{2.64}$$

Where the momentum density is now $\frac{\mathbf{E} \times \mathbf{H}}{c^2}$, and

$$\frac{\partial (T_{\mu\nu})_\mathrm{Abr}}{\partial x_\nu} = f_\mu^\mathrm{A}. \tag{2.65}$$

Once again $f_0^\mathrm{A} = -\mathbf{E} \cdot \mathbf{J}_\mathrm{f}$ is the rate of work done per unit volume, however now $f_i^\mathrm{A} = f_i^\mathrm{M} + \epsilon_0 (\epsilon_\mathrm{r} - 1) \frac{\partial}{\partial t} \mathbf{E} \times \mathbf{B}$, where f_i^M is the Lorentz force density as given by the Minkowski tensor. The Abraham force density term is more familiar to us if we write it in another form. We use the relationship $\epsilon_0 \chi_\mathrm{e} \mathbf{E} = \mathbf{P}$ where $\chi_\mathrm{e} = \epsilon_\mathrm{r} - 1$ and where ϵ_r is the relative susceptibility (note $\mathbf{D} = \epsilon_0 \epsilon_\mathrm{r} \mathbf{E}$). The

force density term may then be written as $\mathbf{f}^{\mathrm{A}} = \frac{\partial}{\partial t}(\mathbf{P} \times \mathbf{B})$ which is our old friend the Abraham force density Eq. (2.38)! Here we can clearly see that the difference between the Abraham and Minkowski representation comes down to bookkeeping. During the derivation of the Abraham energy-momentum tensor, we simply took the Abraham force density out of what we assumed to be the electromagnetic momentum, and grouped it in with the mechanical momentum associated with the medium itself. A physical interpretation of these results will have to wait until Chapter 4.

Chapter 3

Interferometry

3.1 Introduction

Atomic interferometry involves coherently manipulating the translational, and/or temporal, evolution of atoms in order to obtain extremely precise information about a physical system. The idea extends principles more familiar in optical interferomtery to atoms. The wave nature of atoms and molecules allows us to interfere these particles with their de Broglie wavelength playing the role of the optical wavelength. In particular, atom interferometry offers a unique window from which to view the Aharonov-Bohm, Aharonov-Casher, and He-McKellar-Wilkens phases. These effects are only accessible to experiments which are able to interfere atoms - revealing the phase nature of atoms, which is not present in the classical theory. In this section we will review the path integral formulation of quantum mechanics which will lead us to a simple way to calculate the quantum phase picked up by atoms due to various perturbations. With the necessary mathematical tools under our belt, we introduce the Mach-Zehnder (MZ) interferometer and apply a traveling wave of light along each ineterfer-

ometer arm in order to induce an HMW phase. These two arms are spatially separated and subjected to different traveling waves. The atom beam, being coherently split into a superposition of two different translational states, now experiences a different environment in each arm, and hence each state evolves differently. Recombining the two states then produces an interference pattern revealing information about how the atoms couple with the environment. We show that under a carefully set up experiment, it is possible for the first time, to observe the optical He-McKellar-Wilkens phase. Two other setups are then introduced: the Kapitza-Dirac interferometer, and the Laguerre beam interferometer. These experiments offer alternative opportunities to probe the small geometric phase.

3.2 Path Integrals

In this section we introduce Feynman's approach to path integrals. We begin with a classical treatment of the problem, and then move to a quantum interferometric system. For a more detailed derivation see [72].

3.2.1 Classical Mechanics

Consider the two points $(\mathbf{x}_a, t_a)$ and $(\mathbf{x}_b, t_b)$. There are infinitely many paths $\Gamma_1, \Gamma_2, ...$ linking them, but only one Γ_{cl} is actually taken by the particle for a given initial momentum $\mathbf{p}_0$. This path is determined from the classical Lagrangian of the system

$$L(\mathbf{x}, \dot{\mathbf{x}}) = \frac{1}{2} m\dot{x}^2 - V(\mathbf{x}), \tag{3.1}$$

through the principle of least action (PLA). The PLA states that Γ_{cl} is the path which extremizes the classical action

$$S(\Gamma_{\text{cl}}) = \int_{t_a}^{t_b} L(\mathbf{x}(t), \dot{\mathbf{x}}(t))\, dt. \tag{3.2}$$

To find the path which extremizes the action S we consider a variation $\epsilon\boldsymbol{\eta}(t)$ in the classical path. The action is then written as

$$S(\Gamma) = \int_{t_a}^{t_b} L(\mathbf{x}(t) + \epsilon\boldsymbol{\eta}(t), \dot{\mathbf{x}}(t) + \epsilon\dot{\boldsymbol{\eta}}(t))\, dt. \tag{3.3}$$

If we require this to be extremal with respect to ϵ, then we must solve for

$$\frac{d}{d\epsilon} \int_{t_a}^{t_b} L(\mathbf{x}(t) + \epsilon\boldsymbol{\eta}(t), \dot{\mathbf{x}}(t) + \epsilon\dot{\boldsymbol{\eta}}(t))\, dt = 0. \tag{3.4}$$

This implies that

$$\int_{t_a}^{t_b} \left(\frac{\partial L}{\partial \mathbf{x}} \cdot \boldsymbol{\eta}(t) + \frac{\partial L}{\partial \dot{\mathbf{x}}} \cdot \dot{\boldsymbol{\eta}}(t) \right) dt = 0. \tag{3.5}$$

This may be rewritten by making use of integration by parts on the second term

$$\int_{t_a}^{t_b} \frac{\partial L}{\partial \dot{\mathbf{x}}} \cdot \dot{\boldsymbol{\eta}}(t)\, dt = \left[\frac{\partial L}{\partial \dot{\mathbf{x}}} \cdot \boldsymbol{\eta}(t) \right]_{t_a}^{t_b} - \int_{t_a}^{t_b} \boldsymbol{\eta}(t) \cdot \frac{d}{dt} \frac{\partial L}{\partial \dot{\mathbf{x}}}\, dt. \tag{3.6}$$

The first term on the right side is zero since we require the variation $\eta(t)$ to be zero at the boundaries. This then leads to

$$\int_{t_a}^{t_b} \left[\frac{\partial L}{\partial \mathbf{x}} \cdot \boldsymbol{\eta}(t) - \boldsymbol{\eta}(t) \cdot \frac{d}{dt} \frac{\partial L}{\partial \dot{\mathbf{x}}} \right] dt = 0. \tag{3.7}$$

Since $\boldsymbol{\eta}(t)$ is arbitrary other than vanishing at the end points, this implies that:

$$\frac{\partial L}{\partial \mathbf{x}} - \frac{d}{dt} \frac{\partial L}{\partial \dot{\mathbf{x}}} = 0, \tag{3.8}$$

which we recognize as the Euler-Lagrange equation. The Hamiltonian is defined as

$$H = \mathbf{p} \cdot \dot{\mathbf{x}} - L, \tag{3.9}$$

where the canonical momentum $\mathbf{p}$ is given by

$$\mathbf{p} = \frac{\partial L}{\partial \dot{\mathbf{x}}}. \tag{3.10}$$

3.2.2 The Quantum Propagator

The final state $|\psi(t_b)\rangle$ of a quantum system is determined through an evolution operator U acting on the initial state $|\psi(t_a)\rangle$

$$|\psi(t_b)\rangle = U\left(t_a, t_b\right)|\psi(t_a)\rangle\,. \tag{3.11}$$

This allows us to write the projection of the final state onto the coordinate basis as

$$\begin{aligned}\psi(\mathbf{x}_b, t_b) &= \langle \mathbf{x}_b|\psi(t_b)\rangle = \langle \mathbf{x}_b|U\left(t_a, t_b\right)|\psi(t_a)\rangle \\ &= \int d\mathbf{x}_a\ \langle \mathbf{x}_b|U\left(t_a, t_b\right)|\mathbf{x}_a\rangle\,\langle \mathbf{x}_a|\psi(t_a)\rangle\,.\end{aligned} \tag{3.12}$$

The strength of the evolution operator formalism lies in its ability to deal with compositions

$$U\left(t_a, t_c\right) = U\left(t_a, t_b\right)U\left(t_b, t_c\right). \tag{3.13}$$

Feynman postulated that the propagator can be thought of as a sum of contributions from all possible paths

$$\langle \mathbf{x}_b|U|\mathbf{x}_a\rangle = \mathcal{N}\sum_{\Gamma} e^{\frac{iS_\Gamma}{\hbar}}, \tag{3.14}$$

where $\mathcal{N}$ is a normalization constant, and $\sum_\Gamma$ denotes the sum over all possible paths. $S_\Gamma/\hbar$ in Eq. (3.14) varies rapidly and therefore induces destructive interference - unless the path Γ is an extremum. In this case, constructive interference occurs between neighbouring paths. Therefore, only paths very near to the classical path actually contribute in Eq. (3.14).

Let us now consider quadratic Lagrangians of the form

$$L = a(t)\dot{x}^2 + b(t)x\dot{x} + c(t)x^2 + d(t)\dot{x} + e(t)x + f(t), \tag{3.15}$$

and suppose we introduce a small perturbation to the classical path $\mathbf{x}(t) = \mathbf{x}_{\rm cl}(t) + \boldsymbol{\eta}(t)$. We make sure the boundary terms still match. Then the propagator can be written as

$$\langle \mathbf{x}_b | U | \mathbf{x}_a \rangle = \int D\boldsymbol{\eta}(t)\, e^{\frac{i}{\hbar} S[\mathbf{x}_{\rm cl} + \boldsymbol{\eta}(t)]}, \tag{3.16}$$

where $\int D\boldsymbol{\eta}(t)$ is an integral over all path perturbations $\boldsymbol{\eta}(t)$. Here we have neglected writing the normalization factor since we are only interested in the phase. Plugging in the quadratic Lagrangian Eq. (3.15) into Eq. (3.16) yields

$$\begin{aligned} \langle \mathbf{x}_b | U | \mathbf{x}_a \rangle &= e^{\frac{i}{\hbar} S_{\rm cl}} \left[\int D\boldsymbol{\eta}(t) \exp\left(\frac{i}{\hbar} S' \right) \right] \\ S' &= \int_{t_a}^{t_b} dt \left[a(t)\eta^2(t) + b(t)\boldsymbol{\eta}(t) \cdot \dot{\boldsymbol{\eta}}(t) + c(t)\eta^2 \right]. \end{aligned} \tag{3.17}$$

Here we have dropped all terms linear in $\boldsymbol{\eta}$ and $\dot{\boldsymbol{\eta}}$ as they represent first order variations in the action around the extremum path and therefore are zero by definition. Terms that are independent of $\boldsymbol{\eta}$ or $\dot{\boldsymbol{\eta}}$ are factored out in $S_{\rm cl}$. This only leaves the three quadratic terms in Eq. (3.17). As these terms are independent of the boundary points $\mathbf{x}_a$ and $\mathbf{x}_b$, this allows us to write the propagator as

$$\langle \mathbf{x}_b | U | \mathbf{x}_a \rangle = F\left(t_a, t_b\right) e^{\frac{i}{\hbar} S_{\rm cl}}, \tag{3.18}$$

and hence

$$\psi\left(\mathbf{x}_b, t_b\right) = F\left(t_a, t_b\right) \int dx_a \, e^{\frac{i}{\hbar} S_{\mathrm{cl}}[\mathbf{x}_a, t_a; \mathbf{x}_b, t_b]} \psi\left(\mathbf{x}_a, t_a\right). \tag{3.19}$$

Consider now an initial state, which is a plane wave, given by

$$\psi\left(\mathbf{x}_a, t_a\right) = \frac{1}{\sqrt{2\pi\hbar}} e^{\frac{i(\mathbf{p}_0 \cdot \mathbf{x}_a - E_0 t)}{\hbar}}, \tag{3.20}$$

with initial momentum $\mathbf{p}_0$. The classical action S_{cl} is a function only of the end points $S_{\mathrm{cl}}(\mathbf{x}_a, t_a; \mathbf{x}_b; t_b)$. A stationary point corresponds to a point along the classical trajectory (i.e points which correspond to extremums of the actions). In this case we assume $\mathbf{x}_a$ is different from the classical stationary point $\mathbf{x}_0$.

We can expand the initial wavefunction around the stationary point $\mathbf{x}_0$

$$\begin{aligned} \psi\left(\mathbf{x}_0 + \boldsymbol{\eta}, t_a\right) &= \frac{1}{\sqrt{2\pi\hbar}} e^{\frac{i(\mathbf{p}_0 \cdot (\mathbf{x}_0 + \boldsymbol{\eta}) - E_0 t)}{\hbar}} \\ &= \frac{1}{\sqrt{2\pi\hbar}} e^{\frac{i(\mathbf{p}_0 \cdot \mathbf{x}_0 - E_0 t)}{\hbar}} e^{\frac{i\mathbf{p}_0 \cdot \boldsymbol{\eta}}{\hbar}}. \end{aligned} \tag{3.21}$$

Any quadratic Lagrangian can always be expanded around the stationary point $\mathbf{x}_0$ to second order as

$$S_{cl}[\mathbf{x}_0 + \boldsymbol{\eta}, t_a;\, \mathbf{x}_b, t_b] = S_{\mathrm{cl}}[\mathbf{x}_0, t_a;\, \mathbf{x}_b, t_b] - \mathbf{p}_0 \cdot \boldsymbol{\eta} + C\left(t_a, t_b\right) \eta^2, \tag{3.22}$$

where

$$\mathbf{p}_0 = -\frac{\partial}{\partial x_0} S_{\mathrm{cl}}[\mathbf{x}_0, t_a;\, \mathbf{x}_b, t_b], \tag{3.23}$$

$$C\left(t_a, t_b\right) = \frac{1}{2} \frac{\partial^2}{\partial {x_0}^2} S_{\mathrm{cl}}[\mathbf{x}_0, t_a;\, \mathbf{x}_b, t_b]. \tag{3.24}$$

Using the result from Eq. (3.19) then allows us to write

$$\begin{aligned}\psi\left(\mathbf{x}_b, t_b\right) &= F\left(t_a, t_b\right) \int d\boldsymbol{\eta}\, e^{\frac{i}{\hbar} S_{\mathrm{cl}}[\mathbf{x}_0+\boldsymbol{\eta}, t_a; \mathbf{x}_b, t_b]} \psi\left(\mathbf{x}_0+\boldsymbol{\eta}, t_a\right) \\ &= F\left(t_a, t_b\right) \int d\boldsymbol{\eta}\, e^{\frac{i}{\hbar}\left(S_{\mathrm{cl}}[\mathbf{x}_0, t_a; \mathbf{x}_b, t_b] - \mathbf{p}_0 \cdot \boldsymbol{\eta} + C(t_a, t_b)\eta^2 + \mathbf{p}_0 \cdot \boldsymbol{\eta}\right)} \frac{1}{\sqrt{2\pi\hbar}} e^{\frac{i(\mathbf{p}_0 \cdot \mathbf{x}_0 - E_0 t)}{\hbar}}.\end{aligned} \tag{3.25}$$

Here we have simply substituted in our expanded action Eq. (3.22) and wave function Eq. (3.21). Noting that

$$\psi(\mathbf{x}_0, t_a) = \frac{1}{\sqrt{2\pi\hbar}} e^{\frac{i(\mathbf{p}_0 \cdot \mathbf{x}_0 - E_0 t)}{\hbar}}, \tag{3.26}$$

and

$$\int d\boldsymbol{\eta} e^{\frac{iC(t_a, t_b)\eta^2}{\hbar}} = \left[\frac{i\pi\hbar}{C(t_a, t_b)}\right]^{\frac{1}{2}}, \tag{3.27}$$

we can write this as

$$\begin{aligned}\psi\left(\mathbf{x}_b, t_b\right) &= F\left(t_a, t_b\right) e^{\frac{i}{\hbar} S_{\mathrm{cl}}[\mathbf{x}_0, t_a; \mathbf{x}_b, t_b]} \psi\left(\mathbf{x}_0, t_a\right) \int d\boldsymbol{\eta} e^{\frac{iC\eta^2}{\hbar}} \\ &= \left[\frac{i\pi\hbar}{C\left(t_a, t_b\right)}\right]^{1/2} F\left(t_a, t_b\right) e^{\frac{i}{\hbar} S_{\mathrm{cl}}[\mathbf{x}_0, t_a; \mathbf{x}_b, t_b]} \psi\left(\mathbf{x}_0, t_a\right).\end{aligned} \tag{3.28}$$

Thus we see that the phase of the final wavefunction is given by the action acting along the classical path plus the initial phase of the wavefunction.

3.2.3 Perturbations

Let us finally see how small perturbations to the Lagrangian, such as those measured in an interferometer, influence the phase. To begin with, let's con-

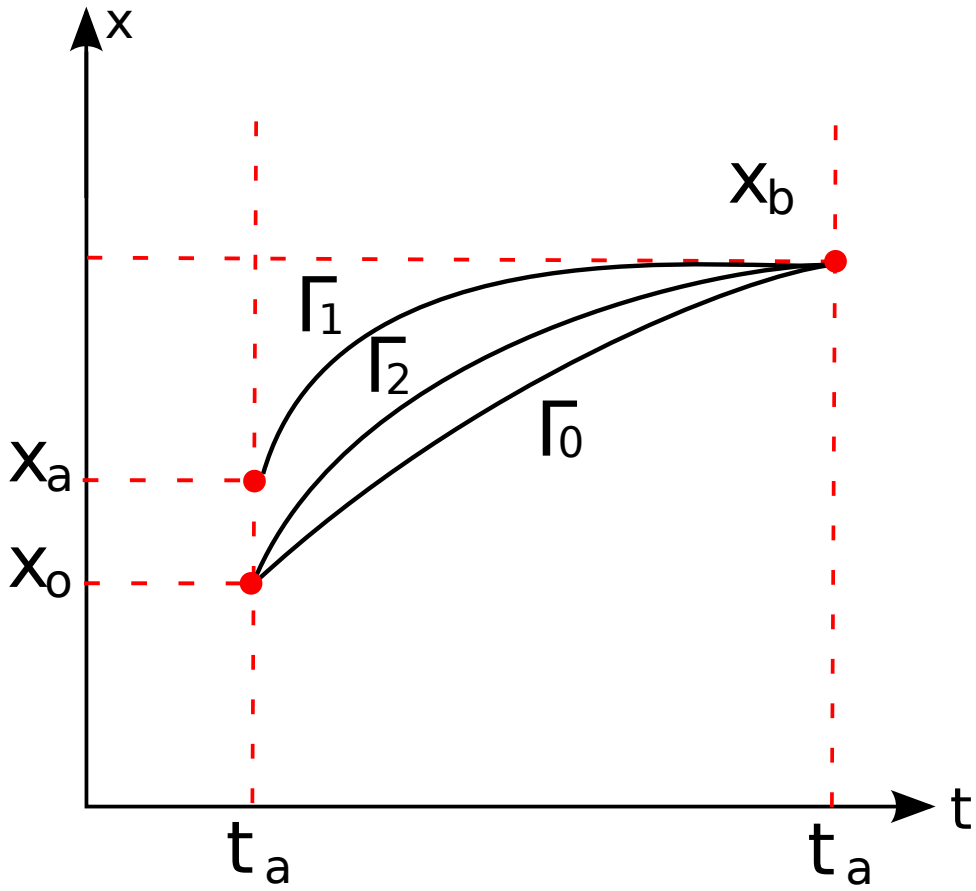

Figure 3.1: A visual representation of the perturbed (Γ_2) and unperturbed (Γ_0, Γ_1) paths taken between perturbed ($\mathbf{x}_a$) and unperturbed ($\mathbf{x}_0$) boundary points.

sider a scenario in which the starting position $\mathbf{x}_0$ is shifted to a new starting point $\mathbf{x}_a$. Here we are assuming $\mathbf{x}_0$ corresponds to a point of stationary phase just as it did in the previous subsection. We are therefore assuming that we are slightly off the classical path, and we wish to find a constraint on this perturbation which will still allow us to approximately use the original classical path. Here we define the classical path Γ_1 from $\mathbf{x}_a$ to the end point $\mathbf{x}_b$ under the initial momentum $\mathbf{p}_0$. This will be different from the classical path Γ_0 from $\mathbf{x}_0$ to $\mathbf{x}_b$. Ignoring the amplitude factor F, we expand the wavefunction and the action about the stationary point $\mathbf{x}_a$

$$\begin{aligned}\psi(\mathbf{x}_b,t_b) &= \frac{1}{\sqrt{2\pi\hbar}} e^{\frac{i(\mathbf{p}_0\cdot\mathbf{x}_a - E_0 t)}{\hbar}} e^{\frac{i}{\hbar}S_{\mathrm{cl}}[\mathbf{x}_a,t_a;\mathbf{x}_b,t_b]} \\ &= \frac{1}{\sqrt{2\pi\hbar}} e^{\frac{i(\mathbf{p}_0\cdot[\mathbf{x}_0+(\mathbf{x}_a-\mathbf{x}_0)]-E_0 t)}{\hbar}} e^{\frac{i}{\hbar}\left(S_{\mathrm{cl}}[\mathbf{x}_a,t_a;\mathbf{x}_b,t_b]-\mathbf{p}_0(\mathbf{x}_a-\mathbf{x}_0)+C(\mathbf{x}_a-\mathbf{x}_0)^2\right]} \\ &= \psi(\mathbf{x}_0,t_a)\, e^{\frac{i}{\hbar}S_{\mathrm{cl}}[\mathbf{x}_0,t_a;\mathbf{x}_b,t_b]} e^{\frac{iC(\mathbf{x}_a-\mathbf{x}_0)^2}{\hbar}}. \end{aligned} \tag{3.29}$$

If we then assume that the starting point $\mathbf{x}_a$ is close enough to the stationary point $\mathbf{x}_0$ to satisfy

$$\frac{C(\mathbf{x}_a-\mathbf{x}_0)^2}{\hbar} \ll 1, \tag{3.30}$$

then we can approximate the final wavefunction $\psi(\mathbf{x}_b,t_b)$ simply by evolving a neighbouring wavefunction along the original classical path!

With this preliminary result, we can tackle the effect that a perturbation has on the phase of a wavefunction. Consider the Lagrangian

$$L = L_0 + \epsilon L_1, \tag{3.31}$$

with $\epsilon \ll 1$. We wish to approximate the perturbed wavefunction

$$\psi_1(\mathbf{x}_b, t_b) = \psi(\mathbf{x}_a, t_a)\, e^{\frac{i}{\hbar}\int_{\Gamma_1}(L_0+\epsilon L_1)\,dt}, \tag{3.32}$$

and write it in terms of the unperturbed wavefunction

$$\psi_0(\mathbf{x}_b, t_b) = \psi(\mathbf{x}_0, t_a)\, e^{\frac{i}{\hbar}\int_{\Gamma_0} L_0\,dt}. \tag{3.33}$$

Here we have neglected the amplitude factors as we are only interested in the phase. This is because typically the phase is experimentally sensitive, while the amplitude will vary much more slowly in general. Γ_1 is the classical trajectory followed in the perturbed Lagrangian from the perturbed point $\mathbf{x}_a$ to the final point $\mathbf{x}_b$. Γ_0 is defined as the classical trajectory followed by the particle from the initial point $\mathbf{x}_0$ to $\mathbf{x}_b$ with initial unperturbed momentum $\mathbf{p}_0$. If the two starting points are sufficiently close that they satisfy Eq. (3.30), then as we showed, we can write

$$\psi(\mathbf{x}_a, t_a)\, e^{\frac{i}{\hbar}\int_{\Gamma_1}(L_0+\epsilon L_1)\,dt} \approx \psi(\mathbf{x}_0, t_a)\, e^{\frac{i}{\hbar}\int_{\Gamma_2}(L_0+\epsilon L_1)\,dt}. \tag{3.34}$$

Here Γ_2 is the classical path linking the unperturbed boundary points $\mathbf{x}_0$ and $\mathbf{x}_b$ under the perturbed Lagrangian. Although the boundary terms now match, the initial momentum and the Lagrangian are still different giving rise to this altered classical path. The path Γ_2 is an extremum for the perturbed Lagrangian, and hence

$$\int_{\Gamma_2} L\,dt \approx \int_{\Gamma_0} \left(L + O(\epsilon^2)\right)\,dt. \tag{3.35}$$

Thus to first order we can write

$$\psi_1(\mathbf{x}_b, t_b) = \psi(\mathbf{x}_0, t_a)\, e^{\frac{i}{\hbar}\oint_{\Gamma_0}(L_0+\epsilon L_1)\,dt} = \psi_0(\mathbf{x}_b, t_b)\, e^{\frac{i}{\hbar}\int_{\Gamma_0}\epsilon L_1\,dt}. \tag{3.36}$$

This shows that so long as condition Eq. (3.30) is met, we can derive the phase due to any perturbation to first order by integrating the perturbation along the unperturbed path.

3.3 The Mach-Zehnder Interferometer

In this section we consider a Mach-Zehnder interferometer arrangement which can be used to detect the optical HMW phase. The interferomter uses three optical gratings which first order Bragg scatter a collimated and velocity selected beam of ^{7}Li atoms. Lithium is chosen due to its relatively small polarizability and its small mass which provides the atom beam with a sizable recoil velocity. This choice of using an atom with a small polarizability seems counter intuitive, but as we shall see, it works to our advantage here. Along one of the arms, we apply a traveling wave laser beam as seen in figure 3.2. The laser beam is then retro-reflected back along the other arm. Each arm is 60 cm in length and the atoms are fired through at a velocity of 3×10^3 m/s. High atom velocities are preferable as the HMW phase depends on the interaction distance, and not on the interaction time, whereas by limiting the interaction time, we can reduce visibility issues caused by spontaneous emission. The transverse velocity of a highly collimated beam is on the order of 10 cm/s. The atom will then pick up an HMW phase shift $\phi_{\text{HMW}} = -\hbar^{-1} \oint [\alpha \mathbf{E} \times \mathbf{B}] \cdot d\mathbf{r}$ due to the presence of the laser along the lower arm and the opposite phase along the upper path.

The difficulty in realizing this effect experimentally hangs on the ability to maximize the contribution due to the HMW phase, while suppressing spontaneous emission. The HMW phase is incredibly small and requires a large laser intensity to become visible. The danger in pushing the intensity too high is that decoherence due to spontaneous emission can smear out any trace of the HMW effect. Spontaneous emission is the process by which an already excited atom emits a photon to drop down to a lower energy state. In this section we

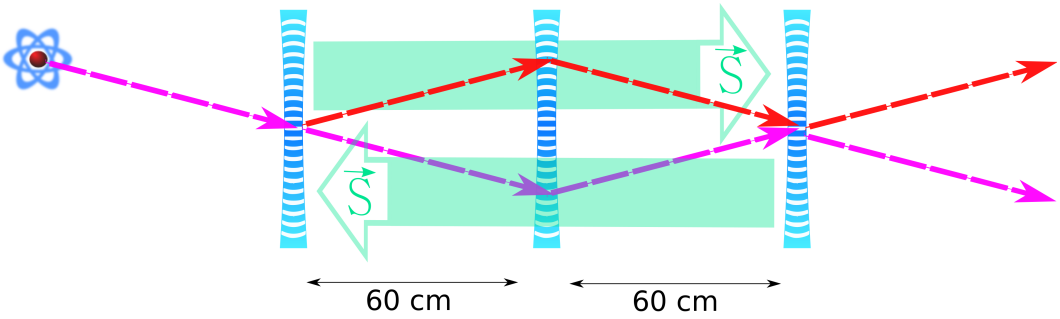

Figure 3.2: A Mach-Zehnder inteferometer made with 3 laser standing wave laser gratings and with a travelling wave laser beam applied along the lower arm and retro-reflected back along the upper arm. The atom beam undergoes first order Bragg scattering at the first standing wave laser which splits the atoms into a coherent superposition of the two arms of the interferometer. The atoms pick up an HMW phase as they travel down the arms along/against the applied laser, proportional to the Poynting vector $\epsilon_0 \mathbf{E} \times \mathbf{B}$.

will discuss Rayleigh scattering, which describes an initially unexcited atom interacting with off-resonant light. Rayleigh scattering can be thought of as the off resonant version of spontaneous emission and includes the entire process of becoming excited, emitting a photon, and dropping back to a lower energy level. The Rayleigh scattering rate of photons out of the laser beam by each atom γ_R is given by

$$\gamma_{\mathrm{R}} = \frac{\mathrm{I}\alpha^2\mathrm{k}^3}{6\pi\epsilon_0^2\mathrm{c}\hbar}, \tag{3.37}$$

where $I = \frac{1}{2}c\epsilon_0 E^2$ is the intensity of the laser beam. Here we see the wisdom of choosing an atom with a smaller polarizability. The HMW phase scales as $\alpha(\omega)$, while the scattering rate scales as $\alpha^2(\omega)$. It is therefore in our interest to make $\alpha(\omega)$ as small as possible, while still being able to detect the HMW phase. Consider a beam of ^{7}Li irradiated by a laser detuned from the D1 line by $\Delta/2\pi = 150$ GHz (the transition frequency being 4.47×10^{14} Hz). At such large detunings, the corresponding dynamic (frequency-dependent)

polarizability $\alpha(\omega)$ can then be found from [73]

$$\alpha(\omega) \approx \frac{\omega_0^2 \alpha_0}{\omega^2 - \omega_0^2} \tag{3.38}$$

where $\alpha_0 = 2.705 \times 10^{-39}$ F $\cdot$ m^2 [74] is the static ground state polarizability of ^{7}Li. Under a $\Delta/2\pi = 150$ GHz detuning, the corresponding polarizability is $\alpha(\omega) = 4 \times 10^{-36}$ F $\cdot$ m^2. We find that with these parameters, the intensity required to obtain a modest HMW phase shift of 0.2 radians along the 120 cm arm is $I = 1.7 \times 10^2$ W/cm^2. Plugging this into Eq. (3.37) gives $\gamma_{\mathrm{R}} = 5.1 \times 10^2\,\mathrm{s}^{-1}$, which corresponds to a 9% chance of a spontaneous event occurring during the 40 μs transit across the interferometer.

The main objective of the experiment is to differentiate the different perturbations present in the experiment. These perturbations fall into two distinct categories: the velocity dependent phase contributions (Stark, Sagnac), and the velocity independent phase terms (HMW, Doppler, diffraction). Here it is worth identifying what we mean by velocity dependent and independent terms. Velocity *dependent* perturbations in the Lagrangian such as the HMW term $\mathbf{v} \cdot (\mathbf{d} \times \mathbf{B})$, become velocity *independent* phase contributions when integrated over time $\int \mathbf{v} \cdot (\mathbf{d} \times \mathbf{B})\, dt \rightarrow \int (\mathbf{d} \times \mathbf{B}) \cdot d\mathbf{r}$. Similarly, terms in the Lagrangian such as the Stark energy $\frac{1}{2}\alpha E^2$ which are independent of velocity, pick up a *velocity dependence* due to the time integral when we consider the phase effects. Going forth, we shall always refer to the phase contribution (i.e the action rather than the Lagrangian contribution) when discussing velocity independent/dependent perturbations.

The second benefit of working with an optical beam over a static field - it eliminates the Aharonov-Casher and Zeeman effects. This is because both of

these effects are due to the interaction energy $\boldsymbol{\mu} \cdot \mathbf{B}$. The magnetic moment $\boldsymbol{\mu}$ is given by

$$\boldsymbol{\mu} = \frac{q}{2m_e c} \left(\mathbf{L} + 2\mathbf{S} \right), \tag{3.39}$$

where $\mathbf{L}$ is the electron angular momentum operator, and $\mathbf{S}$ is the electron spin operator. Notice now that $\mathbf{L}$ and $\mathbf{S}$ depend on the state of the atom. However, the transition rate of the atom is given by the Rabi frequency $\Omega_R = \frac{d_{ab} \cdot E_0}{\hbar}$, where d_{ab} is the dipole matrix element. This tells us that the frequency at which the magnetic moment oscillates is Ω_R which is approximately 4 GHz for our arrangement. However, since the magnetic component of the laser field itself oscillates at an optical frequency on the order of 10^{15} Hz, the product of the two will integrate to zero over a Rabi cycle. Hence, both the Zeeman and AC effects are not present when dealing with optical lasers. Put another way, while the electric dipole moment is induced by the electromagnetic laser (i.e. it did not exist prior to the laser acting on the atom), the magnetic moment is not.

We begin by considering the Lorentz force acting on an atom while entering and traveling inside the laser beam. The Lorentz force in the i'th direction is

$$\mathbf{F}_i(\mathbf{x}_\mathrm{a}, t) = \alpha \mathbf{E}(\mathbf{x}_\mathrm{a}, t) \cdot \frac{\partial}{\partial x_i} \mathbf{E}(\mathbf{x}_\mathrm{a}, t) + \alpha \frac{\partial}{\partial t} \left(\mathbf{E}(\mathbf{x}_\mathrm{a}, t) \times \mathbf{B}(\mathbf{x}_\mathrm{a}, t) \right)_i . \tag{3.40}$$

We may write the electric and magnetic fields in our configuration as

$$\mathbf{E}(x, t) = \mathcal{E}(x) \cos\left(\omega t - kx\right) \hat{\mathbf{z}} \tag{3.41}$$

$$\mathbf{B}(x, t) = \mathcal{B}(x) \cos\left(\omega t - kx\right) \hat{\mathbf{y}}. \tag{3.42}$$

If we look at average force (averaged over an optical period T)

$$\begin{aligned}\langle F(x)\rangle &= \frac{1}{T}\int_t^{t+T} f(x)\,dt = \alpha\mathcal{E}(x)\frac{\partial}{\partial x}\mathcal{E}(x)\frac{1}{T}\int_t^{t+T}\cos^2(kx-\omega t)\,dt \\ &+ 2k\alpha\mathcal{E}^2(x)\frac{1}{T}\int_t^{t+T}\sin(kx-\omega t)\cos(kx-\omega t)\,dt \\ &- 2\omega\alpha\mathcal{E}(x)\mathcal{B}(x)\int_t^{t+T}\sin(kx-\omega t)\cos(kx-\omega t)\,dt. \end{aligned} \tag{3.43}$$

The second and third force terms integrate to zero, and thus we are only left with the optical dipole force

$$\langle F(x)\rangle = \frac{1}{2}\alpha\mathcal{E}(x)\frac{\partial}{\partial x}\mathcal{E}(x). \tag{3.44}$$

This result follows since, surprisingly, it is the partial derivative of the Abraham term that appears in the force equation, and not the total derivative. This can be seen by applying the Euler-Lagrange equations to the Lagrangian Eq. (1.23)

$$L = \frac{1}{2}mv^2 + \mathbf{d}\cdot(\mathbf{E}+\mathbf{v}\times\mathbf{B}) + \boldsymbol{\mu}\cdot(\mathbf{B}-\mathbf{v}\times\mathbf{E}/c^2). \tag{3.45}$$

As we mentioned above, the third term vanishes due to the magnetic moment being independent of the applied laser. Using the convective derivative $\frac{d}{dt} = \mathbf{v}\cdot\nabla + \frac{\partial}{\partial t}$ we find

$$\begin{aligned} m\mathbf{a} &= \frac{d}{dt}(\mathbf{d}\times\mathbf{B}) + \nabla[\mathbf{d}\cdot\mathbf{E} - \mathbf{v}\cdot(\mathbf{d}\times\mathbf{B})] \\ &= \frac{\partial}{\partial t}(\mathbf{d}\times\mathbf{B}) + \mathbf{v}\cdot\nabla(\mathbf{d}\times\mathbf{B}) + \nabla[\mathbf{d}\cdot\mathbf{E} - \mathbf{v}\cdot(\mathbf{d}\times\mathbf{B})] \\ &= \frac{\partial}{\partial t}(\mathbf{d}\times\mathbf{B}) + \nabla(\mathbf{d}\cdot\mathbf{E}). \end{aligned} \tag{3.46}$$

If there is perfect symmetry between the overlap of the upper laser beam with the upper arm of the interferometer and the lower laser beam with the lower arm of the interferometer, then the second term in Eq. (3.46) cancels out in its contribution to the dynamic phase.

We now consider the velocity dependent phase perturbations - the Stark, and Sagnac effects. Given the parameters mentioned previously, the Stark energy at peak intensity is $\frac{1}{2}\alpha E^2 = 2.5\times10^{-27}$J. The corresponding phase shift over one of the 120 cm arms is $\phi_S = 1.0\times10^4$ rad during the 40 μs transit. It is therefore desirable to configure the upper and lower beams to be as symmetric as possible in order to cancel as much of this phase as possible. However, a zero output reading does not necessarily imply that both interferometer arms are contributing equally - since any phase shift difference of $2N\pi$ will yield the same null result. Therefore, the intensity must be ramped up slowly from zero to assure both beams are equally aligned. Let us for the time being suppose that a small alignment asymmetry leads to total Stark phase difference between the two arms of 1 radian. How then can we separate the velocity independent geometric phase shifts we are interested in from the Stark shift? We can do so by varying the initial velocity $\mathbf{v}_0$ of the atoms. The time it takes for an atom to traverse the interaction zone is $T = L/v_0$. Here $L = 1.2$ m is the distance over which the atom interacts with the laser beam. The total velocity $\mathbf{v}$ is the sum of components from the initial velocity $\mathbf{v}_0$ and the perpendicular recoil velocity $\mathbf{v}_{\rm rec} = 2\hbar\mathbf{k}_{\rm L}/m$. From this we find the distance traveled by the atom is

$$d = \sqrt{L^2 + \frac{4\hbar^2 k_L^2 L^2}{m^2 v_0^2}} \approx L\left(1 + \frac{2\hbar^2 k_{\rm L}^2}{m^2 v_0^2}\right) \tag{3.47}$$

We note that while the time $T = L/v_0$ spent in the interaction region is

inversely proportional to the initial velocity v_0, the correction to the distance traveled d grows only as the inverse square of v_0. Therefore to first order, $d \approx L$. This behavior is significant since the phase generated by the Stark shift

$$\phi_{\mathrm{S}} = \frac{1}{\hbar} \int \left(\frac{1}{2} \alpha E^2 \right) dt, \tag{3.48}$$

depends on the time spent in the interaction region, while the phase generated by the HMW term

$$\phi_{\mathrm{HMW}} = -\frac{1}{\hbar} \int (\mathbf{d} \times \mathbf{B}) \cdot d\mathbf{r}, \tag{3.49}$$

depends on the distance traveled in the interaction region. Varying the initial velocity leaves the velocity independent phase terms such as ϕ_{HMW} constant to first order, while allowing us to isolate the velocity dependent terms such as ϕ_{S}. The output intensity of the interferometer can thus be written as

$$I(T) = \langle I \rangle \left[1 + \mathcal{V} \cos \left(C_1 T + C_2 \right) \right], \tag{3.50}$$

where

$$\mathcal{V} = \frac{I_{\max} - I_{\min}}{I_{\max} + I_{\min}}, \tag{3.51}$$

is the fringe visibility, C_1 corresponds to the phase due to perturbations dependent on time, and C_2 the phase due to perturbations independent of time. The visibility $\mathcal{V}$ is degraded by spontaneous emission. In the limit where the separation distance d between the two arms of the interferometer is much greater than the laser wavelength $d \gg \lambda_{\mathrm{L}}$, a single photon scattered by an atom is enough to destroy the coherence because it becomes possible to localize the atom to one of the two paths, breaking the superposition state [75]. In our setup, we necessarily must fall in this regime as it is paramount that the two

paths be separated enough so that each independently interacts with its own traveling wave laser beam. Using the recoil velocity of ^{7}Li $\mathbf{v}_{\text{rec}} = 9\,\text{cm/s}$, we obtain a maximum separation distance of 35 μm which would lead to complete decoherence if spontaneous emission occurs. The 9% of atoms that do undergo spontaneous emission then contribute to the background noise which slightly lowers fringe visibility.

By taking measurements with different initial velocities [62], one obtains an output interference pattern of the form $\cos(C_1T + C_2)$. We must check that the uncertainty in our time measurement δT does not precipitate a large time dependent phase uncertainty which would mask the contribution from C_2. To see that this is not the case, we note that an uncertainty in velocity δv_0 will alter C_1T through

$$C_1T = \frac{C_1L}{v_0} = \frac{C_1L}{v_0 + \delta v_0} \approx \frac{C_1L}{v_0}\left(1 - \frac{\delta v_0}{v_0}\right), \tag{3.52}$$

where L is the length of the interaction region and v_0 is the mean atomic beam velocity. The velocity uncertainty therefore leads to a time dependent phase uncertainty

$$\delta\phi \approx -\frac{C_1L}{v_0}\frac{\delta v_0}{v_0}. \tag{3.53}$$

Using atomic beam phase choppers [76], we may measure the average beam velocity to within 0.1%. We then find that the uncertainty in C_1T is $\delta\phi \approx 1$ mrad. It is therefore possible to measure C_1 by varying v_0 and hence T. By observing the output phase's sinusoidal variation near a node as T is varied in small increments, C_1 can be obtained by finding the slope. The velocity can be altered by seeding the ^{7}Li with a noble gas. Vigué et al. for example

use krypton ($\mathbf{v} = 744 \pm 18$ m/s), argon ($\mathbf{v} = 1062 \pm 20$ m/s), and neon ($\mathbf{v} = 1520 \pm 38$ m/s) [62]. The mean velocity varies as $1/\sqrt{M}$, where M is the mass of the carrier gas [61].

Note that C_1 contains both the Stark phase and the Sagnac phase, which is due to the Earth's rotation. In the interferometry experiment preformed by Vigue [62], with similar parameters, they measured the effect of the Sagnac phase to be on the order of ≈ 0.65 rad. This phase is dependent on the latitude at which the experiment is preformed and can be calculated out, or measured with the two traveling lasers switched off.

We must also take into account the velocity distribution associated with a supersonic atomic beam. This threatens to mask the HMW phase and decrease the fringe visibility. The normalized longitudinal velocity distribution is approximated by [63]

$$P(v) = \frac{S_{\|}}{v_0\sqrt{\pi}} \exp\left[-\left(\frac{(v - v_0)\, S_{\|}}{v_0}\right)^2\right], \tag{3.54}$$

where v_0 is the mean velocity, and $S_{\|} = v_0/\left(\sqrt{2}\sigma\right)$ is the parallel speed ratio which is a function of the RMS σ of the velocity distribution around the mean velocity. The velocity distribution modifies the transmission signal

$$\langle I \rangle = I_0 \int dv P(v) \left[1 + \mathcal{V} \cos(\phi)\right]. \tag{3.55}$$

Let

$$\langle \phi \rangle = \int dv P(v) \phi(v), \tag{3.56}$$

$$\delta\phi = \phi(v) - \langle \phi \rangle. \tag{3.57}$$

Substituting these terms into Eq. (3.55) and expanding the cosine term to third order in $\delta\phi$, one obtains [63]

$$\langle I \rangle = I_0 \left[1 + \mathcal{V}_m \cos\left(\phi_m\right)\right], \tag{3.58}$$

where we define the modified terms $\phi_m = \phi - \langle(\delta\phi)^3/6\rangle$ and $\mathcal{V}_m = \mathcal{V}\left[1 - \langle(\delta\phi)^2/2\rangle\right]$. Let us examine how this affects the Stark phase. The velocity distribution will act to modify the Stark term by ${\phi_S}' = \phi_S - \langle(\delta\phi_S)^3/6\rangle$. The value of $\delta\phi_S$ in our arrangement would then be approximately

$$\delta\phi \approx \phi_S \frac{\Delta v}{v}. \tag{3.59}$$

Suppose that, as suggested above, the two beams are arranged such that the mean output phase contribution due to the Stark shift can be reduced to within 1 radian ($\phi_S \approx 1$). Even with a generous velocity dispersion ratio $\Delta v/v = 10\%$ [64] we find ${\phi_S}' \approx \phi_S$ and therefore we can neglect the effects of the velocity distribution.

We now consider the velocity independent phases contained in C_2, beginning with the Doppler shifted Stark phase,

$$\phi_{\text{Doppler}} = \exp\left[\frac{i}{\hbar}\int \frac{1}{2}\alpha E^2 \left(\frac{\mathbf{k}_L \cdot \mathbf{v}}{\Delta}\right) dt\right]. \tag{3.60}$$

Eq. (3.60) can be derived by noting that the Doppler shift manifests itself through the polarizability [65]

$$\alpha = \frac{\Delta |d_{ab}|^2 E_0}{\hbar\left[\Delta^2 + \frac{\Gamma^2}{4} + \frac{\Omega^2}{2}\right]}. \tag{3.61}$$

Here d_{ab} is the dipole matrix element of the transition, Γ is the linewidth, $\Delta = \omega_{\mathrm{L}} - \omega_{\mathrm{a}}$ is the detuning and Ω is the Rabi frequency. In the large detuning regime, the polarizability is approximately inversely proportional to the detuning. A moving atom experiences a Doppler shifted detuning

$$\frac{1}{\Delta_{\mathrm{Doppler}}} = \frac{-1}{\omega_a - \left(1 + \frac{\mathbf{v}}{c}\right)\omega_L} \approx \frac{1}{\Delta}\left(1 + \frac{\mathbf{k}_L \cdot \mathbf{v}}{\Delta}\right) \tag{3.62}$$

Therefore the Doppler shifted Stark energy is

$$\frac{1}{2}\alpha E^2 \left(1 + \frac{\mathbf{k}_L \cdot \mathbf{v}}{\Delta}\right) \tag{3.63}$$

The first term is the rest frame Stark energy, while the second term yields Eq. (3.60). Unfortunately for us, the Doppler shifted phase can be rewritten in a form very nearly mimicking the HMW phase: $\phi_{\mathrm{Doppler}} = \frac{\omega}{\Delta}\phi_{\mathrm{HMW}}$. However, we see that $\phi_{\mathrm{HMW}} \propto 1/\Delta$, and $\phi_{\mathrm{Doppler}} \propto 1/\Delta^2$. Using this difference, it is possible to distinguish the two perturbations by manipulating the detuning. Note that because $\omega_{\mathrm{L}} > \Delta$, then $\phi_{\mathrm{Doppler}} > \phi_{\mathrm{HMW}}$ for all monochromatic plane wave lasers (5000 times larger!). We can, however, make the HMW phase larger than the Doppler phase by using two traveling beams which are oppositely detuned from the transition frequency.

Figure 3.3 shows four configurations with blue (blue arrows) and red (red arrows) detuned beams. In configuration (A), the beams are blue detuned from the atomic transition frequency, while in (B) the beams are red detuned. Between configurations (A) and (B) the sign of the HMW phase reverses sign, while the Doppler term changes by a factor of ω_R/ω_B, where the subscripts (R,B) indicate red/blue detuned beams. Note that in configurations (A) and

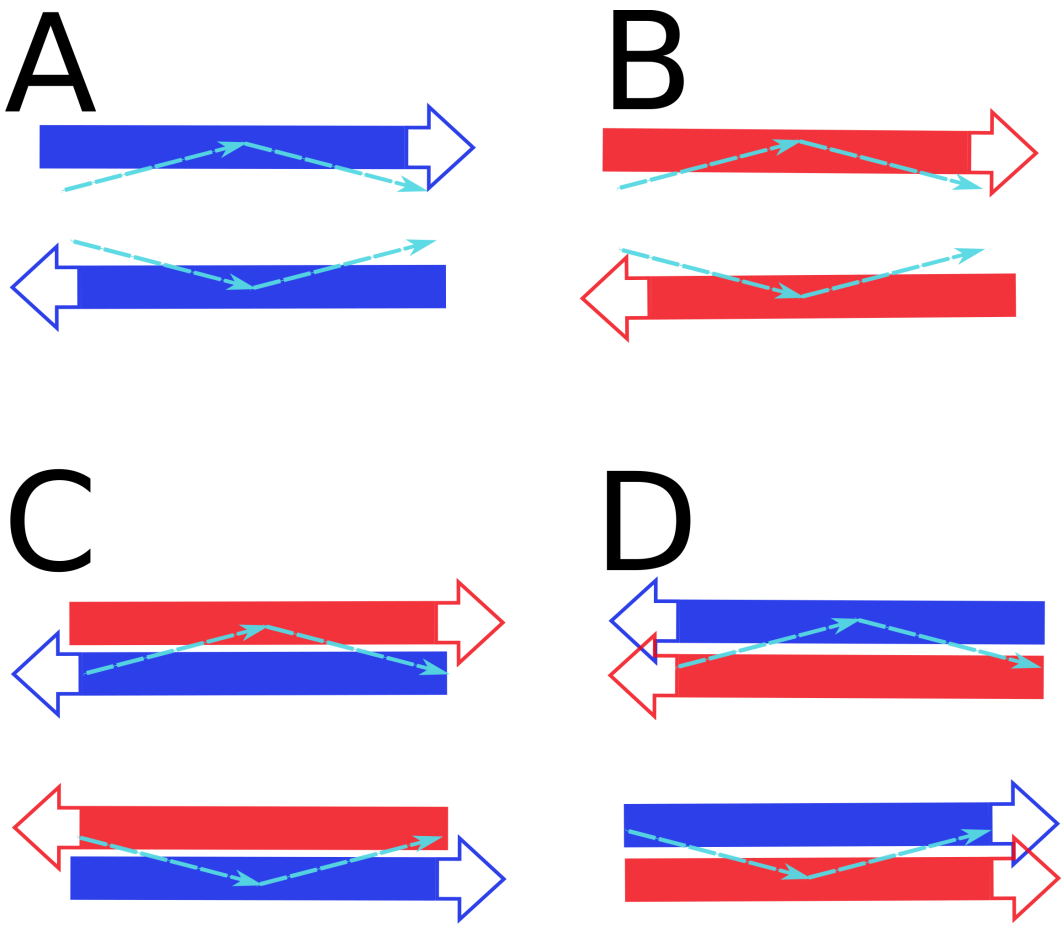

Figure 3.3: Four different configurations are shown which help distinguish the HMW phase from the Doppler shifted Stark effect. The blue color indicates a positive detuning, while red indicates the beam is negatively detuned.

(B), the Doppler phase will be a factor of ω/Δ larger than the HMW phase, which makes detecting the HMW phase rather difficult. We overcome this issue by considering configuration (C) in which we overlap two oppositely traveling beams - one red detuned, and the other symmetrically blue detuned. The HMW term doubles in value relative to configuration (B), while the Doppler term has been cut to half that of the new HMW phase. This is a unique situation in which the HMW term is actually larger than the Doppler phase allowing for us to observe the HMW phase clearly over the Doppler phase. Finally in configuration (D) both blue and red detuned beams are traveling in the same direction. The HMW phase here is identically zero since the blue detuned beam contributes an equal and opposite HMW phase to the atom, while the Doppler term acquires an energy shift of $\frac{1}{2}\alpha E^2 \frac{(\mathbf{k}_{LR}+\mathbf{k}_{LB})\cdot\mathbf{v}}{\Delta}$. This configuration allows us to isolate the Doppler phase in order to obtain a precise value for this term.

Finally we mention the diffraction phase ϕ_d which is caused by the Bragg scattering standing waves responsible for splitting the atom beam. The phase is dependent on the positions of the standing wave mirrors (i.e the phase of the beam splitting standing wave produced by each mirror.) y_1, y_2, y_3 [62]

$$\phi_d = 2k_{\mathrm{SW}}\left(y_1 - y_2 + y_3\right) \tag{3.64}$$

where k_{SW} is the standing wave laser wave number. The diffraction phase can be calculated *a priori* and is then subtracted out of the final output signal.

We have shown that Mach-Zehnder inteferometer provides a means to observe the optical HMW phase. By using an optical laser, we effectively remove the Zeeman and Aharonov-Casher phase shifts from contaminating the ob-

served shift. The output intensity of the MZ interferometer can be divided into time dependent and time independent phases. Thus it is possible to separate out the velocity dependent phases (Stark, Sagnac) from the velocity independent phases (HMW, Doppler, diffraction). It is the Doppler term which provides the most trouble for such an experiment. However, even though the Doppler shift is much larger than the HMW phase for a single traveling plane wave, we can use different symmetric arrangements, as indicated in figure 3.3, to quench its effect and promote the HMW phase. In particular, using two oppositely traveling, symmetrically blue and red detuned lasers, we can make the HMW phase

$$\phi_{\mathrm{HMW}} = -\frac{1}{\hbar}\int (\mathbf{d}\times\mathbf{B})\cdot d\mathbf{r}, \tag{3.65}$$

twice as large as the Doppler phase shift, thus revealing this enigmatic effect.

3.4 The Kapitza-Dirac Interferometer

Here we consider a long thin Bose Einstein condensate placed in a uniform traveling wave laser beam. We assume the BEC is initially magnetically trapped and confined in some region, while a plane wave laser is switched on. The trap is then turned off and a standing pulse is applied to the BEC. The standing wave pulse acts as a beam splitter. The reason we want the laser on before the standing pulse is because we want to only observe the HMW phase shift without having to deal with the classical forces associated with entering a laser beam. As a result of the first pulse, the atoms are put into a superposition of the $|\pm 2n_r\hbar k\rangle$ momentum states, and the ground state. Here k is the recoil momentum and n_r is the refractive index of the BEC. After 1 ms of free propagation, a second standing pulse is applied which kicks some of the $|\pm 2n_r\hbar k\rangle$ group back into the ground state and produces an interference pattern which may then be imaged. This set up closely follows the work done by Pritchard's group [35], where we have modified the experiment to include a traveling optical laser beam acting on the BEC. The choice of using ^{7}Li over ^{87}Rb comes down to having a smaller polarizability (remember the HMW phase scales as α, while spontaneous emission scales as α^2), and a smaller mass - which leads to a greater recoil velocity.

The dipole potential created by a standing wave pulse is given by [77]

$$U(\mathbf{x},t) = \frac{\hbar\Omega_R^2}{\Delta} f^2(t)\sin^2(n_r k\mathbf{x}). \tag{3.66}$$

Where Ω_R is the Rabi frequency and Δ is the detuning away from the atomic transition frequency. Here we have assumed $\Delta \gg \Gamma/4$, where Γ is the sponta-

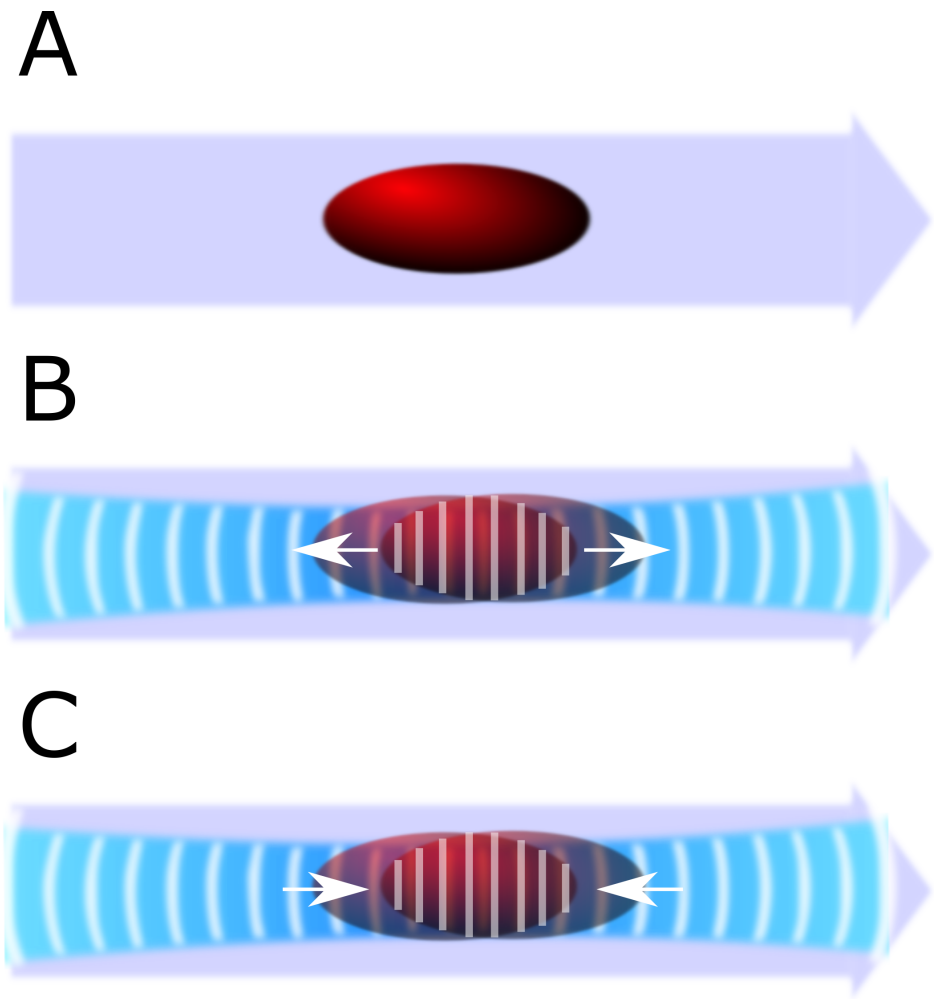

Figure 3.4: In (A) the initial configuration is a ^{7}Li BEC in a harmonic trap illuminated by a laser. (B) The trap is then switched off and the BEC is pulsed with a standing wave of laser light which scatters a fraction of the atoms into $|\pm 2\hbar n_r k\rangle$ states. (C) After a delay of 1 ms, a second standing pulse scatters these atoms back into the ground state.

neous decay rate. The time envelope f can be any function, but here we assume it is a simple step function resulting in a square wave pulse. In the Raman-Nath approximation, the wave function immediately following a Kapitza-Dirac pulse is [78, 35]

$$|\psi\rangle = |\psi_0\rangle\, e^{\frac{-i}{\hbar}\int dt'\, U(x,t')} = |\psi_0\rangle\, e^{\frac{-i}{2\Delta}\Omega_R^2\tau} e^{\frac{i}{2\Delta}\Omega_R^2\tau\cos(2n_r kx)}. \tag{3.67}$$

Here we have defined $\tau = \int dt' f^2(t')$ which for a square wave pulse is simply the interaction time $\tau = t_{\text{int}}$. Note that in the Kapitza-Dirac regime we are assuming short interaction times relative to the recoil frequency (i.e. $t \ll 1/\omega_{\text{rec}}$), and hence during the pulse we assume the atomic motion is negligible. Making use of the identity

$$e^{iA\cos(B)} = \sum_{m=-\infty}^{\infty} i^m J_m(A) e^{imB}, \tag{3.68}$$

we rewrite the wave function in terms of Bessel functions of the first kind in the position space representation

$$\langle x|\psi\rangle = \langle x|\psi_0\rangle\, e^{\frac{-i\Omega_R^2\tau}{2\Delta}} \sum_{m=-\infty}^{\infty} i^m J_m\left(\frac{\Omega_R^2\tau}{2\Delta}\right) e^{i2mn_r kx}. \tag{3.69}$$

In the position space representation $\langle \mathbf{x}, \psi_0\rangle = \langle \mathbf{x}, 0 n_r kx\rangle \to 1$. This allows us to write the state after the initial Kapitza-Dirac pulse as:

$$|\psi\rangle = e^{\frac{-i\Omega_R^2\tau}{2\Delta}} \sum_{m=-\infty}^{\infty} i^m J_m\left(\frac{\Omega_R^2\tau}{2\Delta}\right) |2mn_r\hbar k\rangle\,. \tag{3.70}$$

From here on, we will only keep the three terms corresponding to $m = (-1, 0, 1)$ as the other terms are much smaller, corresponding to a negligible

fraction of atoms in these higher momentum states. The Hamiltonian after the first pulse has acted is given by

$$\begin{aligned} \hat{H} &= \frac{\left(\hat{P} + \mathbf{d} \times \mathbf{B}\right)^2}{2m} - \frac{1}{2}\alpha E^2 \\ &= \frac{\hat{P}^2 + 2\mathbf{d} \times \mathbf{B}\hat{P} + (\mathbf{d} \times \mathbf{B})^2}{2m} - \frac{1}{2}\alpha E^2. \end{aligned} \tag{3.71}$$

This is true since the Abraham term $\mathbf{d} \times \mathbf{B}$ is a constant in this setup and so commutes with the momentum operator. Since plane waves are eigenstates of this Hamiltonian, the eigenvalue of the term $\hat{P}$ is

$$\hat{P}e^{\pm i2n_r kx} = \pm 2n_r \hbar k e^{\pm i2n_r kx}, \tag{3.72}$$

and therefore

$$\hat{H}e^{\pm i2n_r kx} = \left[\frac{(\pm 2n_r \hbar k + \mathbf{d} \times \mathbf{B})^2}{2m} - \frac{1}{2}\alpha E^2\right] e^{\pm i2n_r kx}. \tag{3.73}$$

We will drop the global phase factor appearing in front of the summation in what follows. From here we can determine the state of the wave function ψ at

any time t after the pulse:

$$\begin{aligned}
|\psi(t+\tau)\rangle &= e^{\frac{-i\hat{H}t}{\hbar}}|\psi(0)\rangle \\
&= J_0\left(\frac{\Omega_R^2\tau}{2\Delta}\right)e^{\frac{-i}{\hbar}\left[\frac{(\mathbf{d}\times\mathbf{B})^2}{2m}-\frac{1}{2}\alpha E^2\right]t}|0n_r\hbar k\rangle \\
&+ iJ_1\left(\frac{\Omega_R^2\tau}{2\Delta}\right)\left(e^{i2n_rkx-\frac{it}{\hbar}\left[\frac{(2n_r\hbar k+\mathbf{d}\times\mathbf{B})^2}{2m}-\frac{1}{2}\alpha E^2\right]}\right)|2n_r\hbar k\rangle \\
&+ iJ_1\left(\frac{\Omega_R^2\tau}{2\Delta}\right)\left(e^{-i2n_rkx-\frac{it}{\hbar}\left[\frac{(-2n_r\hbar k+\mathbf{d}\times\mathbf{B})^2}{2m}-\frac{1}{2}\alpha E^2\right]}\right)|-2n_r\hbar k\rangle \\
&= e^{\frac{-it}{\hbar}\left(\frac{(\mathbf{d}\times\mathbf{B})^2}{2m}-\frac{1}{2}\alpha E^2\right)}\left[J_0\left(\frac{\Omega_R^2\tau}{2\Delta}\right)|0n_r\hbar k\rangle\right. \\
&+ iJ_1\left(\frac{\Omega_R^2\tau}{2\Delta}\right)e^{i\left(2n_rkx-\frac{4\hbar^2n_r^2k^2t}{2m\hbar}-2n_rk\frac{\mathbf{d}\times\mathbf{B}}{m}t\right)}|2n_r\hbar k\rangle \\
&+ \left.iJ_1\left(\frac{\Omega_R^2\tau}{2\Delta}\right)e^{i\left(-2n_rkx-\frac{4\hbar^2n_r^2k^2t}{2m\hbar}+2n_rk\frac{\mathbf{d}\times\mathbf{B}}{m}t\right)}|-2n_r\hbar k\rangle\right]. \quad (3.74)
\end{aligned}$$

Here we have made use of the identity $J_{-m}(\theta) = (-1)^m J_m(\theta)$. During this time τ, the phases of the $|\pm 2n_rk\rangle$ states evolve at a different rate from those in the ground state.

We next apply another standing wave pulse to this wave function - partially recombining the momentum states. We are interested in finding the probability of finding the atoms in the ground state $|0n_r\hbar k\rangle$ after this second pulse, so we are only interested in the $|0n_r\hbar k\rangle$ terms,

$$\begin{aligned}
|\psi(t+2\tau)\rangle &= e^{\frac{-it}{\hbar}\left(\frac{(\mathbf{d}\times\mathbf{B})^2}{2m}-\frac{1}{2}\alpha E^2\right)}\left[J_0^2\left(\frac{\Omega_R^2\tau}{2\Delta}\right)|0n_r\hbar k\rangle\right. \\
&- J_1^2\left(\frac{\Omega_R^2\tau}{2\Delta}\right)e^{i\left(2n_rkx-\frac{4\hbar^2n_r^2k^2t}{2m\hbar}-2n_rk\frac{\mathbf{d}\times\mathbf{B}}{m}t\right)}|0n_r\hbar k\rangle \\
&- \left.J_1^2\left(\frac{\Omega_R^2\tau}{2\Delta}\right)e^{i\left(-2n_rkx-\frac{4\hbar^2n_r^2k^2t}{2m\hbar}+2n_rk\frac{\mathbf{d}\times\mathbf{B}}{m}t\right)}|0n_r\hbar k\rangle\right].
\end{aligned} \quad (3.75)$$

The probability p_0 of finding the atoms in the ground state $|0n_r\hbar k\rangle$ is

$$\begin{aligned} p_0 &= |\langle\psi(t+2\tau)|0n_r\hbar k\rangle|^2 = J_0^4\left(\frac{\Omega_R^2\tau}{2\Delta}\right) \\ &- 4J_0^2\left(\frac{\Omega_R^2\tau}{2\Delta}\right)J_1^2\left(\frac{\Omega_R^2\tau}{2\Delta}\right)\cos\left(\frac{4\hbar^2 n_r^2 k^2 t}{2m\hbar}\right) \\ &\times \cos\left(2n_r kx - 2\frac{\mathbf{d}\times\mathbf{B}}{m}n_r kt\right) \\ &+ 4J_1^4\left(\frac{\Omega_R^2\tau}{2\Delta}\right)\cos^2\left(2n_r kx - 2\frac{\mathbf{d}\times\mathbf{B}}{m}n_r kt\right). \end{aligned} \tag{3.76}$$

The third term can be dropped as $J_0^2 J_1^2 \gg J_1^4$ for short times. Thus far we have neglected the impact that the Doppler shifted Stark term would have on our ability to see the HMW phase. Without the Doppler shift, the Stark energy $\frac{1}{2}\alpha E^2$ does not affect the probability since it contributes equally to all momentum states. The Doppler shift presents itself through the detuning

$$\Delta_\pm \approx \Delta\left(1 \pm \frac{\omega_{\mathrm{L}}}{\Delta}\frac{\mathrm{v}}{\mathrm{c}}\right). \tag{3.77}$$

The Doppler shifted Stark term is therefore

$$\frac{1}{2}\alpha\left(1 \mp \frac{\omega_{\mathrm{L}}}{\Delta}\frac{\mathrm{v}}{\mathrm{c}}\right)\mathrm{E}^2, \tag{3.78}$$

for blue(-) and red(+) detuning respectively. If we include this term, the

probability amplitude becomes

$$\begin{aligned} p_0 &= |\langle\psi(t+2\tau)|0n_r\hbar k\rangle|^2 = J_0^4 \\ &-4J_0^2J_1^2\cos\left(\frac{4\hbar^2n_r^2k^2t}{2m\hbar}\right)\cos\left(2n_rkx-2\frac{\mathbf{d}\times\mathbf{B}}{m}n_rkt+\frac{1}{2}\alpha E^2\frac{\omega_L}{\hbar\Delta}\frac{v}{c}t\right) \\ &+4J_1^4\cos^2\left(2n_rkx-2\frac{\mathbf{d}\times\mathbf{B}}{m}n_rkt+\frac{1}{2}\alpha E^2\frac{\omega_L}{\hbar\Delta}\frac{v}{c}t\right) \\ &= J_0^4-4J_0^2J_1^2\cos\left(\frac{4\hbar^2n_r^2k^2t}{2m\hbar}\right)\cos\left(2n_rkx-2\alpha E^2\frac{n_rkt}{mc}\left(1-\frac{\omega_L}{2\Delta}\right)\right). \end{aligned} \tag{3.79}$$

In the last line we have dropped the J_1^4 term as it is much smaller than the others. In Eq. (3.79) we see that the Doppler term depends on the detuning of the laser Δ in the polarizability α (which is proportional to $1/\Delta$), the laser frequency ω_L, and the detuning itself Δ. Therefore, by switching between red and blue detuned lasers the Doppler term will simply change in magnitude through the frequency as the other two terms will cancel the sign change out. The HMW term on the other hand, will not change magnitude (as it doesn't contain a frequency term), but it will change signs with the detuning. Thus, one can distinguish the two effects by performing the experiment twice. Once using a blue, and once using a red detuned traveling wave laser.

The HMW phase is incredibly small and requires a large laser intensity to become visible. The HMW frequency is $2\frac{\mathbf{d}\times\mathbf{B}}{m}n_rk$. If we use $\alpha = 4\times10^{-36}\,\mathrm{F\cdot m^2}$ as we did in the previous section (corresponding to a detuning of $\Delta/2\pi = 150$ GHz), then we require a laser intensity of $\mathrm{I} = 6\times10^6\,\mathrm{W/cm^2}$ to obtain a phase shift of 1 radian during the $\tau = 1$ ms propagation.

Spontaneous emission is a major concern as it affects the visibility of the

interference fringes required to observe the HMW effect. If the separation distance d between the out-coupled sample of atoms in the state $|2\hbar n_r k\rangle$ and the ground atoms $|0\hbar n_r k\rangle$ is larger than the wavelength of the probe laser interacting with the sample, then any spontaneous emission would destroy the coherence of the experiment. This follows from the fact that under such circumstances, a spontaneous event would allow an observer to positively identify the sample from which the photon was emitted. This would then break the superposition state of the two samples, thus eliminating the ability to interfere the two states. This, however, is not the case here. Let us take the dimensions of the condensate to be 300 μm $\times$ 20 μm [79]. The recoil velocity of lithium is approximately $\mathbf{v}_{\text{rec}} = 9$ cm/s. Therefore, during the 1 ms that the two samples are separating, the total separation distance is $d = 1.8 \times 10^{-4}$ m. Therefore the majority of the condensate overlaps throughout the process. Pritchard's group [75] has measured the effects of spontaneous emission on decoherence and found that for such small separation distances the fringe contrast will not be overly diminished.

In free space, such an intensity output would be difficult to achieve, but by placing the atom in a ring cavity (Figure 3.5) we can enhance the intensity by a factor of $2\mathcal{F}/\pi$ [27], where $\mathcal{F}$ is the finesse of the cavity system. The cavity finesse required will of course depend on the intensity of the pump laser. A caveat of placing the atom in a cavity system is that a back action of the atom on the intra-cavity field can alter the light field. An example of this is collective atom recoil lasing (CARL) where the atoms collectively scatter light from one travelling mode to the other resulting in a accelerating force on the atoms. Such an effect would obviously be undesirable as it would add an extra layer of complication to disentangling the HMW phase from other effects. For

a single atom massively detuned from the cavity mode, even for such high intensities such as those required to see the HMW phase, the CARL threshold is not reached [80, 81] and the back action effects may safely be ignored.

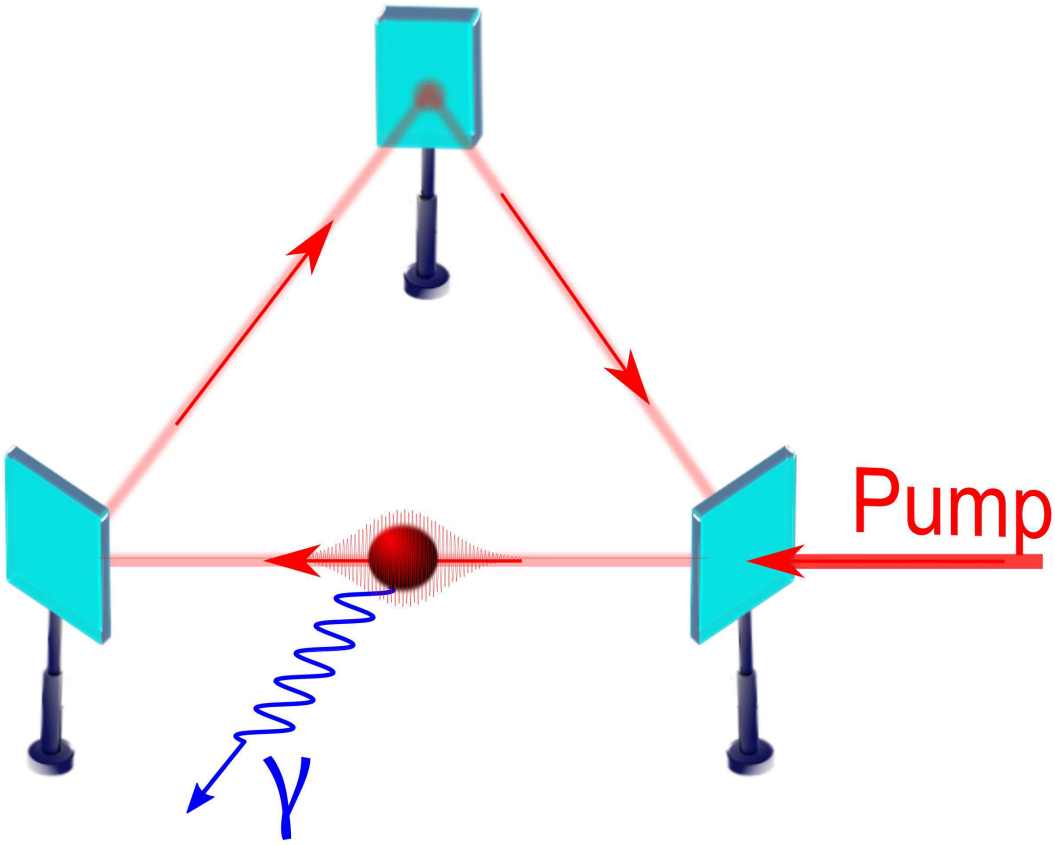

Figure 3.5: A schematic for the high finesse ring cavity setup used to enhance the intensity of the traveling wave. The cavity mode must be massively detuned from the atomic transition in order to suppress spontaneous emission γ.

Using a Kaptiza-Dirac pulse of wavelength $\lambda = 671\,\mathrm{nm}$ the value of the recoil term is $n_r\hbar kx = 3.4 \times 10^3$, while $\frac{4\hbar^2 n_r^2 k^2 t}{2m\hbar}$ is approximately twice the size of the recoil term. The Abraham term which is responsible for the HMW phase is $2\frac{\mathbf{d}\times\mathbf{B}}{m} n_r k\,\mathrm{t} = 9.5\,\mathrm{t/s}$.

In figure 3.6 we plot the probability of finding the atom in the ground state Eq. (3.76) as a function of propagation time, with and without the HMW phase using these values. The red line shows the probability to find the atoms in the ground state without the HMW phase, while the solid blue lines include the HMW phase. In figure 3.7 we plot the Fourier transform using a propagation time of τ =1 ms, sampled at a frequency of 1μs. Although the magnitude of the fourier peaks between the two predictions is apparent, it is difficult to discern the frequency shift.

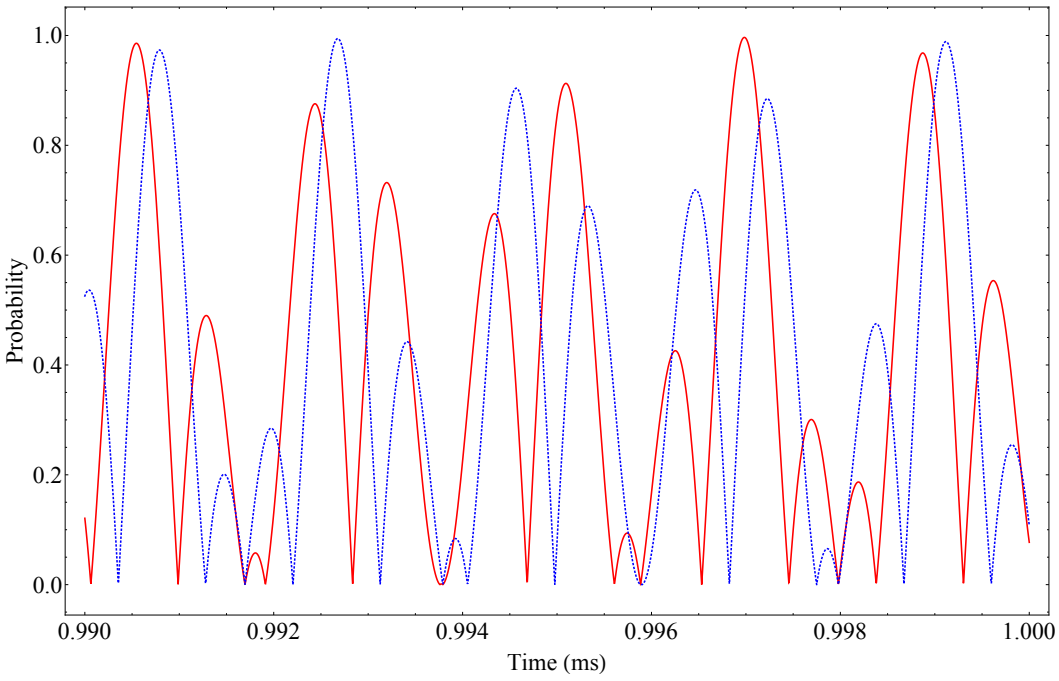

Figure 3.6: A plot of the probability of finding the atoms in the ground state $p_0 = |\langle\psi(t+2\tau)|0n\hbar k\rangle|^2$. The red line show the probability of finding the atoms in the ground state without the HMW phase, while the blue line includes the HMW phase. The intensity of the laser is $I_1 = 6\times10^6\,\mathrm{W/cm^2}$ detuned to $\Delta = 150/2\pi$ GHz. The total propagation time is τ =1 ms.

A possible enhancing technique which may also be implemented to increase the size of the Röntgen term is to consider large momentum transfer beam-splitters (LMT). Thus far we have only considered 2-photon recoil momentum

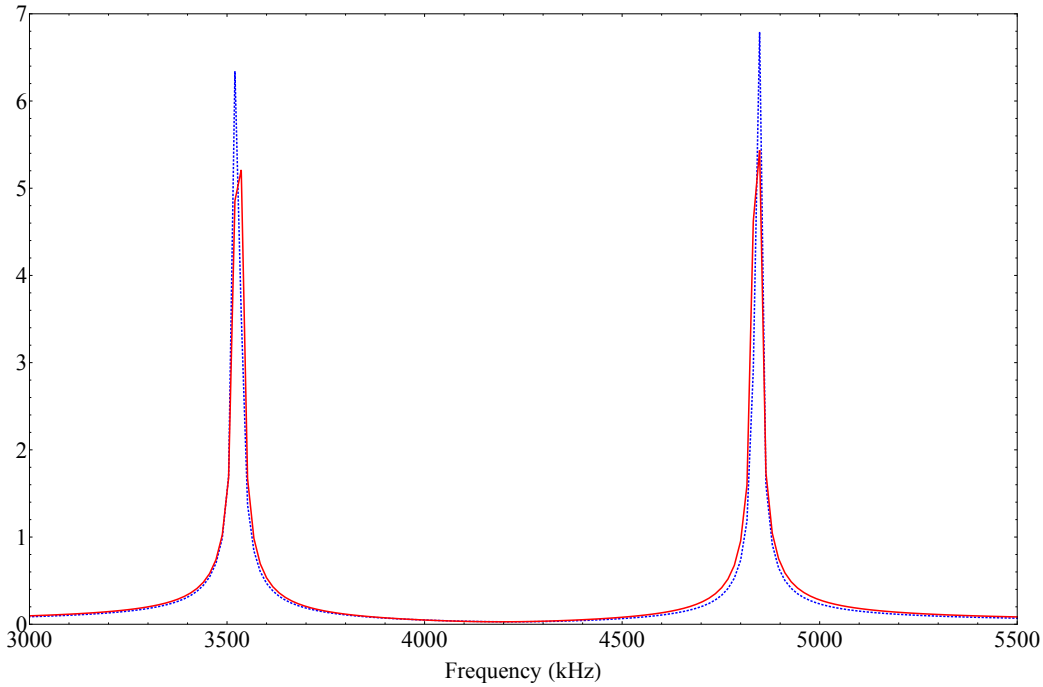

Figure 3.7: The time-discrete Fourier transform of Eq. (3.76) using τ =1 ms of total propagation time. The dotted blue line shows the Fourier transform without the HMW phase, while the red line includes the HMW phase. The effect of the HMW phase on the Fourier transform is most apparent in the magnitude change, while the frequency shift is difficult to see.

kicks. However, it is possible to use large momentum transfers on the order of $10n_r\hbar k - 100n_r\hbar k$ [82]. Using such an LMT, we could significantly increase the effects of the HMW phase. This however also works against us by increasing the separation distance between samples, and hence decreasing the fringe visibility. A better option is to simply increase the intensity slightly at the cost of a modest decrease in visibility due to spontaneous emission. In Figures 3.8 and 3.9 we plot Eq. (3.76) and the time-discrete Fourier transform using an intensity of $I_2 = 6 \times 10^7\,\mathrm{W/cm^2}$.

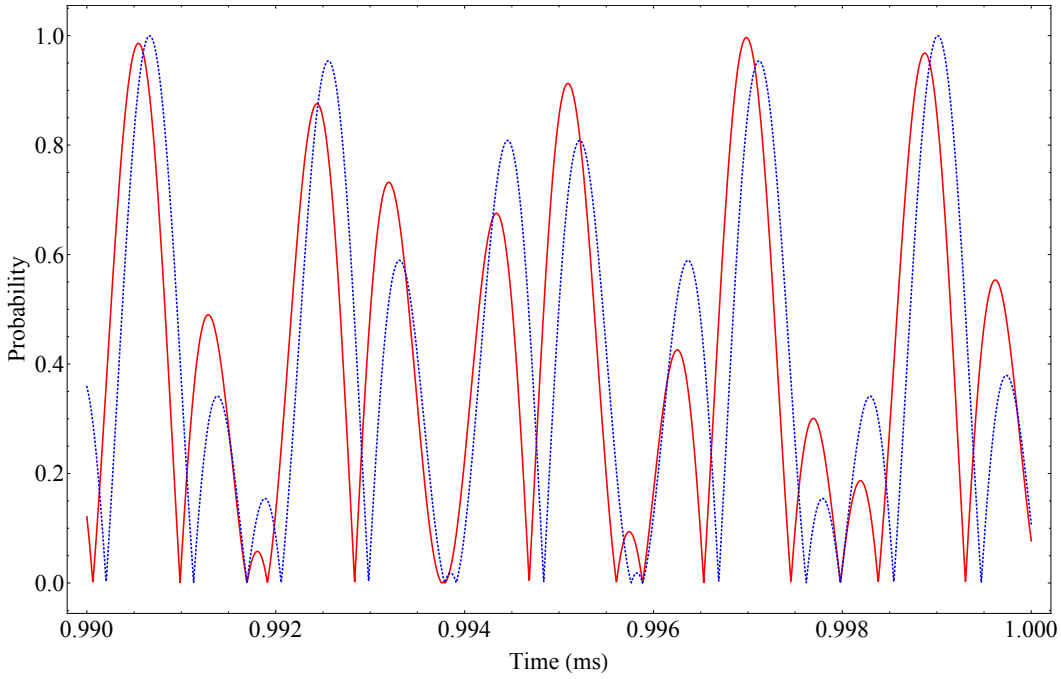

Figure 3.8: A plot of the probability of finding the atoms in the ground state $\mathrm{p_0} = |\,\langle\psi(\mathrm{x,t}+2\tau)|0\mathrm{n}\hbar\mathrm{k}\rangle\,|^2$ vs. propagation time. The red line show the probability of finding the atoms in the ground state without the HMW phase, while the blue line include the HMW phase. Here the difference between the two is more apparent. The intensity of the laser is set to $I_2 = 6 \times 10^7\,\mathrm{W/cm^2}$.

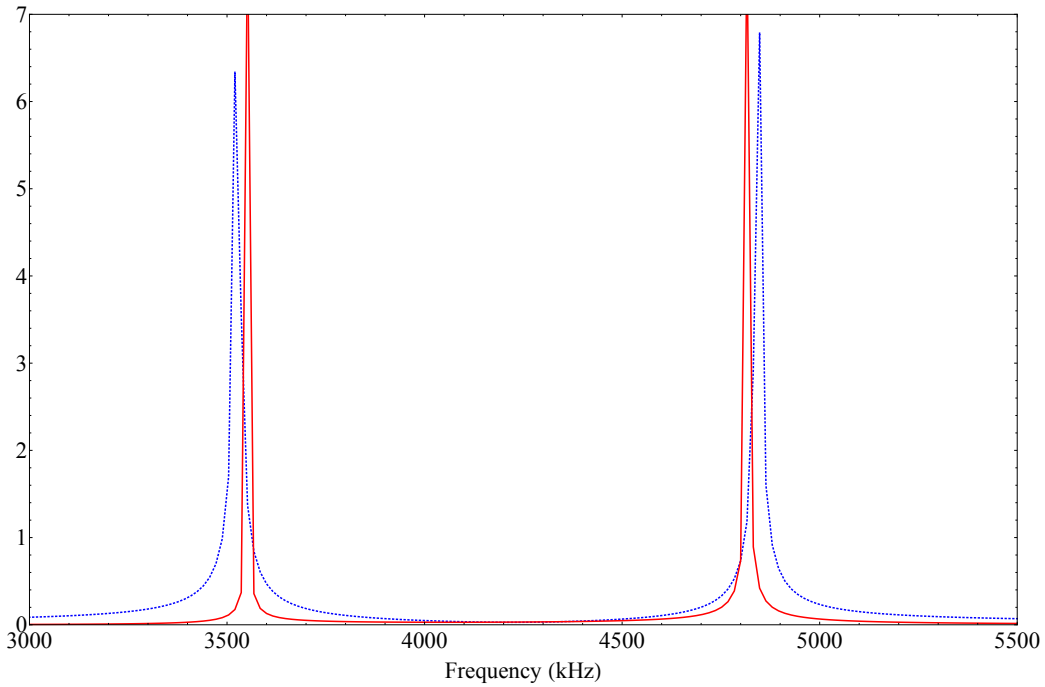

Figure 3.9: The time-discrete Fourier transform of Eq. (3.76) using an increased intensity $I_2 = 9.7 \times 10^7\,\mathrm{W/cm^2}$. The separation between the peaks is more obvious here.

3.5 Laguerre Beam Interferometer

Laguerre-Gaussian (LG) laser beams provide yet another avenue to observing the HMW phase. LG beams have a Poynting vector which swirls around the direction of propagation, giving it an orbital angular momentum. This forms a little circuit for an HMW interferometer to act as long as the atoms can be guided around the circuit. The setup we consider in this section is a trapped BEC in a time-orbiting magnetic ring trap as outlined in [83, 84]. The BEC is irradiated with a single LG beam. Note that this is different from typical setups [85] in which the Laguerre-Gauss beam is accompanied by a counter-propagating ordinary Gaussian-profile beam. In that case, the interference of the two beams creates a standing wave profile, producing a dipole force on the BEC which is responsible for the transfer of angular momentum. On the contrary, what we wish to show is that the HMW phase and the Abraham force can be observed from a setup in which only a single LG beam is present. This section is slightly different from the other two as here we wish to observe the Lorentz force in action. As was mentioned in Chapter 2, there are two components to the optical Lorentz force: the well known optical dipole force, and the illusive Abraham force. We investigate a simple arrangement in which the presense of the Abraham force can be easily detected. Consider an LG mode $L^l_{m=0}$, linearly polarized in the transverse x-direction as shown in figure 3.10. The magnitude of the Laguerre-Gauss mode u^l_0 at $z = 0$ can be written in cylindrical coordinates as [86]

$$u^l_0(r,\phi) = A_0\sqrt{\frac{2}{\pi w_0^2}}\sqrt{\frac{1}{l!}}\exp\left(\frac{-2r^2}{w_0^2}\right)\left(\frac{\sqrt{2}r}{w_0}\right)^l \exp\left(il\phi\right), \tag{3.80}$$

where A_0 is the amplitude, and w_0 is the beam waist. The vector potential

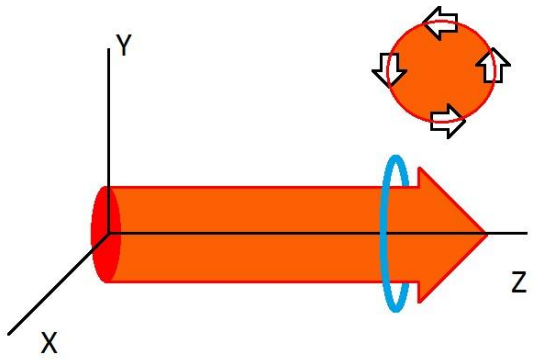

Figure 3.10: A Laguerre-Gauss beam with linear polarization acts on an atomic circuit trap. In upper right frame we show a cross-section of the beam which has an azimuthal component giving the Poynting vector a non-zero circulation. The blue ring here represents the ring trap.

$\mathbf{A}(\mathbf{r}, \boldsymbol{\phi}, \mathbf{z})$ associated with such a mode can be written as

$$\mathbf{A}(r, \phi, z) = u_0^l(r, \phi) \exp i(kz - \omega t)\hat{\mathbf{x}}. \tag{3.81}$$

The electric and magnetic fields may then be obtained in the Lorentz gauge ($\nabla \cdot \mathbf{A} + \frac{1}{c^2}\frac{\partial V}{\partial t} = 0$, where V is the scalar potential) via

$$\begin{aligned} \mathbf{E}(r, \phi, z) &= -\nabla V - \frac{\partial \mathbf{A}}{\partial t} = i\omega \left(\mathbf{A}(r, \phi, z) + \frac{\nabla \left(\nabla \cdot \mathbf{A}(r, \phi, z) \right)}{k^2} \right) \\ \mathbf{B}(r, \phi, z) &= \nabla \times \mathbf{A}(r, \phi, z). \end{aligned} \tag{3.82}$$

We apply the paraxial approximation to Eq. (3.82) (i.e dropping all second order derivatives) and obtain

$$\begin{aligned}\mathbf{E}(r,\phi,z) &= i\omega u((r,\phi))\exp i(kz-\omega t)\hat{\mathbf{x}} - c\frac{\partial u(r,\phi)}{\partial x}\exp i(kz-\omega t)\hat{\mathbf{z}}\\ \mathbf{B}(r,\phi,z) &= iku(r,\phi)\exp i(kz-\omega t)\hat{\mathbf{y}} - \frac{\partial u(r,\phi)}{\partial x}\exp i(kz-\omega t)\hat{\mathbf{z}}.\end{aligned} \tag{3.83}$$

We are interested in calculating the HMW phase. We begin by finding the real component of $\mathbf{E}\times\mathbf{B}$ using Eq. (3.83)

$$\mathbf{E}\times\mathbf{B}^* = \left(i\omega u(r,\phi)\frac{\partial u^*(r,\phi)}{\partial x}\right)\hat{\mathbf{x}} + \left(i\omega u^*(r,\phi)\frac{\partial u(r,\phi)}{\partial y}\right)\hat{\mathbf{y}} + \left(\omega k\left|u(r,\phi)\right|^2\right)\hat{\mathbf{z}}. \tag{3.84}$$

Eqn. (3.84) can be rewritten in cylindrical coordinates as

$$\mathbf{E}\times\mathbf{B}^* = i\omega u(r,\phi)\left(\frac{\partial}{\partial r}\hat{\mathbf{r}} + \frac{1}{r}\frac{\partial}{\partial\phi}\hat{\boldsymbol{\phi}}\right)u^*(r,\phi) + \left(\omega k\left|u(r,\phi)\right|^2\right)\hat{\mathbf{z}}. \tag{3.85}$$

From Eq. (3.84) and Eq. (3.80) we can calculate the azimuthal component of $\mathbf{E}\times\mathbf{B}^*$.

$$\left(\mathbf{E}\times\mathbf{B}^*\right)_\phi = -\frac{A_0^2\,\omega\phi\,2^{l+1}}{\pi\,w_0^{2l+2}\,(l-1)!}r^{2l-1}\exp\left(\frac{-4r^2}{w_0^2}\right). \tag{3.86}$$

This term is the only component responsible for rotating the BEC around the toroidal trap. However, since we also wish to write the LG mode in terms of the output power of the laser P, we also want the z-component of $\mathbf{E}\times\mathbf{B}^*$ in order to find the intensity of the laser. We are using the fact that the z-component is the dominant term, and hence we can approximate the total

intensity by only considering the z-component.

$$(\mathbf{E}\times\mathbf{B}^*)_z = \frac{\omega k A_0^2\, 2^{l+1}}{\pi w_0^{2l+2}\, l!}\, r^{2l} \exp\left(\frac{-4r^2}{w_0^2}\right). \tag{3.87}$$

The intensity is then given by $I \approx \frac{1}{2}\epsilon_0 c^2 (\mathbf{E}\times\mathbf{B})_z$. Plugging in Eqn. (3.87) and integrating over the area gives the power P

$$P = \int_0^{2\pi}\int_0^{\infty} \left(\frac{1}{2}\epsilon_0 c^2 \mathbf{E}\times\mathbf{B}^*\right)_z r\, dr\, d\phi = \frac{\omega k A_0^2\, 2^{-l-1}\,\Gamma[1+l]}{l!}, \tag{3.88}$$

where Γ is the gamma function. Solving for the amplitude A_0 we obtain

$$A_0 = \left(\frac{2l!\, P}{\epsilon_0 c^2 \omega k\, 2^{-l-1}\,\Gamma[1+l]}\right)^{\frac{1}{2}} \tag{3.89}$$

Although in this section we are interested in the Abraham force, it is worth digressing to consider the phase shift induced by the HMW effect. The term in the action responsible for giving rise to the HMW phase has been shown to be due to the Röntgen interaction

$$S_{\text{HMW}} = \int \alpha \mathbf{v}\cdot(\mathbf{B}\times\mathbf{E})\, dt = -\int \alpha\,(\mathbf{E}\times\mathbf{B})\cdot d\mathbf{l} \tag{3.90}$$

Plugging in Eq. (3.88) into Eq. (3.86) and integrating around a circuit of radius R:

$$S_{\text{HMW}} = -\frac{\alpha A_0^2\,\omega 2^{l+2}}{w_0^{2l+2}\,(l-1)!}\, R^{2l-1} \exp\left(\frac{-4R^2}{w_0^2}\right). \tag{3.91}$$

The maximum HMW phase occurs at a radius of

$$R = \frac{\omega}{2}\left(l-\frac{1}{2}\right)^{\frac{1}{2}}. \tag{3.92}$$

Therefore we would ideally want our trap to confine the atoms to a circuit of this radius. Then assuming a power of 1 Watt, an angular state of $l = 1$, and a beam waist of $w_0 = 100\,\mu$m, we find the induced HMW phase acquired by traveling one lap around the ring trap is $\phi_{\text{HMW}} \approx 1$ rad. Recently Willke's [86] group was able to generate high order (u_3^3) Laguerre-Gauss beams with high laser power (83 Watts) which could further push the induced HMW phase higher if desired.

The experimental setup we now consider for observing the optical Abraham force is shown in 3.11. A BEC of ^{7}Li atoms is initially confined in a ring trap. A Laguerre-Gauss beam is then switched on. Without the Abraham term, the only component of the Lorentz force responsible for acting on the BEC would be the optical dipole force $\mathbf{F}_1 = \alpha\frac{1}{2}\nabla E^2$. During the time that the LG beam is being switched on, the electric field amplitude has a time dependence that can be described as $E_\phi(z,t) = \mathcal{E}(\omega t - kz)cos(\omega t - kz)$. Therefore, the force experienced by the BEC during the switch on is given by

$$\bar{\mathbf{F}} = \frac{1}{2}\alpha k\mathcal{E}(\omega t - kz)\mathcal{E}'(\omega t - kz)\hat{\boldsymbol{\phi}}. \tag{3.93}$$

This optical dipole force would have the effect of rotating the BEC in a clockwise direction (for a red detuned LG beam). On the other hand, if the Abraham force is present, the total time averaged azimuthal force on the BEC would be

$$\bar{\mathbf{F}} = \frac{1}{2}\alpha\left[k\mathcal{E}(\omega t - kz)\mathcal{E}'(\omega t - kz) - \frac{2\omega}{c}\mathcal{E}(\omega t - kz)\mathcal{E}'(\omega t - kz)\right]\hat{\boldsymbol{\phi}}, \tag{3.94}$$

which yields an aziumthal force in the opposite direction! Thus we can corroborate the existence of the Abraham force by observing the rotational direction of the BEC.

3.6 Summary and Conclusions

In this section we explored three different arrangements: the Mach-Zehnder, Kapitza-Dirac, and Laguerre-Gauss interferometers. The Mach-Zehnder interferometer is the strongest potential candidate due to its simple geometry, and obtainable parameters. The most difficult task is aligning the red and blue detuned beams precisely enough to ensure that an equal Stark shift is observed in both arrangements. The Kapitza-Dirac interferometer suffers from spontaneous emission due to the high intensity laser required to resolve the HMW shift. It does, however, have the advantage of not having to deal with classical forces, unlike the other two setups which must go through pains to cancel out the effects due to the dipole and Abraham force. In the Laguerre-Gauss arrangement, we actually desire to see the classical Lorentz force to act on the BEC. In this setup we were interested in observing the flow direction of the BEC as an LG beam was switched on. Without the Abraham force, we expect the BEC to be rotated clockwise, while with it, we expect counterclockwise rotation. We showed that the HMW phase and the Abraham force are intimately tied together through the Lagrangian term (the Röntgen interaction) $\mathbf{v} \cdot (\mathbf{d} \times \mathbf{B})$. As we shall show in the next chapter, this term is responsible for both the geometric (HMW) and dynamic (Abraham) effects observed in these three experiments.

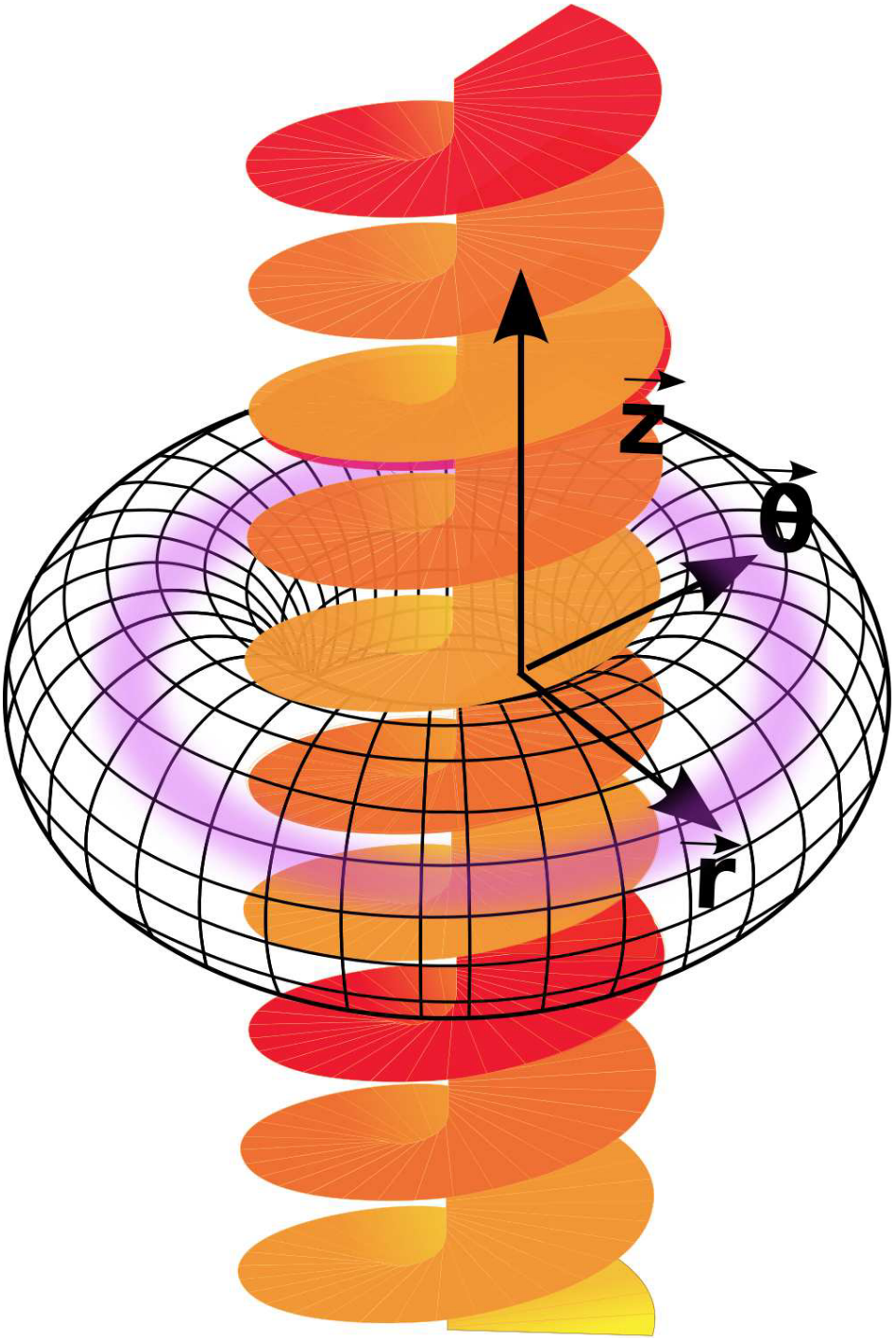

Figure 3.11: An interferometer setup utilizing a Laguerre-Gauss beam with linear polarization. Atoms are trapped in a time-orbiting magnetic ring trap while they interact with a time-varying LG beam. These atoms experience an azimuthal force which will drive rotation around the trap. The direction of rotation will prove or disprove the existence of the Abraham force.

Chapter 4

Quantum Representations

4.1 Introduction

In this section, we show that while both forms of the electromagnetic momentum density are correct, they correspond to different representations of the Hamiltonian. In fact, they are linked to two different representations of the direct coupling Hamiltonian which we show to be tied intimately with the Aharonov-Casher and the He-McKellar-Wilkens phases. The two geometric phases are shown to be related through a unitary transformation. In addition, we show that the HMW and AC phases can be viewed as being either geometric or dynamic in nature. In other words, depending on the representation used, the HMW phase can be viewed as a geometric phase arising from the canonical momentum of the Hamiltonian, or as a dynamic phase arising from the Abraham force. This section is inspired by Loudon et al [41] in which they first connected the canonical/kinetic atomic momentum with the Minkowski/Abraham momentum.

4.2 The Abraham/Minkowski representation

We begin with the Lagrangian for a dielectric composed of polarizable/magnetizable atoms interacting with an electromagnetic field.

$$L = \sum_i \frac{1}{2} m_i \dot{x}_i^2 + \frac{1}{2} \int \left(\epsilon \dot{A}^2 - \frac{1}{\mu} \left(\nabla \times \mathbf{A} \right)^2 \right) d^3\mathbf{r}, \tag{4.1}$$

where $\mathbf{A}$ is the vector potential, μ is the permeability, and ϵ is the permittivity. The sum is over individual atoms. The canonical momentum of the atoms $\mathbf{p}$ and the field $\mathbf{\Pi}$ is given by

$$\mathbf{p} = \frac{\partial L}{\partial \dot{\mathbf{x}}} = \sum_i m_i \dot{\mathbf{x}}_i, \tag{4.2}$$

$$\mathbf{\Pi} = \frac{\partial L}{\partial \dot{\mathbf{A}}} = \epsilon \dot{\mathbf{A}}. \tag{4.3}$$

Therefore, the corresponding Hamiltonian is given by

$$H = \frac{\partial L}{\partial \dot{\mathbf{x}}} \dot{\mathbf{x}} + \frac{\partial L}{\partial \dot{\mathbf{A}}} \dot{\mathbf{A}} - L = \sum_i \frac{p_i^2}{2m_i} + \frac{1}{2} \int \left(\frac{\Pi^2}{\epsilon} + \frac{1}{\mu} \left(\nabla \times \mathbf{A} \right)^2 \right) d^3\mathbf{r}. \tag{4.4}$$

Using the definitions for the electric and magnetic fields in the Coulomb gauge

$$\mathbf{E} = -\frac{\partial \mathbf{A}}{\partial t}, \tag{4.5}$$

$$\mathbf{B} = \nabla \times \mathbf{A}, \tag{4.6}$$

along with the linear auxiliary field definitions

$$\mathbf{D} = \epsilon\mathbf{E} = \epsilon_0\mathbf{E} + \mathbf{P} = \epsilon_0\mathbf{E} + \sum_i \mathbf{d}\delta(\mathbf{r} - \mathbf{r}_i), \tag{4.7}$$

$$\mathbf{H} = \frac{\mathbf{B}}{\mu} = \frac{1}{\mu_0}\mathbf{B} - \mathbf{M} = \frac{\mathbf{B}}{\mu_0} - \sum_i \mathbf{m}\delta(\mathbf{r} - \mathbf{r}_i), \tag{4.8}$$

we arrive at the correct form for the energy of the system

$$H = \sum_i \frac{1}{2} m_i \dot{x}_i^2 + \frac{1}{2}\int (\mathbf{D}\cdot\mathbf{E} + \mathbf{H}\cdot\mathbf{B})\, d^3\mathbf{r}. \tag{4.9}$$

Here $\mathbf{P}$ is the polarization, $\mathbf{d}$ is the dipole moment, $\mathbf{M}$ is the magnetization, and $\mathbf{m}$ is the magnetic moment. Note that $\frac{1}{2}\int (\mathbf{D}\cdot\mathbf{E} + \mathbf{H}\cdot\mathbf{B})\, d^3\mathbf{r}$ is a function of position due to electric/magnetic moments contained in $\mathbf{D}/\mathbf{H}$. However, Eq. (4.1) is not the whole story. In the reference frame the atoms, the Lorentz transformed fields are $\bar{\mathbf{E}} = \mathbf{E} + \mathbf{v}\times\mathbf{B}$ and $\bar{\mathbf{B}} = \mathbf{B} - \epsilon_0\mu_0\,(\mathbf{v}\times\mathbf{E})$ (to first order in v/c). Hence, the Lagrangian for moving atoms is found by substituting in $\bar{\mathbf{E}}$ and $\bar{\mathbf{B}}$ for the lab frame electric and magnetic fields $\mathbf{E}$ and $\mathbf{B}$ in Eq. (4.1).

$$\begin{aligned}
L &= \sum_i \frac{1}{2} m_i \dot{x}_i^2 + \sum_i \frac{1}{2}\int \epsilon \left(-\dot{\mathbf{A}} + \dot{\mathbf{x}}_i \times (\nabla\times\mathbf{A})\right)^2 d^3\mathbf{r} \\
&- \sum_i \frac{1}{2}\int \frac{1}{\mu}\left(\nabla\times\mathbf{A} + \frac{1}{c^2}(\dot{\mathbf{x}}_i\times\dot{\mathbf{A}})\right)^2 d^3\mathbf{r} \\
&= \sum_i \frac{1}{2} m_i v_i^2 + \frac{1}{2}\int (\mathbf{D}\cdot\mathbf{E} - \mathbf{H}\cdot\mathbf{B})\, d^3\mathbf{r} \\
&- \sum_i \int \mathbf{v}_i\cdot(\mathbf{D}\times\mathbf{B})\, d^3\mathbf{r} + \sum_i \int \mathbf{v}_i\cdot\frac{\mathbf{E}\times\mathbf{H}}{c^2}\, d^3\mathbf{r} + \text{H.O.}
\end{aligned} \tag{4.10}$$

The canonical momentum for the atoms and field is then given by

$$\begin{aligned}
\mathbf{p}_i &= m\mathbf{v}_i - \int \left(\mathbf{D}_i \times \mathbf{B} - \frac{\mathbf{E} \times \mathbf{H}_i}{c^2} \right) d^3\mathbf{r} \\
&\equiv m\mathbf{v}_i - \mathbf{d}_i \times \mathbf{B}_i - \frac{\mathbf{E}_i \times \mathbf{m}_i}{c^2}, \qquad (4.11) \\
\mathbf{\Pi} &\approx \frac{\partial L}{\partial \dot{\mathbf{A}}} = \epsilon \dot{\mathbf{A}}. \qquad (4.12)
\end{aligned}$$

We have dropped higher order terms in the canonical field momentum $\mathbf{\Pi}$. The subscript i associated with the fields indicate that the field is evaluated at the position of atom i. The corresponding Hamiltonian is then found to be

$$\begin{aligned}
H &= \sum_i \frac{1}{2m_i} \left(\mathbf{p}_i + \mathbf{d}_i \times \mathbf{B}_i + \frac{\mathbf{E}_i \times \mathbf{m}_i}{c^2} \right)^2 \\
&+ \frac{1}{2} \int \left(\mathbf{D} \cdot \mathbf{E} + \mathbf{H} \cdot \mathbf{B} \right) d^3\mathbf{r}. \qquad (4.13)
\end{aligned}$$

The Schrödinger equation for the Hamiltonian is therefore given by

$$\begin{aligned}
i\hbar\dot{\psi}(\mathbf{r},t) &= \sum_i \frac{1}{2m_i} \left(\mathbf{p}_i + \mathbf{d}_i \times \mathbf{B}_i + \frac{\mathbf{E}_i \times \mathbf{m}_i}{c^2} \right)^2 \psi(\mathbf{r},t) \\
&+ \left(\frac{1}{2} \int \left(\mathbf{D} \cdot \mathbf{E} + \mathbf{H} \cdot \mathbf{B} \right) d^3\mathbf{r} \right) \psi(\mathbf{r},t). \qquad (4.14)
\end{aligned}$$

The last term in Eq. (4.14) may be rewritten by making use of Poynting's theorem [70] :

$$\mathbf{E} \cdot \mathbf{J}_\mathrm{f} = -\frac{1}{2} \frac{\partial}{\partial t} \left(\mathbf{D} \cdot \mathbf{E} + \mathbf{B} \cdot \mathbf{H} \right) - \nabla \cdot \left(\mathbf{E} \times \mathbf{H} \right). \qquad (4.15)$$

Since there are no free currents, $\mathbf{J}_{\mathrm{f}} = 0$. This allows us to write

$$\frac{1}{2}\left(\mathbf{D}\cdot\mathbf{E}+\mathbf{B}\cdot\mathbf{H}\right) = -\int_{-\infty}^{t} \nabla\cdot\left(\mathbf{E}\times\mathbf{H}\right)\, dt'. \tag{4.16}$$

Consider a plane wave pulse of the form

$$\mathbf{E}(x,t) = \mathcal{E}(kx-\omega t)\cos\left(kx-\omega t\right). \tag{4.17}$$

For such a field, we can rewrite the second term in Eq. (4.16) using a change in variables:

$$\frac{\partial}{\partial x} \rightarrow -\frac{1}{c}\frac{\partial}{\partial t}. \tag{4.18}$$

Thus for a field of the form given by Eq. (4.17), Poynting's theorem allows us to write

$$\frac{1}{2}\left(\mathbf{D}\cdot\mathbf{E}+\mathbf{B}\cdot\mathbf{H}\right) = c\frac{\partial}{\partial t}\int_{-\infty}^{t}\left(\frac{\mathbf{E}\times\mathbf{H}}{c^2}\right)\, dt' = c\frac{\mathbf{E}\times\mathbf{H}}{c^2}. \tag{4.19}$$

Substituting this into Eq. (4.14) gives

$$i\hbar\dot{\psi}(\mathbf{r},t) = \sum_i \frac{1}{2m_i}\left(\mathbf{p}_i+\mathbf{d}_i\times\mathbf{B}_i+\frac{\mathbf{E}_i\times\mathbf{m}_i}{c^2}\right)^2\psi(\mathbf{r},t)+c\mathbf{S}_{\mathrm{Abr}}\psi(\mathbf{r},t). \tag{4.20}$$

The second term on right is the energy due to the Abraham momentum

$$\mathbf{S}_{\mathrm{Abr}}(\mathbf{r},t) = \int\frac{\mathbf{E}\times\mathbf{H}}{c^2}\, d^3\mathbf{r}. \tag{4.21}$$

Eq. (4.20) is what we will call the Abraham representation. The first term on the right is of course the kinetic momentum of the atom. Note that both the AC and the HMW effect arise in this representation as dynamic phases

through the kinetic momentum [87]

$$m\mathbf{v} = m\frac{\partial H}{\partial \mathbf{p}} = \mathbf{p} + \mathbf{d}\times\mathbf{B} + \frac{\mathbf{E}\times\mathbf{m}}{c^2}. \tag{4.22}$$

The dynamic phase due to the kinetic energy is then given by

$$\theta_{\rm dyn} = -\frac{1}{\hbar}\int_{-\infty}^{t}\frac{1}{2}m\mathbf{v}\cdot\mathbf{v}\,dt' = -\frac{1}{2\hbar}\int_{-\infty}^{\mathbf{r}} m\mathbf{v}\cdot d\mathbf{r}' = -\frac{1}{2\hbar}\int_{-\infty}^{\mathbf{r}}\left(\mathbf{p}+\mathbf{d}\times\mathbf{B}+\frac{\mathbf{E}\times\mathbf{m}}{c^2}\right)\cdot d\mathbf{r}'. \tag{4.23}$$

The Abraham representation is in no way unique however. We can transform the Schödinger equation into the Minkowski representation through a unitary transformation by writing the wave function as

$$\psi(\mathbf{r},\mathrm{t}) = \Psi(\mathbf{r},\mathrm{t})\exp\left[-\frac{\mathrm{i}}{\hbar}\int_{-\infty}^{\mathbf{r}}\mathbf{S}(\mathbf{r}',\mathrm{t})\cdot\mathrm{d}\mathbf{r}'\right], \tag{4.24}$$

where $\mathbf{S}(\mathbf{r},t)\equiv\sum_i(\mathbf{d}_i\times\mathbf{B}_i+\epsilon_0\mu_0\mathbf{E}_i\times\mathbf{m}_i)$. Substituting this back into Eq. (4.20) gives us (See appendix A.1)

$$\begin{aligned}
& i\hbar\dot{\Psi}(\mathbf{r},t)\ \exp\left[-\frac{i}{\hbar}\int\mathbf{S}(\mathbf{r}',t)\cdot d\mathbf{r}'\right] \\
+\ & \Psi(\mathbf{r},t)\left(\frac{\partial}{\partial t}\int\mathbf{S}(\mathbf{r}',t)\cdot d\mathbf{r}'\right)\exp\left[-\frac{i}{\hbar}\int\mathbf{S}(\mathbf{r}',t)\cdot d\mathbf{r}'\right] \\
=\ & -\sum_i\frac{\hbar^2\left(\nabla_i^2\Psi(\mathbf{r},t)\right)}{2m_i}\exp\left[-\frac{\mathrm{i}}{\hbar}\int\mathbf{S}(\mathbf{r}',t)\cdot d\mathbf{r}'\right] \\
+\ & c\mathbf{S}_{\rm Abr}(\mathbf{r},t)\,\Psi(\mathbf{r},t)\exp\left[-\frac{i}{\hbar}\int\mathbf{S}(\mathbf{r}',t)\cdot d\mathbf{r}'\right].
\end{aligned} \tag{4.25}$$

Cancelling out the unitary term and rearranging gives

$$i\hbar\dot{\Psi}(\mathbf{r},t) = \sum_i\frac{\mathbf{p}_i^2}{2m}\Psi(\mathbf{r},t) - \left(\frac{\partial}{\partial t}\int_{-\infty}^{\mathbf{r}}\mathbf{S}_{\rm Min}\cdot d\mathbf{r}'\right)\Psi(\mathbf{r},t). \tag{4.26}$$

The second term is now the energy due to the Minkowski momentum

$$\mathbf{S}_{\text{Min}} = \int (\mathbf{D} \times \mathbf{B})\, d^3\mathbf{r} \tag{4.27}$$

Once again using Eq. (4.18) and the divergence theorem, we can write Eq. (4.26) as

$$i\hbar\dot{\Psi}(\mathbf{r},t) = \sum_i \frac{\mathbf{p}_i^2}{2m}\Psi(\mathbf{r},t) + c\,\mathbf{S}_{\text{Min}}\Psi(\mathbf{r},t). \tag{4.28}$$

We will refer to this representation as the Minkowski representation. The $\mathbf{p}_i$ term on the right of Eq. (4.28) is now the canonical momentum of the atom as opposed to the kinetic momentum in the Abraham representation.

Suppose we start with the initial wave function ψ_0. From Eq. (4.24) we see if we decided to use the Minkowski formulation and naively plugged in $\Psi = \psi_0$, we would obtain an incorrect result. Using the Minkowski representation forces us to use the initial wave function

$$\Psi(\mathbf{r},t) = \psi_0(\mathbf{r},t)\exp\left[-\frac{\mathrm{i}}{\hbar}\int_{-\infty}^{\mathbf{r}}\sum_i\left(\mathbf{d}_i \times \mathbf{B}_i + \frac{\mathbf{E}_i \times \mathbf{m}_i}{c^2}\right)\cdot d\mathbf{r}'\right]. \tag{4.29}$$

This is precisely the He-McKellar-Wilkens and the Aharonov-Casher phase. The HMW and AC effects appear in the Minkowski representation as geometric phases, in contrast to the dynamic phase portrayal in the Abraham representation.

4.3 Conclusion

We began by showing how the classical Lagrangian for polarizable/magnetizable atoms interacting with an electromagnetic field must be modified by consid-

ering the Lorentz transformed interactions as seen from the atom's reference frame. We were then able to show that the corresponding Hamiltonian yielded the Abraham momentum through Poynting's theorem. By transforming the field through the unitary transformation

$$\exp\left[-\frac{\mathrm{i}}{\hbar}\int_{-\infty}^{\mathbf{r}}\sum_{i}\left(\mathbf{d}_i\times\mathbf{B}_i+\frac{\mathbf{E}_i\times\mathbf{m}_i}{c^2}\right)\cdot d\mathbf{r}'\right]. \tag{4.30}$$

We were able to produce the Minkowski momentum for the field, at the expense of transforming the kinetic momentum of the atom into the canonical momentum

$$\mathbf{p}_{\text{canonical}}=m\mathbf{v}-\mathbf{d}\times\mathbf{B}-\frac{\mathbf{E}\times\mathbf{m}}{c^2}. \tag{4.31}$$

We then showed that if ψ_0 satisfies the Schrödinger equation in the Abraham representation, then

$$\Psi(\mathbf{r},t)=\psi_0(\mathbf{r},t)\exp\left[-\frac{\mathrm{i}}{\hbar}\int_{-\infty}^{\mathbf{r}}\left(\mathbf{d}\times\mathbf{B}+\frac{\mathbf{E}\times\mathbf{m}}{c^2}\right)\cdot d\mathbf{r}'\right] \tag{4.32}$$

satisfies the Schrödinger equation in the Minkowski representation. This generates the AC phase $\phi_{\text{AC}}=-(\hbar c^2)^{-1}\oint[\mathbf{E}(\mathbf{r})\times\mathbf{m}]\cdot dl$ along with the HMW phase $\phi_{\text{HMW}}=\hbar^{-1}\oint[\mathbf{B}(\mathbf{r})\times\mathbf{d}]\cdot dl$. Finally we showed that the AC/HMW effect may be interpreted as emerging from a dynamic or a geometric phase depending on the representation.

Chapter 5

Cavity Momentum

5.1 Introduction

In this section we consider an electromagnetic field in a cavity interacting with a dielectric slab which is allowed to move. The model is solved analytically by making use of a simple δ-function approximation for the central dielectric slab. This system offers a unique opportunity to study the energy and momentum of light in matter. For one, since the light is confined to a cavity, we have a well controlled system which can be precisely manipulated. The central dielectric slab can in theory be replaced with a single atom. The cavity system then acts to enhance the atom's influence on the light since the beam will bounce back and forth many times during the cavity lifetime, interacting with the atom during each pass. During the intervening travel time between cavity mirrors, the light is traveling in free space where there is no ambiguity in photon momentum. As we shall see, we obtain the same conclusions inside the cavity as we did in free space - but for quite distinct reasons.

This chapter follows the work we published on the optical Landau-Zener

effect [88]. In the first section 5.2 we introduce a simple model for the spatial dependence of the dielectric permittivity function inside a double cavity. This model treats the central membrane as a Dirac δ-function which facilitates analytic calculations. In Section 5.3 we find the global static solutions (normal modes) of Maxwell's wave equation subject to this dielectric function. From here we are able to extract the refractive index of the cavity-slab system. In Section 5.4 we determine the optical force on the dielectric slab. Finally in Section 5.5 we use the work-energy theorem to determine the form of the energy-momentum density. Conclusions are drawn in Section 5.6.

5.2 δ-function dielectric model

Consider a double cavity formed from two end mirrors plus a dielectric membrane located between them, as shown Figure 5.1.

A simple theoretical model describing such a double cavity has been given in a classic paper by Lang, Scully and Lamb [89]. For the purposes of solving Maxwell's wave equation in the double cavity, they treated the end mirrors as perfect reflectors and the central membrane as a thin slab of dielectric material which is modelled by a Dirac δ-function spatial profile. The double cavity model is thereby encoded in a dielectric permittivity function of the form

$$\varepsilon(x) = \begin{cases} \varepsilon_0(1 + \frac{a}{\varepsilon_0}\delta(x)) & -L_1 < x < L_2 \\ \infty & \text{elsewhere} \end{cases}, \tag{5.1}$$

where $x = -L_1$, and $x = L_2$ are the positions of the end mirrors. a is a parameter which determines the reflectivity of the central membrane. We have purposely written it in this suggestive manner in anticipation of the findings

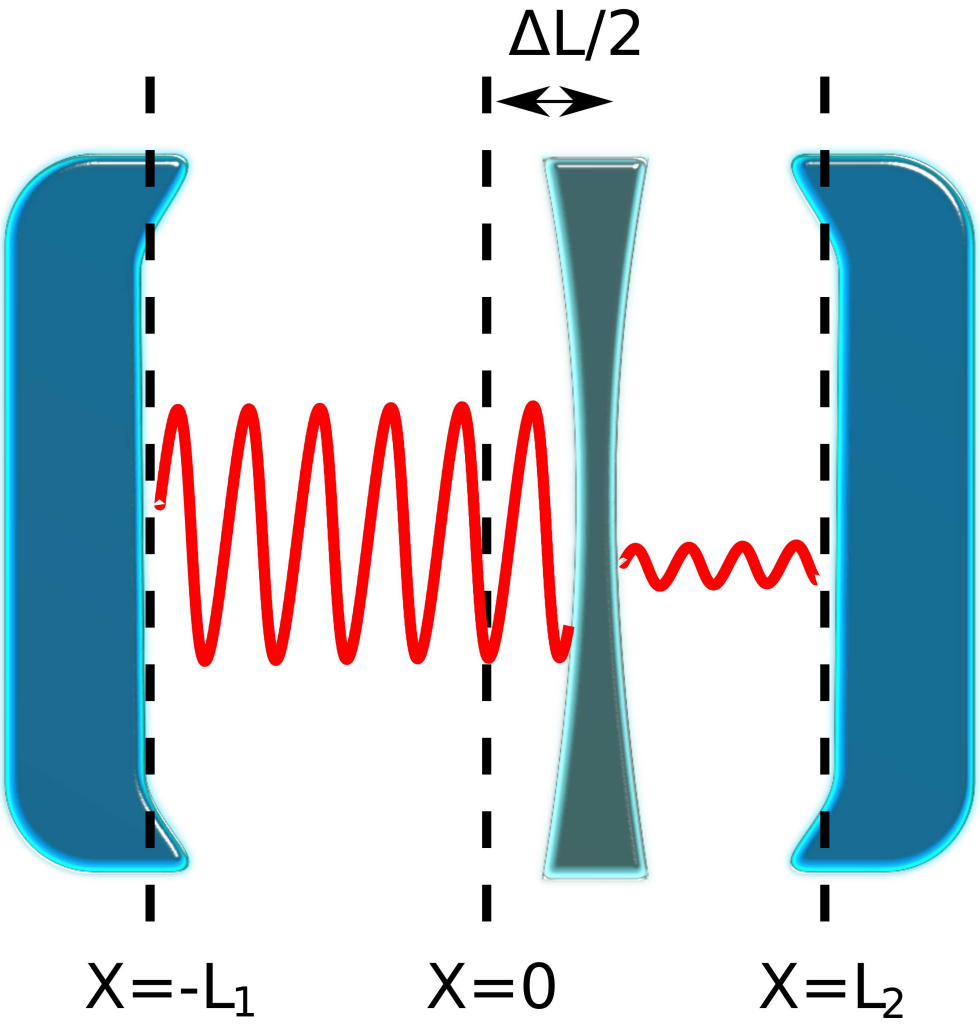

Figure 5.1: Double cavity setup consisting of two perfectly reflecting mirrors, along with a partially transmissive central membrane. $\Delta L \equiv L_1 - L_2$ is the difference in length between the two sub-cavities.

in Appendix B. The total length of the double cavity is $L \equiv L_1 + L_2$, and we also define the difference between the lengths of the two sub-cavities to be $\Delta L \equiv L_1 - L_2$, which is also twice the displacement of the membrane from the center of the whole cavity.

Maxwell's wave equation for the electric field $\mathcal{E}(x,t)$ in the double cavity is

$$\frac{\partial^2 \mathcal{E}(x,t)}{\partial x^2} - \mu_0 \varepsilon_0 (1 + \frac{a}{\varepsilon_0}\delta(x)) \frac{\partial^2 \mathcal{E}(x,t)}{\partial t^2} = 0 \ . \tag{5.2}$$

In Appendix A we compare the force calculations of the δ-membrane model to the standard dipole force equation to obtain a relationship between a and the polarizibility of an atom.

We write the solutions to the Maxwell wave equation as $\mathcal{E}_m(x,t) = U_m(x)\exp(-i\omega_m t)$, where $\omega_m = k_m/\sqrt{\varepsilon_0\mu_0}$ is the angular frequency and $m = 1, 2, 3\ldots$ is an integer labeling the modes. The dimensionless mode functions $U_m(x)$ can be chosen to be orthogonal in the Sturm-Liouville sense by ensuring that they obey

$$\frac{1}{\varepsilon_0}\int_{-L_1}^{L_2} \varepsilon(x) U_l(x) U_m(x) dx = 0, \quad l \neq m. \tag{5.3}$$

Inserting the above form for $\mathcal{E}(x,t)$ into Eq. (5.2) gives

$$\frac{\mathrm{d}^2 U_m(x)}{\mathrm{d}x^2} + k_m^2 (1 + \frac{a}{\varepsilon_0}\delta(x)) U_m(x) = 0 \ . \tag{5.4}$$

Solutions satisfying the boundary conditions $U_m(-L_1) = U_m(L_2) = 0$ are given by

$$U_m(x) = \begin{cases} \mathcal{A}_{Lm} \sin\left[k_m(x + L_1)\right] & -L_1 \leq x \leq 0 \\ \mathcal{A}_{Rm} \sin\left[k_m(x - L_2)\right] & 0 \leq x \leq L_2 \ . \end{cases} \tag{5.5}$$

Assuming the electric field is continuous across the δ-membrane, so that $U_m(0^+) =$

$U_m(0^-)$, we can integrate Eq. (5.4) over a vanishingly small interval containing the membrane and thereby find the last boundary condition $U'_m(0^+) - U'_m(0^-) = -\frac{a}{\varepsilon_0} k_m^2 U_m(0)$.

Combining all the boundary conditions one is led to the following equation for the wave numbers k_m of the allowed modes [89]

$$\cos(k_m \Delta L) - \cos(k_m L) = 2\varepsilon_0 \, \frac{\sin k_m L}{a k_m}. \tag{5.6}$$

This transcendental equation can in general only be solved numerically. However, when ak_m becomes large the sinc function on the right hand side becomes small. The left hand side may then be expanded around its roots and this permits approximate analytic solutions which will be supplied in Section 5.3. We refer to the solutions for the wave number in the case of an empty cavity system (i.e when there is no central membrane) as k_0.

5.3 Analytic Results

The mode amplitudes $\mathcal{A}_{Lm}$ and $\mathcal{A}_{Rm}$ on the two sides of the membrane will now be calculated. From the continuity condition for the field across the membrane we find that

$$\frac{\mathcal{A}_{Lm}}{\mathcal{A}_{Rm}} = -\frac{\sin(k_m L_2)}{\sin(k_m L_1)} = -\frac{\sin[k_m(L - \Delta L)/2]}{\sin[k_m(L + \Delta L)/2]}. \tag{5.7}$$

Throughout this paper we make use of results obtained by considering a closed cavity system. Although not physical, the results approximate an open cavity system in which the end mirrors are much more reflective than the central membrane. To see this consider a double cavity system in which the two

end mirrors are not perfectly reflective. This scenario is fundamentally very different from the case in which we have perfectly reflecting end mirrors. In the latter case, the mirror position determines the allowed wavenumbers of the system. In the former case, the positioning does not change the wavenumber of the pumped laser, it only changes the amplitude. We wish to find the amplitude ratios of the left and right mode as a function of central membrane position. To accomplish this, we solve Maxwell's equations in the four zones (the two left and right sub-cavities, along with the two regions to the left and right of the cavity system). We treat the mirrors as delta potentials similar to how we treated the dielectric membrane. Using the ansatz that in each region we have a plane wave propagating to the right and a plane wave propagating to the left, we may solve for the amplitude of the waves by matching boundary values. Continuity of the electric field at the mirrors give the following relations (see figure 5.2):

$$Ae^{ikx_1} + Be^{ikx_1} = Ce^{ikx_1} + De^{ikx_1}, \tag{5.8}$$

$$C + D = E + F, \tag{5.9}$$

$$Ee^{ikx_3} + Fe^{ikx_3} = Ge^{ikx_3}. \tag{5.10}$$

Integrating over an infinitesimal region about each delta mirror gives the final 3 relations:

$$\frac{i}{k}\left(-Ae^{ikx_1} + Be^{ikx_1} + Ce^{ikx_1} - De^{ikx_1}\right) = \frac{a_{\mathrm{L}}}{\epsilon_0}\left(Ae^{ikx_1} + Be^{ikx_1}\right), \tag{5.11}$$

$$\frac{i}{k}\left(-C + D + E - F\right) = \frac{a}{\epsilon_0}\left(C + D\right), \tag{5.12}$$

$$\frac{i}{k}\left(-Ee^{ikx_3} + Fe^{ikx_3} + Ge^{ikx_3}\right) = \frac{a_{\mathrm{R}}}{\epsilon_0}\left(Ee^{ikx_3} + Fe^{ikx_3}\right). \tag{5.13}$$

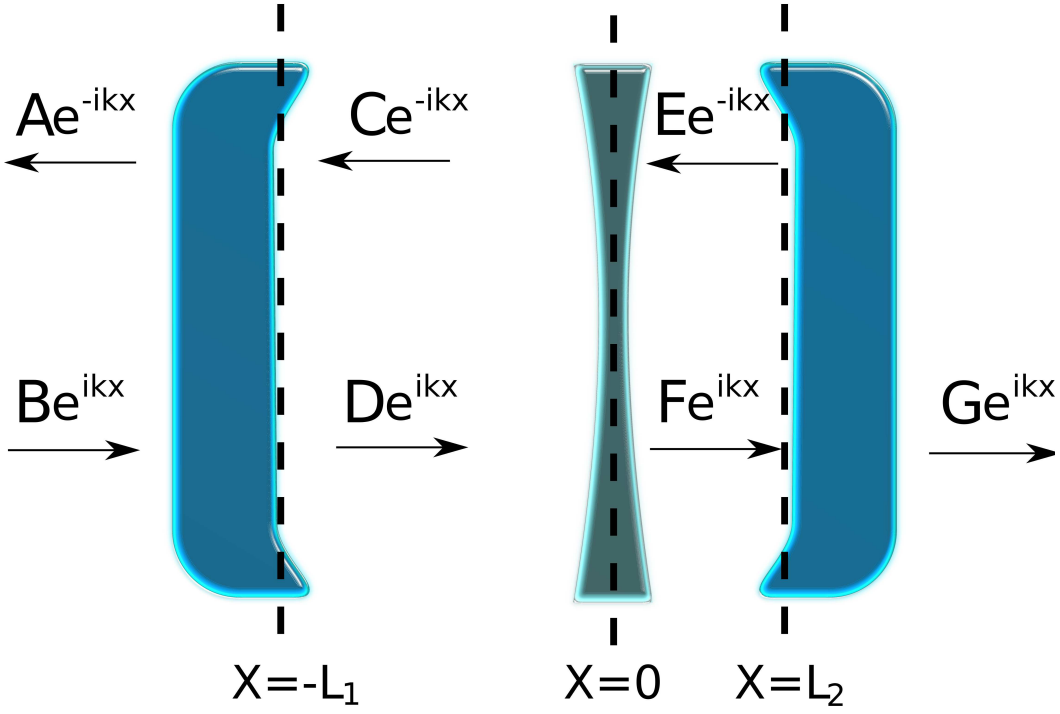

Figure 5.2: A schematic decomposition of the different traveling waves both inside and outside of the cavity system. Using Maxwell's equations along with proper boundary conditions, it is possible to determine the amplitude ratio of the left sub-cavity field, relative to the right sub-cavity field.

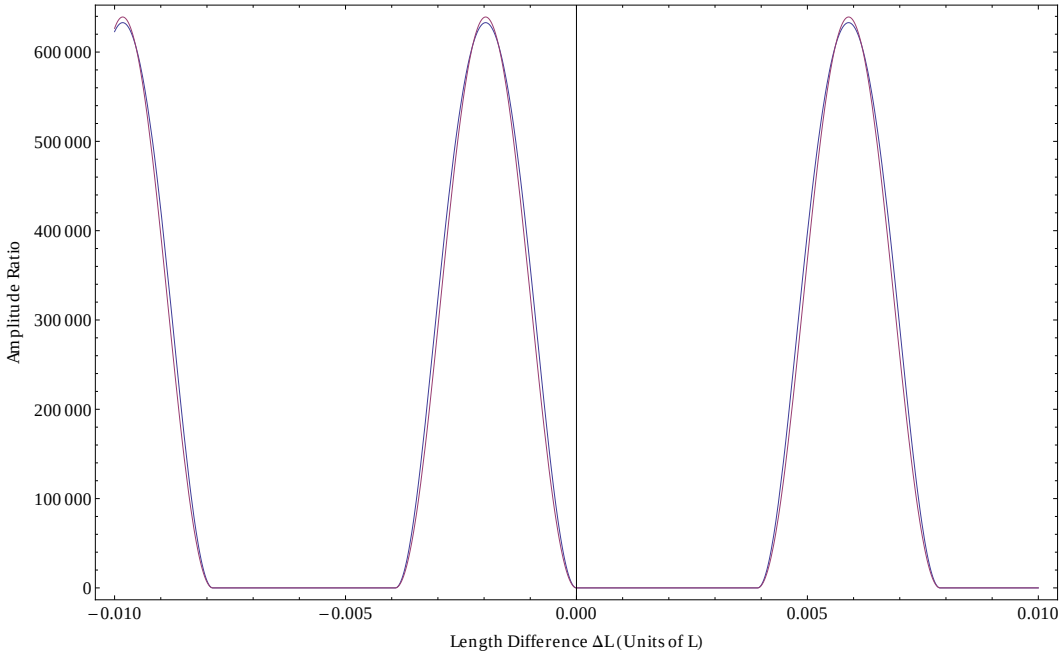

Figure 5.3: The relative amplitude ratio Eq. (5.7) is plotted (red) along side numeric solutions obtained using Maxwell's equations in an open cavity system (blue). In the open system, the outer mirrors were set to be 10 times more reflective than the central membrane.

Where a_{L}, a_{L}, and a are the left, right, and central mirror strengths as given by Eq. (5.1). We set $A = 1$ and then numerically solve this system of equations and determine the amplitude ratio of the left cavity relative to the right cavity. In figure 5.3 we compare the amplitude ratio found in Eq. (5.7) with numerical solutions obtained for an open cavity system. The end mirrors are assumed to be 10 times more reflective than the central membrane. We see that the field distribution coincides very well with the closed cavity.

We now turn back to the transcendental equation Eq. (5.6) . It is possible to find an analytic solution for the wave number k_m when a is very small as it is for a low density atomic cloud. When a is very small, the right side of Eq. (5.6) must still be of order one since the left side is of order one, therefore $\sin kL$ must be very close to zero. We can then expand $k_m L$ about $m\pi$ to first

order

$$\cos(k_m \triangle L) \pm 1 = \mp \frac{2\varepsilon_0 L}{a} \left(\frac{L}{m\pi} \left(k_m - \frac{m\pi}{L} \right) \right). \tag{5.14}$$

Where the upper signs correspond to odd m while lower signs give the result for even m. Now $\cos(k\Delta L)$ has a k in the argument, however as this doesn't deviate from $m\pi$ much, it is reasonable for small values of a to replace it with $m\pi$ as the cosine function is insensitive to such small perturbations

$$k_m = \mp \frac{am\pi}{2\varepsilon_0 L^2} \left(\cos(m\pi \frac{\triangle L}{L}) \pm 1 \right) + \frac{m\pi}{L}. \tag{5.15}$$

Note that the upper signs correspond to odd m and lower signs to even m respectively. In Figure 5.4 we plot Eq. (5.15) against the numeric solution for the wave number to show that the analytic approximation is sufficiently close to the numeric solution. We see that the overlap is near perfect for $a = 10^{-5}$.

We now ask ourselves what the effective refractive index is for the system. For this we use Eq. (5.15) for the wave number k_m and rewrite it in a form that allows us to extract the effective index of refraction n_r

$$k_m = \frac{m\pi}{L} \left[\mp \frac{a}{2\varepsilon_0 L} \left(\cos(m\pi \frac{\triangle L}{L}) \pm 1 \right) + 1 \right] = k_0 n_r, \tag{5.16}$$

and we see that

$$n_r = \left[\mp \frac{a}{2\varepsilon_0 L} \left(\cos(m\pi \frac{\triangle L}{L}) \pm 1 \right) + 1 \right]. \tag{5.17}$$

For the remainder of this chapter we will assume m is even and work with the odd wavemodes k_{odd}. Confusingly, an even m gives rise to an odd wavemode and vice versa. For a membrane position near $\Delta L = 0$, we can expand the

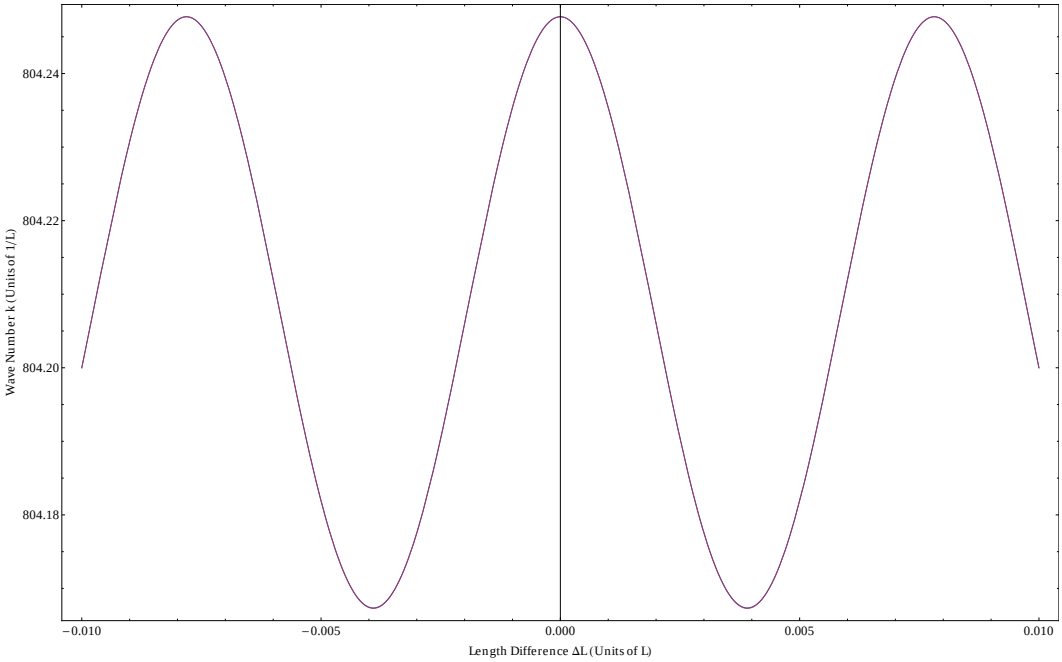

Figure 5.4: Wavenumber is plotted as a function of central membrane position. The analytic result Eq. (5.15) is in blue, and the exact numerical solution is plotted in red. In the plot the value of a, which controls the strength of the δ-potential, is set at $a = 10^{-5}$.

refractive index to second order as

$$n_r \approx 1 - \frac{am^2\pi^2}{4\epsilon_0 L^3}(\Delta L)^2. \tag{5.18}$$

We will return to this result shortly.

5.4 The Force on the Central Membrane

We turn to the problem of calculating the electromagnetic force on the central membrane. The optical force is the rate at which momentum is being extracted from the electromagnetic field due to the presence of the membrane. This will then allow us to calculate the average photon momentum inside the cavity for a given membrane position ΔL. The force is given by Eq. (2.30)

$$F = \oint_S \overleftrightarrow{T} \cdot da - \varepsilon_0\mu_0 \frac{\partial}{\partial t}\int_V S d\tau, \tag{5.19}$$

where $\overleftrightarrow{T}$ is the Maxwell stress tensor defined as

$$T_{xx} = \frac{\varepsilon_0}{2}\left(\mathcal{E}_x^2 - \mathcal{E}_y^2 - \mathcal{E}_z^2\right) + \frac{1}{2\mu_0}\left(B_x^2 - B_y^2 - B_z^2\right), \tag{5.20}$$

$$T_{xy} = \varepsilon_0\left(\mathcal{E}_x\mathcal{E}_y\right) + \frac{1}{\mu_0}\left(B_xB_y\right). \tag{5.21}$$

S in Eq. (5.19) is the Poynting vector, which we neglect for the time being, i.e. let us first consider only the force due to the stress tensor $\overleftrightarrow{T}$. Integrating about a Gaussian pillbox containing the central membrane gives [90] (see figure 5.1).

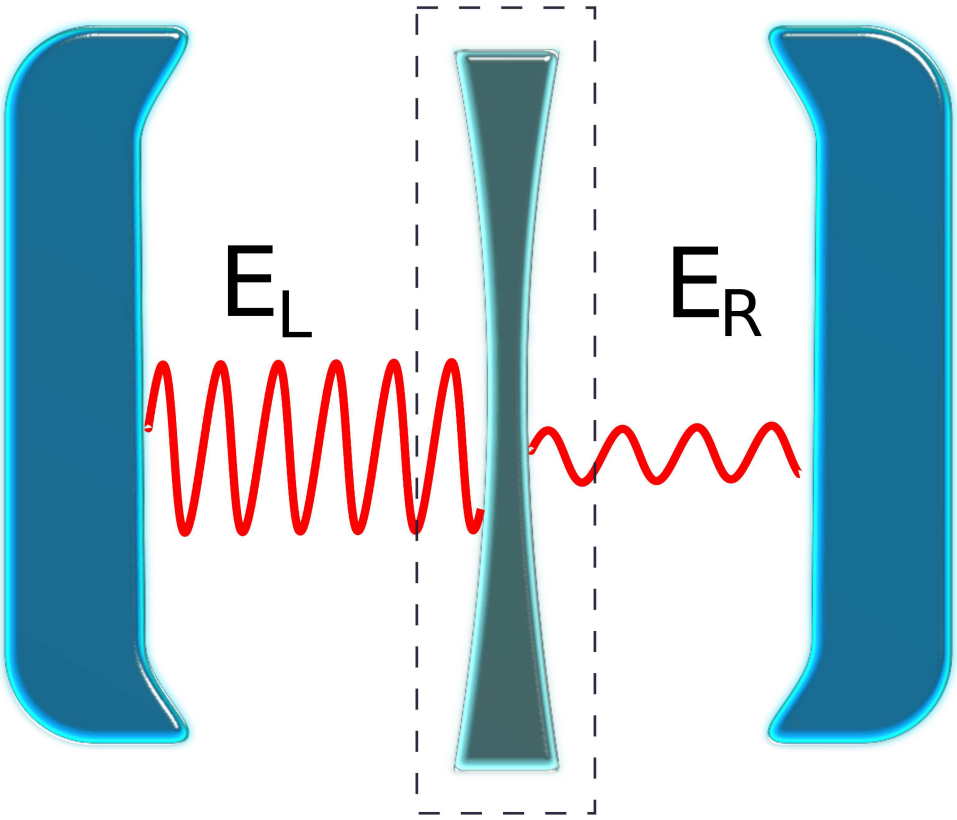

Figure 5.5: The force is found by integrating the Maxwell stress tensor around a small pillbox containing the central membrane.

$$\begin{aligned} F &= \frac{\varepsilon_0}{2}\left(|\mathcal{E}_{Lm}|^2 - |\mathcal{E}_{Rm}|^2\right) \\ &= \left(\frac{\varepsilon_0}{2}|\mathcal{E}_{Rm}|^2\right)\left(\left|\frac{\sin(k_m L_2)}{\sin(k_m L_1)}\right|^2 - 1\right). \end{aligned} \tag{5.22}$$

Where $\mathcal{E}_{Lm}$ and $\mathcal{E}_{Rm}$ are the electromagnetic fields to the left and right of the central membrane respectively. Note that here what we call the force F is really the radiation pressure (force/area). We have made use of Eq. (5.7) in writing the left field $\mathcal{E}_{Lm}$ in terms of the right. The second factor in Eq. (5.22) tells us that the force is proportional to the amplitude ratio between the modes on the left and right of the central membrane as is expected with radiative pressure. The first factor tells us that the force is proportional to the intensity of the field. When the central membrane is at $\Delta L = 0$, then $\mathcal{E}_{Rm} = \mathcal{E}$ and we can write the total electromagnetic energy per unit area as

$$E_{\text{total}} = \int_0^L \varepsilon_0 |\mathcal{E}|^2 \, dl = \frac{\varepsilon_0 |\mathcal{E}_{Rm}|^2 L}{2}. \tag{5.23}$$

For small deviations around $\Delta L = 0$, we make the approximation

$$\frac{\varepsilon_0 |\mathcal{E}_{Rm}|^2 L}{2} \approx E_{\text{total}}. \tag{5.24}$$

This approximation allows us to write the first factor in Eq. (5.22) simply as E_{total}:

$$F = \frac{E_{\text{total}}}{L}\left(\left|\frac{\sin(k_m L_2)}{\sin(k_m L_1)}\right|^2 - 1\right). \tag{5.25}$$

As we are interested in determining the average force per photon, we divide

Eq. (5.25) by the number of photons n_{photon}. It is assumed that the total number of photons in the cavity is conserved during adiabatic motion of the membrane

$$n_{\text{photon}} = \frac{E_{\text{total}}}{\hbar c k_0}. \tag{5.26}$$

This gives the average force per photon

$$F = \frac{\hbar c k_0}{L}\left(\left|\frac{\sin(k_m L_2)}{\sin(k_m L_1)}\right|^2 - 1\right). \tag{5.27}$$

We can further simplify this expression by noting that for very small a we can approximate the amplitude ratio factor in Eq. (5.27) to first order

$$\left|\frac{\sin(k_m L_2)}{\sin(k_m L_1)}\right|^2 \approx \frac{\frac{\varepsilon_0 L}{am\pi} - \frac{1}{2}\sin(m\pi\frac{\triangle L}{L})}{\frac{\varepsilon_0 L}{am\pi} + \frac{1}{2}\sin(m\pi\frac{\triangle L}{L})}. \tag{5.28}$$

Substituting this into Eq. (5.27) and simplifying yields

$$F_{\text{Min}} = -\hbar k_0 c \frac{am\pi}{\varepsilon_0 L^2}\sin(m\pi\frac{\triangle L}{L}). \tag{5.29}$$

We have written the force here with a subscript, foreshadowing results from the next section.

5.5 Energy and Momentum

In this section we want to determine how much energy is required to realize a given membrane configuration. It is assumed that the polarizbility factor α is very small, and we make use of the analytic results obtained in Sections 5.3 and 5.4. The work-energy theorem tells us how much energy must be used by

the field in moving the central membrane to some position $\triangle L$.

$$\mathcal{E}_{\text{field}} = -\int F\, dx. \tag{5.30}$$

Substituting in the force Eq. (5.29)

$$\begin{aligned}
\mathcal{E}_{\text{field}} &= -\int F_{Min} \frac{d\,(\triangle L)}{2} \\
&= \int_0^{\triangle L} \hbar k_0 c \frac{\alpha m \pi}{2L^2} \sin(m\pi \frac{\triangle L'}{L}) d\,(\triangle L') \\
&= -\hbar c k_0 \left[\frac{\alpha}{2L} \left(\cos(m\pi \frac{\triangle L}{L}) - 1 \right) \right] \\
&\approx \hbar c k_0 \frac{a m^2 \pi^2}{4\epsilon_0 L^3} (\Delta L)^2.
\end{aligned} \tag{5.31}$$

Eq. (5.31) tells us is the energy per photon $\mathcal{E}_{\text{field}}$ used to move the membrane from the centered position $\triangle L = 0$, to some other position $\triangle L$. By subtracting $\mathcal{E}_{\text{field}}$ from the initial photon energy $\hbar c k_0$, we arrive at an expression for the energy per photon remaining in the system

$$\mathcal{E}_{\text{photon}} = \hbar c k_0 \left(1 - \frac{a m^2 \pi^2}{4\epsilon_0 L^3} (\Delta L)^2 \right). \tag{5.32}$$

Then using Eq. (5.18), we can rewrite this in terms of the refractive index

$$\mathcal{E}_{\text{photon}} = \hbar c k_0 n_r. \tag{5.33}$$

To obtain the momentum we note that the electromagnetic fields are propagating in a vacuum, and hence we divide Eq. (5.32) by c and obtain the Minkowski momentum $\mathbf{p}_{\text{min}} = \hbar k_0 n_r$.

Let us now go back to the Maxwell force Eq. (5.19). In the derivation which resulted in us obtaining the Minkowski momentum, we only considered the force, and hence the momentum, due to the stress tensor term. We now take into account the momentum contribution from the Poynting vector term. The Poynting (or Abraham) radiation pressure (force/area) is

$$F_{\text{Poynting}} = -\frac{\partial}{\partial t}\int_{L_1}^{L_2} (\epsilon_0 \mathbf{E} \times \mathbf{B})\,. \tag{5.34}$$

We can rewrite the Poynting vector in terms of the left and right electric field amplitudes

$$F_{\text{Poynting}} = -\epsilon_0 \frac{\partial}{\partial t}\left(|\mathcal{E}_{Lm}|^2 L_1 + |\mathcal{E}_{Rm}|^2 L_2\right). \tag{5.35}$$

After some manipulation (see appendix B), we obtain a simplified expression for the force

$$F_{\text{Poynting}} = \frac{\partial}{\partial t}\left(\hbar k_0 \frac{a m^2 \pi^2}{2\epsilon L^3}(\Delta L)^2\right). \tag{5.36}$$

The momentum $\mathbf{p}_{\text{Poynting}}$ transferred to the system by moving the membrane to ΔL is found by integrating this force with respect to time

$$\mathbf{p}_{\text{Poynting}} = \hbar k_0 \frac{a m^2 \pi^2}{2\epsilon L^3}(\Delta L)^2. \tag{5.37}$$

We found earlier that the momentum $\mathbf{p}_{\text{min}}$ of the photons inside the cavity due to the Maxwell stress tensor Eq. (5.32) is given by

$$\mathbf{p}_{\text{min}} = \hbar k_0 \left(1 - \frac{a m^2 \pi^2}{4\epsilon_0 L^3}(\Delta L)^2\right). \tag{5.38}$$

If we now include the momentum $\mathbf{p}_{\text{Poynting}}$ we find the total momentum of the

photons to be

$$\begin{aligned}
\mathbf{p}_{\text{total}} &= \hbar k_0 \left(1 - \frac{am^2\pi^2}{4\epsilon_0 L^3}(\Delta L)^2\right) + \hbar k_0 \frac{am^2\pi^2}{2\epsilon_0 L^3}(\Delta L)^2 \\
&= \hbar k_0 \left(1 + \frac{am^2\pi^2}{4\epsilon_0 L^3}(\Delta L)^2\right) \\
&\approx \frac{\hbar k_0}{1 - \frac{am^2\pi^2}{4\epsilon_0 L^3}(\Delta L)^2} = \frac{\hbar k_0}{n_r} = \mathbf{p_{abr}}.
\end{aligned} \tag{5.39}$$

We have arrived the Abraham momentum!

5.6 Conclusion

The Minkowski-Abraham paradox was shown to result from the Poynting term in the Maxwell force equation

$$F = \oint_S \overleftrightarrow{T} \cdot da - \varepsilon_0 \mu_0 \frac{\partial}{\partial t} \int_V S d\tau. \tag{5.40}$$

This result is consistent with our findings from the previous chapters, even though we arrived at it by quite different means. Note that the Poynting term here is not equal to the Abraham force term $\mathbf{f}^{\text{A}} = \frac{\partial}{\partial t}(\mathbf{P} \times \mathbf{B})$ responsible for the difference between the two momenta in the previous chapters. We began by showing how the refractive index arises as a result of the superposition between left and right traveling modes inside the cavity. This calculation required us to consider a perfectly reflecting cavity, however, it was shown that so long as the cavity mirrors were significantly more reflective than the central membrane, this approximation holds. This result is particularly interesting since in the perfectly reflecting cavity scenario, the mirror positions determine the allowed wavenumber in the cavity. While in the more physical, open cavity

system, the position of the mirrors only affects the amplitude of the modes, yet they both converge to the same solution when the ratio of mirror reflectivity to membrane reflectivity is large. We were then able to calculate the force from these modes acting on the central dielectric membrane to determine the momentum transferred from the electromagnetic fields to the membrane. The resulting electromagnetic momentum was shown to be of either the Minkowski or Abraham form depending on whether or not the Poynting term in the Maxwell force equation is included.

Chapter 6

Conclusions and Outlook

6.1 Conclusions

Why is it so many experiments tend to favor the Minkowski representation over the Abraham form? The reason lies with the Abraham (Poynting) force $\mathbf{F}^{\mathrm{A}} = \alpha \frac{\partial}{\partial t}(\mathbf{E} \times \mathbf{B})$. As we saw in Section 2, this only becomes relevant in certain situations. We saw that this force averages to zero over an optical cycle unless the fields have a time-dependent amplitude. The momentum transferred is only dependent on the initial and final amplitude of the field. Therefore not only do we require the electromagnetic field amplitude to be time dependent, but also that the field not be pulsed (i.e turned on and then off quickly). This makes it difficult to observe in an experiment. However, if one considers the momentum gained from an electromagnetic field due to a field which is initially at zero and is then turned up to some maximal strength $E_{\max}$, one finds the Abraham force contribution is twice as much as that due to the gradient force. Of course for a pulsed field, the Abraham force will contribute zero total momentum as the initial and final amplitudes are both the same. Thus

the Abraham force is observable, and in fact greater than the optical dipole force, during this initial amplitude switch on period. The reason why the Abraham force has been so elusive, is because we have been doing the wrong experiments. At the outset of this thesis, one of the end goals was to understand why certain experiments observed the Minkowski versus the Abraham momentum. Let us go back and review two of the cornerstone experiments which produced seemingly conflicting conclusions and see if we can make sense of the results.

The first experiment we reexamine was performed by Pritchard and Ketterle [35]. The setup consisted of an elongated ^{87}Rb Bose-Einstein condensate contained in a magnetic trap. They used a $\lambda = 780$ nm standing wave pulse which acted for 5 μs to out couple approximately 5% of the atoms. After waiting 600 μs a second pulse was applied which recombined some of the atoms from this group with the original ground state group, producing at interference pattern. Using ballistic imaging they were able to resolve the momentum states and conclude that the atoms had acquired a momentum kick proportional to the refractive index of the gas, thus corroborating Minkowki's claim. We immediately see the issue here however. By pulsing a standing wave, they have ensured that the Abraham force will contribute nothing for two reasons. Firstly, a standing wave has no net Poynting vector, and hence the Abraham force will be zero. Secondly, even if there was a small net Poynting vector associated with the laser, after the full pulse cycle, the initial and final amplitudes of the pulse are the same, and hence the momentum transferred due to the Abraham force must be zero.

The second experiment was performed by Ulf Leonhardt and Nan Peng [36]. In this experiment they shone a laser onto the surface of water and

oil. By observing the surface bulge they were able to conclude that the electromagnetic momentum coincided with the Abraham momentum. How can we make sense of this with what we've learned? The difference between the Pritchard-Ketterle experiment and this one is the nature of the light beam. In the Leonhardt experiment, the surface of the liquid sees an electric field amplitude which switches on from zero to some maximum value. During this process the Abraham force $\mathbf{F}^A = \alpha \frac{\partial}{\partial t}(\mathbf{E} \times \mathbf{B})$ is nonzero - unlike in the Pritchard experiment. As was mentioned earlier, under these conditions the Abraham force contribution is twice that of the dipole force (and in the opposite direction). Therefore, it is no wonder that Leonhardt's group observed an outward bulge, indicative of the Abraham momentum.

What is the take home message after all this? Let's go back and take a look at Poynting's theorem in the Minkowski and the Abraham representation. In the Minkowski representation, Eq. (2.56), we have

$$\tilde{\mathbf{f}} + \frac{\partial}{\partial t}\left[\mathbf{D} \times \mathbf{B}\right] = \nabla \cdot \left(\mathbf{E}\mathbf{D} + \mathbf{H}\mathbf{B} - \frac{1}{2}\mathbf{I}\left(\mathbf{D} \cdot \mathbf{E} + \mathbf{H} \cdot \mathbf{B}\right)\right), \tag{6.1}$$

where we identify $\tilde{\mathbf{f}}$ with the rate of change of mechanical momentum. What this equation is telling us is that

$$\frac{\partial}{\partial t}\left(\tilde{\mathbf{P}}_{\text{mechanical}}\right) + \frac{\partial}{\partial t}\left(\tilde{\mathbf{P}}_{\text{electromagnetic}}\right) = \nabla \cdot \mathbf{W}_{\text{total}}, \tag{6.2}$$

where $\tilde{\mathbf{P}}_{\text{mechanical}}$ is the mechanical momentum of the material, $\tilde{\mathbf{P}}_{\text{electromagnetic}}$ is the electromagnetic momentum, and $\mathbf{W}_{\text{total}}$ is the total work done. Now just as we had previously done in Section 2, we subtract $\varepsilon_0\left(\varepsilon_{\mathbf{r}} + 1\right)\frac{\partial}{\partial t}(\mathbf{E} \times \mathbf{B})$

from both sides. This gives us

$$\mathbf{f} + \frac{\partial}{\partial t}\frac{\mathbf{E}\times\mathbf{H}}{c^2} = \nabla\cdot\left(\mathbf{ED} + \mathbf{HB} - \frac{1}{2}\mathbf{I}\left(\mathbf{D}\cdot\mathbf{E} + \mathbf{H}\cdot\mathbf{B}\right)\right), \tag{6.3}$$

where $\mathbf{f} = \tilde{\mathbf{f}} + \frac{\partial}{\partial t}(\mathbf{P}\times\mathbf{B})$. Now in the Abraham representation, we identify $\mathbf{f}$ with the change in mechanical momentum $\frac{\partial}{\partial t}\mathbf{P}_{\text{mechanical}}$ and $\frac{\mathbf{E}\times\mathbf{H}}{c^2}$ with the change in electromagnetic momentum $\mathbf{P}_{\text{electromagnetic}}$. So how does this fit in with the fact that Minkowski form is the representation most often claimed in the literature? Consider again the Abraham force density $\frac{\partial}{\partial t}(\mathbf{P}\times\mathbf{B})$ which is responsible for the difference between $\tilde{\mathbf{f}}$ and $\mathbf{f}$. As we mentioned above, a typical experiment will not observe the Abraham force, and hence will measure the force density on the system to be simply $\tilde{\mathbf{f}}$. In doing so however, they will be led erroneously to conclude that the corresponding electromagnetic field momentum is $\tilde{\mathbf{P}}_{\text{electromagnetic}}$ in Eq. (6.1) and hence the Minkowski momentum.

Appendices

Appendix A

Appendix to Chapter 4

In this appendix I derive some of the fundamental results of this thesis. Details omitted in the body of the thesis are shown here. In the first subsection I fully derive the Abraham representation and show all steps. In the second subsection I show how to derive the direct coupling Hamiltonian from the minimal coupling representation. Finally in the third subsection I show how one can derive the direct coupling Hamiltonian through a gauge transformation.

A.1 Appendix: Abraham Representation Expansion

In this section we go through the derivation of the Minkowski Hamiltonian given by Eq. (4.28). The Schrodinger equation in the Abraham representation is given by Eq. (4.20)

$$i\hbar\dot{\psi}(\mathbf{r},t) = \sum_i \frac{1}{2m_i}\left(\mathbf{p}_i + \mathbf{d}_i \times \mathbf{B}_i + \frac{\mathbf{E}_i \times \mathbf{m}_i}{c^2}\right)^2 \psi(\mathbf{r},t) + c\mathbf{S}_{\mathrm{Abr}}\psi(\mathbf{r},t). \quad \text{(A.1)}$$

Here we have written

$$\mathbf{S}_{\mathrm{Abr}} = \int \frac{\mathbf{E}\times\mathbf{H}}{c^2}\, dV. \quad \text{(A.2)}$$

$$\psi(\mathbf{r},\mathrm{t}) = \Psi(\mathbf{r},\mathrm{t}) \exp\left[-\frac{\mathrm{i}}{\hbar}\int_{-\infty}^{\mathbf{r}} \mathbf{S}(\mathbf{r}',\mathrm{t})\cdot \mathrm{d}\mathbf{r}'\right], \quad \text{(A.3)}$$

where $\mathbf{S}(\mathbf{r},t) \equiv \sum_i (\mathbf{d}_i \times \mathbf{B}_i + \epsilon_0\mu_0 \mathbf{E}_i \times \mathbf{m}_i)$ This yields

$$\begin{aligned} & i\hbar\dot{\Psi} + \Psi \left(\frac{\partial}{\partial t} \int_0^{\mathbf{x}} \mathbf{S}\, dx' \right) \\ = \; & -\hbar^2(\nabla^2\Psi) + 2i\hbar(\nabla\Psi)\mathbf{S}_{\mathrm{A}} + \Psi S^2 + i\hbar\Psi(\nabla\mathbf{S}) \\ & -2i\hbar(\nabla\Psi)\mathbf{S} - i\hbar\Psi(\nabla\mathbf{S}) - 2\Psi\mathbf{S}^2 \\ & -2i\hbar(\nabla\Psi)(\mathbf{d}\times\mathbf{B}) - i\hbar\Psi(\nabla(\mathbf{d}\times\mathbf{B})) - 2\Psi\mathbf{S}(\mathbf{d}\times\mathbf{B}) \\ & +\Psi\left(\mathbf{S}^2 + (\mathbf{d}\times\mathbf{B})^2 + 2\mathbf{S}(\mathbf{d}\times\mathbf{B})\right) \\ & -\Psi \int \frac{1}{2}\left(\mathbf{D}\cdot\mathbf{E} + \mathbf{H}\cdot\mathbf{B}\right) dV. \end{aligned} \tag{A.4}$$

Here we have omitted writing out the phase factor

$$\exp\left[-\frac{i}{\hbar}\int_0^{\mathbf{x}} \mathbf{S}\, dx'\right], \tag{A.5}$$

as it appears multiplying every term and will be factored out. Canceling terms leaves us with

$$\begin{aligned} & i\hbar\dot{\Psi} + \Psi \left(\frac{\partial}{\partial t} \int_0^{\mathbf{x}} \mathbf{S}\, dx' \right) \\ = \; & -\hbar^2(\nabla^2\Psi) - 2i\hbar(\nabla\Psi)(\mathbf{d}\times\mathbf{B}) - i\hbar\Psi(\nabla(\mathbf{d}\times\mathbf{B})) \\ & +\Psi(\mathbf{d}\times\mathbf{B})^2 - \Psi \int \frac{1}{2}\left(\mathbf{D}\cdot\mathbf{E} + \mathbf{H}\cdot\mathbf{B}\right) dV. \end{aligned} \tag{A.6}$$

Factoring terms, this can be rearranged into

$$i\hbar\dot{\Psi} = \left(\frac{(\mathbf{P} + \mathbf{d}\times\mathbf{B})^2}{2M} - \int \frac{1}{2}\left(\mathbf{D}\cdot\mathbf{E} + \mathbf{H}\cdot\mathbf{B}\right) dV - \frac{\partial}{\partial t}\int_0^{\mathbf{x}} \mathbf{S}\, dx' \right) \Psi. \tag{A.7}$$

A.2 Appendix: The Göppert-Mayer Transformation

We begin with the minimal coupling Hamiltonian for a system of charges interacting with an electromagnetic field

$$H(\mathbf{x},t) = \sum_j \frac{1}{2m_j} \left[\mathbf{p}_j - q_j\, \mathbf{A}(0,t)\right]^2 + V_c(\mathbf{x}), \tag{A.8}$$

where $\mathbf{A}(\mathbf{x},t)$ is the vector potential, e_j is the charge, and $V_{\rm c}(\mathbf{x})$ is the scalar potential energy of the system. In the long-wavelength approximation, we have assumed the spatial variation of $\mathbf{A}(\mathbf{x},t)$ is negligible. We therefore choose the location of the system of charges considered to be at $\mathbf{x}=0$ and set $\mathbf{A}(\mathbf{x},t) = \mathbf{A}(0,t)$. The corresponding Schrödinger equation for the minimal coupling Hamiltonian is given by

$$i\hbar\dot{\psi}(\mathbf{x},t) = \left[\sum_j \frac{1}{2m_j} \left[\mathbf{p}_j - q_j\, \mathbf{A}(0,t)\right]^2 + V_{\rm c}(\mathbf{x})\right] \psi(\mathbf{x},t). \tag{A.9}$$

The unitary transformation responsible for giving rise to the electric dipole interaction (direct coupling representation) is given by the Göppert-Mayer transformation (GMT)

$$\Theta(t) = \exp\left[\frac{i}{\hbar}\sum_j q_j\, \mathbf{r}_j \cdot \mathbf{A}(0,t)\right] = \exp\left[\frac{i}{\hbar}\mathbf{d}\cdot\mathbf{A}(0,t)\right], \tag{A.10}$$

where

$$\mathbf{d} = \sum_j e_j\, \mathbf{r}_j. \tag{A.11}$$

We rewrite the wave function ψ as

$$\psi(\mathbf{x},t) = \Theta(t)\Psi(\mathbf{x},t) = \exp\left[\frac{i}{\hbar}\mathbf{d}\cdot\mathbf{A}(0,t)\right]\Psi(\mathbf{x},t). \tag{A.12}$$

Substituting this into Eq. (A.9) yields This yields

$$\begin{aligned} & i\hbar\dot{\Psi}(\mathbf{x},t)\Theta(t) + \Psi(\mathbf{x},t)\Theta(t)\ (\mathbf{d}\cdot\mathbf{E}(0,t)) = \\ & -\Psi(\mathbf{x},t)\Theta(t)\left(i\sum_j \frac{e_j}{2m_j c}\mathbf{A}(0,t)\right)^2 \\ - \quad & \nabla\Psi(\mathbf{x},t)\Theta(t)\left(2i\hbar\sum_j \frac{e_j}{2m_j}\mathbf{A}(0,t)\right) \\ - \quad & \hbar^2\nabla^2\Psi(\mathbf{x},t)\Theta(t) + 2\Psi(\mathbf{x},t)\Theta(t)\left(i\sum_j \frac{e_j}{2m_j}\mathbf{A}(0,t)\right)^2 \\ + \quad & \nabla\Psi(\mathbf{x},t)\Theta(t)\left(2i\hbar\sum_j \frac{e_j}{2m_j}\mathbf{A}(0,t)\right) \\ + \quad & \Psi(\mathbf{x},t)\Theta(t)\left(i\sum_j \frac{e_j}{2m_j}\mathbf{A}(0,t)\right)^2 + \Psi(\mathbf{x},t)\Theta(t)\mathbf{V}_{\mathrm{c}}(\mathbf{x}). \end{aligned} \tag{A.13}$$

Where we have used

$$\mathbf{E}(0,t) = -\frac{\partial\mathbf{A}(0,t)}{\partial t}. \tag{A.14}$$

Canceling terms and rearranging leaves us with

$$i\hbar\dot{\Psi}(\mathbf{x},t) = \left[\frac{\mathbf{P}^2}{2M} - \mathbf{d}\cdot\mathbf{E}(0,t) + \mathbf{V}_{\mathrm{c}}(\mathbf{x})\right]\Psi(\mathbf{x},t). \tag{A.15}$$

Where $\mathbf{P} = \sum_j \mathbf{p}_j$ and $M = \sum_j m_j$ Here we have arrived at the direct coupling representation of the Hamiltonian. This Hamiltonian however, does not include the radiation energy of the fields themselves. Our treatment of the minimal coupling Hamiltonian Eq. (A.9) may be extended further by including the radiation energy of the fields themselves

$$H_{\mathrm{R}} = \frac{1}{2}\int\left(\epsilon_0\mathbf{E}^2(\mathbf{x},t) + \frac{\mathbf{B}^2(\mathbf{x},t)}{\mu_0}\right)dV = \sum_j \hbar\omega_j\left({a_j}^\dagger a_j + \frac{1}{2}\right). \tag{A.16}$$

The question then arises, how does the radiation Hamiltonian transform under the Göppert-Mayer unitary transformation transformation? Clearly if the fields are treated classically, the GMT Eq. (A.10) will commute with the electric field. If however, we consider a quantized field, this is no longer true. In order to determine how the fields transform under a quantized field, we must

promote the vector potential to an operator [91]

$$\mathbf{A}(\mathbf{x},t) = \sum_j \mathcal{A}_{\omega_j} \left[a_j \, \varepsilon_j e^{i(\mathbf{k}_j \cdot \mathbf{x} - \omega t)} + a_j{}^\dagger \, \varepsilon_j e^{-i(\mathbf{k}_j \cdot \mathbf{x} - \omega t)} \right], \tag{A.17}$$

where ε is the polarization, and

$$\mathcal{A}_{\omega_j} = \left[\frac{\hbar}{2\epsilon_0 L^3 \omega_j} \right]^{\frac{1}{2}}. \tag{A.18}$$

The transverse electric field in the Coulomb gauge is given by

$$\mathbf{E}_\perp(\mathbf{x},t) = i \sum_{j,\mu} \mathcal{E}_{\omega_j} \left[a_j \, \varepsilon_j e^{i(\mathbf{k}_j \cdot \mathbf{x} - \omega t)} - a_j{}^\dagger \, \varepsilon_j e^{-i(\mathbf{k}_j \cdot \mathbf{x} - \omega t)} \right], \tag{A.19}$$

where

$$\mathcal{E}_{\omega_j} = \left[\frac{\hbar \omega_j}{2\epsilon_0 L^3} \right]^{\frac{1}{2}}. \tag{A.20}$$

From here it is necessary to determine the commutation relation between the vector potential and electric field.

$$\begin{aligned}
&[\mathbf{A}(\mathbf{x},t), \mathbf{E}_\perp(\mathbf{x}',t)] = \\
&\frac{i\hbar}{2\epsilon_0 L^3} \sum_{j_\perp, j'_\perp} \left(\left[a_j^\dagger, a_{j'} \right] \, e^{i\mathbf{k}_{j'} \cdot \mathbf{x}'} e^{-i\mathbf{k}_j \cdot \mathbf{x}} \right) + \\
&\frac{i\hbar}{2\epsilon_0 L^3} \sum_{j_\perp, j'_\perp} \left(\left[a_{j'}^\dagger, a_j \right] \, e^{i\mathbf{k}_j \cdot \mathbf{x}} e^{-i\mathbf{k}_{j'} \cdot \mathbf{x}'} \right) = \\
&\frac{i\hbar}{2\epsilon_0 L^3} \sum_{j_\perp} \left(e^{i\mathbf{k}_j \cdot (\mathbf{x} - \mathbf{x}')} + e^{-i\mathbf{k}_j \cdot (\mathbf{x} - \mathbf{x}')} \right).
\end{aligned} \tag{A.21}$$

Where we have made use of the relation $[a_j, a_{j'}^\dagger] = \delta_{j,j'}$. In the summation, the notation $j_\perp$ indicates that we are taking the sum over the transverse modes. We convert our sum into an integral through [**?**]

$$\sum_k \to \frac{L^3}{(2\pi)^3} \int d^3k, \tag{A.22}$$

and we make use of the transverse delta function

$$\delta_\perp(\mathbf{x} - \mathbf{x}') = \frac{1}{(2\pi)^3} \int d^3k_\perp \, e^{i\mathbf{k}_j \cdot (\mathbf{x} - \mathbf{x}')}. \tag{A.23}$$

Therefore we find

$$[\mathbf{A}(\mathbf{x},\mathbf{t}),\mathbf{E}_{\perp}(\mathbf{x}',t)] = -\frac{i\hbar}{\epsilon_0}\delta_{\perp}(\mathbf{x}-\mathbf{x}'). \tag{A.24}$$

In order to determine how the electric field transforms under the GMT $\Theta(t)$ we use the property that for any two operators $\mathbf{A}$ and $\mathbf{B}$

$$\exp(i\mathbf{A})\,\mathbf{B}\exp(-i\mathbf{A}) = \mathbf{B} + i[\mathbf{A},\mathbf{B}] + ... \tag{A.25}$$

Using Eq. (A.24) and Eq. (A.25) we find

$$\Theta(t)\mathbf{E}_{\perp}(\mathbf{x},t)\Theta^{\dagger}(t) = \mathbf{E}_{\perp}(\mathbf{x},t) + \frac{1}{\epsilon_0}\mathbf{d}_{\perp}(\mathbf{x},t) = \frac{\mathbf{D}(\mathbf{x},t)}{\epsilon_0}. \tag{A.26}$$

Where $\mathbf{D}$ is the displacement field. Note that for a neutral system $\nabla\cdot\mathbf{D}=0$ and therefore the displacement field is fully transverse which allows us to drop the perpendicular suffix. It can easily be checked that

$$\Theta(t)\mathbf{B}(\mathbf{x},t)\Theta^{\dagger}(t) = \mathbf{B}(\mathbf{x},t), \tag{A.27}$$
$$\Theta(t)\mathbf{A}(\mathbf{x},t)\Theta^{\dagger}(t) = \mathbf{A}(\mathbf{x},t), \tag{A.28}$$
$$\Theta(t)\mathbf{P}(\mathbf{x},t)\Theta^{\dagger}(t) = \mathbf{P}(\mathbf{x},t). \tag{A.29}$$

This allows us to deduce that

$$\Theta(t)\mathbf{D}(\mathbf{x},t)\Theta^{\dagger}(t) = \epsilon_0\mathbf{E}(\mathbf{x},t). \tag{A.30}$$

We can now preform a generalized Göppert-Mayer transformation for the total minimal coupling Hamiltonian

$$\begin{aligned} H_{\mathrm{Min}} &= H_0 + H_{\mathrm{R}} \\ &= \sum_j \frac{1}{2m_j}\left[\mathbf{p}_j - q_j\,\mathbf{A}(\mathbf{0},t)\right]^2 + V_{\mathrm{c}}(\mathbf{x}) \\ &+\frac{1}{2}\int\left(\epsilon_0\mathbf{E}^2(\mathbf{x},t) + \frac{\mathbf{B}^2(\mathbf{x},t)}{\mu_0}\right)dV. \end{aligned} \tag{A.31}$$

We begin with the Schrödinger equation

$$i\hbar\frac{\partial}{\partial t}\psi = H\,\psi, \tag{A.32}$$

and rewrite the wave function as

$$\psi = e^{\frac{i}{\hbar}\mathbf{d}\cdot\mathbf{A}}\Phi. \tag{A.33}$$

This allows us to express the Schrödinger equation in terms of the wave function Φ

$$\begin{aligned} i\hbar\frac{\partial}{\partial t}\Phi = i\hbar\frac{\partial}{\partial t}\left(e^{\frac{i}{\hbar}\mathbf{d}\cdot\mathbf{A}}\psi\right) \\ = \; i\hbar e^{\frac{i}{\hbar}\mathbf{d}\cdot\mathbf{A}}\frac{\partial}{\partial t}\psi - e^{\frac{i}{\hbar}\mathbf{d}\cdot\mathbf{A}}\left(\dot{\mathbf{d}}\cdot\mathbf{A}+\mathbf{d}\cdot\dot{\mathbf{A}}\right)\psi \\ = \; e^{\frac{i}{\hbar}\mathbf{d}\cdot\mathbf{A}}\,H\,\psi - e^{\frac{i}{\hbar}\mathbf{d}\cdot\mathbf{A}}\left(\dot{\mathbf{d}}\cdot\mathbf{A}+\mathbf{d}\cdot\mathbf{E}\right)\psi \\ = \; e^{\frac{i}{\hbar}\mathbf{d}\cdot\mathbf{A}}\,H\,e^{-\frac{i}{\hbar}\mathbf{d}\cdot\mathbf{A}}\Phi - e^{\frac{i}{\hbar}\mathbf{d}\cdot\mathbf{A}}\left(\dot{\mathbf{d}}\cdot\mathbf{A}+\mathbf{d}\cdot\mathbf{E}\right)e^{-\frac{i}{\hbar}\mathbf{d}\cdot\mathbf{A}}\Phi. \end{aligned} \tag{A.34}$$

The Hamiltonian H_{Min} transforms under the generalized GMT in the same way that that it did when the fields were considered classical, with the exception that $\mathbf{E}\rightarrow\mathbf{D}/\epsilon_0$. Therefore under the generalized GMT, the minimal coupling Hamiltonian Eq. (A.31) is transformed into the direct coupling Hamiltonian

$$\begin{aligned} H_{\text{dir}} \;&=\; \frac{\mathbf{P}^2}{2M} - \mathbf{d}\cdot\mathbf{D}(0,t) + \mathbf{V}_{\text{c}} \\ &+\; \frac{1}{2}\int\left(\frac{\mathbf{D}^2(\mathbf{x},t)}{\epsilon_0}+\frac{\mathbf{B}^2(\mathbf{x},t)}{\mu_0}\right)dV. \end{aligned} \tag{A.35}$$

A.3 Appendix: Gauge Transformation - Direct Coupling

In this section, we outline the derivation of the direct coupling Hamiltonian through the use of the Göppert-Mayer gauge to first order in the polarization term. This means we leave out the magnetization field. We begin with the minimal coupling Lagrangian [91]

$$\begin{aligned} L_{\text{min}} &= \frac{1}{2}\sum_n m_n \dot{\mathbf{r}}_n^2 - V_{\text{c}} + \sum_n \left[q_n \dot{\mathbf{r}}_n \mathbf{A}(\mathbf{r}_n, t) - q_n U(\mathbf{r}_n, t)\right] \\ &+ \frac{\epsilon_0}{2}\int \left[\dot{\mathbf{A}}^2(\mathbf{r}, t) - c^2 \left(\nabla \times \mathbf{A}(\mathbf{r}, t)\right)^2\right] d^3\mathbf{r}. \end{aligned} \tag{A.36}$$

Where $\mathbf{A}$ and U are the vector and scalar potential for the external fields, and V_{c} is the Coulomb potential. The corresponding Hamiltonian is given by

$$\begin{aligned} H_{\text{min}} &= \sum_n \frac{1}{2m_n}\left[\mathbf{p}_n - q_n \mathbf{A}(\mathbf{r}_n, t)\right]^2 + V_{\text{c}} + \sum_n q_n U(\mathbf{r}_n, t) \\ &+ \frac{\epsilon_0}{2}\int \left[\dot{\mathbf{A}}^2(\mathbf{r}, t) - c^2 \left(\nabla \times \mathbf{A}(\mathbf{r}, t)\right)^2\right] d^3\mathbf{r}. \end{aligned} \tag{A.37}$$

Here the conjugate momentum and conjugate field are given by

$$\mathbf{p}_n = m_n \dot{\mathbf{r}}_n + q_n \mathbf{A}(\mathbf{r}_n, t), \tag{A.38}$$

$$\mathbf{\Pi}(\mathbf{r}, t) = \epsilon_0 \dot{\mathbf{A}}(\mathbf{r}, t) = -\epsilon_0 \mathbf{E}(\mathbf{r}, t). \tag{A.39}$$

Let us now preform the following gauge transformation

$$\mathbf{A}'(\mathbf{r_n}, t) = \mathbf{A}(\mathbf{r_n}, t) + \nabla\chi(\mathbf{r}_n, t), \tag{A.40}$$

$$U'(\mathbf{r_n}, t) = U(\mathbf{r_n}, t) + \frac{\partial}{\partial t}\chi(\mathbf{r}_n, t). \tag{A.41}$$

Substituting this into the minimal coupling Lagrangian Eq. (A.36), the transformed Lagrangian becomes

$$\begin{aligned} L_{\text{dir}} &= \frac{1}{2}\sum_n m_n \dot{\mathbf{r}}_n - V_c + \sum_n \left[q_n \dot{\mathbf{r}}_n \mathbf{A}'(\mathbf{r}_n, t) - q_n U'(\mathbf{r}_n, t)\right] \\ &+ \frac{\epsilon_0}{2}\int \left[\dot{\mathbf{A}}^2(\mathbf{r}, t) - c^2 \left(\nabla \times \mathbf{A}(\mathbf{r}, t)\right)^2\right] d^3\mathbf{r} \\ &= L_{\text{min}} + \frac{d}{dt}\left[\sum_n q_n \chi(\mathbf{r}_n, t)\right]. \end{aligned} \tag{A.42}$$

This shows that the gauge transformation generated by χ is equivalent to adding

$$\frac{d}{dt}\left[\sum_n q_n\,\chi(\mathbf{r}_n,t)\right], \tag{A.43}$$

to the Lagrangian. The direct coupling Lagrangian is obtained through the Göppert-Mayer generator

$$\chi(\mathbf{r},t) = -\int \mathbf{P}^{\perp}(\mathbf{r},t)\cdot\mathbf{A}(\mathbf{r},t)\,d^3\mathbf{r}. \tag{A.44}$$

Where

$$\mathbf{P}(\mathbf{r}) = \sum_n q_n(\mathbf{r}-\mathbf{R}_n)\delta(\mathbf{r}-\mathbf{R}_n), \tag{A.45}$$

is the electric polarization vector field. The transformed conjugate momentum and conjugate field become

$$\mathbf{p}_n = m_n\dot{\mathbf{r}}, \tag{A.46}$$

$$\mathbf{\Pi}(\mathbf{r},t) = \epsilon_0\dot{\mathbf{A}}(\mathbf{r},t) - \mathbf{P}^{\perp}(\mathbf{r},t) = -\mathbf{D}(\mathbf{r},t). \tag{A.47}$$

Where $\mathbf{D}$ is the displacement field. Note that for a neutral system $\nabla\cdot\mathbf{D}=0$ and therefore the displacement field is fully transverse which allows us to drop the perpendicular suffix. From here we can construct the transformed Hamiltonian

$$\begin{aligned} H_{\text{dir}} &= \sum_n \mathbf{p}_n\cdot\dot{\mathbf{r}}_n + \int \Pi(\mathbf{r},t)\cdot\dot{\mathbf{A}}(\mathbf{x},t)\,d^3\mathbf{r} - L_{\text{dir}} \\ &= \sum_n \frac{1}{2m_n}\mathbf{p}_n^2 + V_c - \frac{1}{\epsilon_0}\int \mathbf{P}^{\perp}(\mathbf{r},t)\cdot\mathbf{D}(\mathbf{r},t)\,d^3\mathbf{r} \\ &+ \frac{\epsilon_0}{2}\int\left[\mathbf{D}^2(\mathbf{r},t) - c^2\left(\nabla\times\mathbf{A}(\mathbf{r},t)\right)^2\right]d^3\mathbf{r}. \end{aligned} \tag{A.48}$$

This is the direct coupling Hamiltonian.

A.4 Appendix: The Direct Coupling Lagrangian

This section follows Thirunamachandran's derivation [91]. The minimal coupling Lagrangian for an atom interacting with an electromagnetic field is given by

$$\begin{aligned} L_{\min} &= \frac{1}{2}\sum_n m_n \dot{\mathbf{r}}_n^2 + \int \mathbf{J}^{\perp}(\mathbf{r})\cdot\mathbf{A}(\mathbf{r})\, d^3\mathbf{r} \\ &+ \frac{\epsilon_0}{2}\int \left[\dot{\mathbf{A}}^2(\mathbf{r},t) - c^2\left(\nabla\times\mathbf{A}(\mathbf{r},t)\right)^2\right] d^3\mathbf{r}. \end{aligned} \tag{A.49}$$

Here $\mathbf{J}^{\perp}$ is the perpendicular component of the current density. In terms of elementary charges e, the current density can be written as

$$\mathbf{J}(\mathbf{r}) = e\sum_n \dot{\mathbf{x}}_n \delta(\mathbf{r}-\mathbf{x}_n). \tag{A.50}$$

This can then be Taylor expanded about some point $\mathbf{R}$:

$$\mathbf{J}_i(\mathbf{r}) = e\sum_n \dot{x}_{n,i}\left[1-(\mathbf{x}_n-\mathbf{R})_j\nabla_j + \frac{1}{2}(\mathbf{x}_n-\mathbf{R})_j(\mathbf{x}_n-\mathbf{R})_k\nabla_j\nabla_k...\right]\delta(\mathbf{r}-\mathbf{R}). \tag{A.51}$$

We can also Taylor expand the charge density ρ around $\mathbf{R}$

$$\rho(\mathbf{r}) = e\sum_n \delta(\mathbf{r}-\mathbf{x}_n) = e\sum_n\left[1-(\mathbf{x}_n-\mathbf{R})_j\nabla_j + \frac{1}{2}(\mathbf{x}_n-\mathbf{R})_j(\mathbf{x}_n-\mathbf{R})_k\nabla_j\nabla_k...\right]\delta(\mathbf{r}-\mathbf{R}). \tag{A.52}$$

This allows us to write the charge density in terms of the net charge density $\rho_{\text{net}}(\mathbf{r}) = e\sum_n \delta(\mathbf{r}-\mathbf{R})$ as

$$\rho(\mathbf{r}) = e\sum_n \delta(\mathbf{r}-\mathbf{x}_n) = \rho_{\text{net}} - \nabla\cdot\mathbf{P}(\mathbf{r}), \tag{A.53}$$

where we have defined the electric polarization field $\mathbf{P}$ as

$$\mathbf{P}(\mathbf{r}) = e\sum_n(\mathbf{x}_n-\mathbf{R})\left[1-\frac{1}{2}(\mathbf{x}_n-\mathbf{R})_j\nabla_j + \frac{1}{6}(\mathbf{x}_n-\mathbf{R})_j(\mathbf{x}_n-\mathbf{R})_k\nabla_j\nabla_k...\right]\delta(\mathbf{r}-\mathbf{R}). \tag{A.54}$$

Now the time derivative of the i'th component of the electric polarization field is given by

$$\begin{aligned}\frac{d\mathbf{P}_i(\mathbf{r})}{dt} &= e\sum_n \dot{x}_{i,n}\left[1-\frac{1}{2}(\mathbf{x}_n-\mathbf{R})_j\nabla_j+\frac{1}{6}(\mathbf{x}_n-\mathbf{R})_j(\mathbf{x}_n-\mathbf{R})_k\nabla_j\nabla_k...\right]\delta(\mathbf{r}-\mathbf{R})\\ &- e\sum_n(\mathbf{x}_n-\mathbf{R})_i\dot{x}_{j,n}\nabla_j\left[\frac{1}{2}-\frac{1}{3}(\mathbf{x}_n-\mathbf{R})_k\nabla_k...\right]\delta(\mathbf{r}-\mathbf{R}). \qquad \text{(A.55)}\end{aligned}$$

Using Eq. (A.51) and Eq. (A.55) we then find

$$\mathbf{J}_i(\mathbf{r})-\frac{d\mathbf{P}_i(\mathbf{r})}{dt}=e\sum_n\left(-\dot{x}_{n,i}(\mathbf{x}_n-\mathbf{R})_j\nabla_j+\dot{x}_{n,j}(\mathbf{x}_n-\mathbf{R})_i\nabla_j\right)\left(\frac{1}{2}-\frac{1}{6}(\mathbf{x}_n-\mathbf{R})_k\nabla_k+...\right)\delta(\mathbf{r}-\mathbf{R}). \qquad \text{(A.56)}$$

This can be rewritten as

$$\mathbf{J}_i(\mathbf{r})-\frac{d\mathbf{P}_i(\mathbf{r})}{dt}=\left[\nabla\times\mathbf{M}(\mathbf{r})\right]_i, \qquad \text{(A.57)}$$

where we have defined the magnetization $\mathbf{M}$ as

$$M_i(\mathbf{r})=e\sum_n\left[(\mathbf{x}_n-\mathbf{R})\times\dot{\mathbf{x}}_n\right]_i\left[\frac{1}{2}-\frac{1}{3}(\mathbf{x}_n-\mathbf{R})_j\nabla_j+...\right]\delta(\mathbf{r}-\mathbf{R}). \qquad \text{(A.58)}$$

We are now ready to preform a gauge transformation on the minimal coupling Lagrangian by adding a total time derivative (which leaves the equations of motion the same)

$$L_{\text{dir}}=L_{\text{min}}-\frac{d}{dt}\int\mathbf{P}^{\perp}(\mathbf{r})\cdot\mathbf{A}(\mathbf{r})\,d^3\mathbf{r}. \qquad \text{(A.59)}$$

Expanding out the gauge transformed Lagrangian:

$$L_{\text{dir}}=L_{\text{min}}-\int\dot{\mathbf{P}}^{\perp}(\mathbf{r})\cdot\mathbf{A}(\mathbf{r})\,d^3\mathbf{r}-\int\mathbf{P}^{\perp}(\mathbf{r})\cdot\dot{\mathbf{A}}(\mathbf{r})\,d^3\mathbf{r}. \qquad \text{(A.60)}$$

Using Eq. (A.57) and the definition of the minimal coupling Lagrangian Eq. (A.49) yields

$$\begin{aligned}L_{\text{dir}} &= \frac{1}{2}\sum_n m_n\dot{\mathbf{r}}_n^2-\int\mathbf{P}^{\perp}(\mathbf{r})\cdot\dot{\mathbf{A}}(\mathbf{r})\,d^3\mathbf{r}+\int(\nabla\times\mathbf{M}(\mathbf{r}))\cdot\mathbf{A}(\mathbf{r})\,d^3\mathbf{r}\\ &+ \frac{\epsilon_0}{2}\int\left[\dot{\mathbf{A}}^2(\mathbf{r},t)-c^2\left(\nabla\times\mathbf{A}(\mathbf{r},t)\right)^2\right]d^3\mathbf{r}. \qquad \text{(A.61)}\end{aligned}$$

This is the direct coupling Lagrangian.

Appendix B

Appendix to Chapter 5

In this appendix I present calculations pertaining to chapter 5.

B.1 Abraham Force in a Cavity

In this section we derive the force contribution due to the poynting component of the Maxwell force equation Eq. (5.19)

$$F_{\text{poynting}} = -\frac{\partial}{\partial t}\int_{L_1}^{L_2} (\epsilon_0 \mathbf{E}\times\mathbf{B})\,. \tag{B.1}$$

Here we follow a strategy similar to that used in deriving the stress-tensor force.

$$\begin{aligned} F_{\text{poynting}} &= -\frac{\epsilon_0}{2c}\frac{\partial}{\partial t}\left(|\mathcal{E}_{Lm}|^2 L_1 + |\mathcal{E}_{Rm}|^2 L_2\right) \\ &= -\frac{\partial}{\partial t}\frac{\epsilon_0 |\mathcal{E}_{Rm}|^2}{2c}\left[\frac{|\mathcal{E}_{Lm}|^2}{|\mathcal{E}_{Rm}|^2}\frac{L+\Delta L}{2} + \frac{L-\Delta L}{2}\right]. \end{aligned} \tag{B.2}$$

We have introduced a factor of $1/2$ here due to integrating the poynting vector. We now make use of the approximation

$$\frac{|\mathcal{E}_{Lm}|^2}{|\mathcal{E}_{Rm}|^2} = \left|\frac{\sin(k_m L_2)}{\sin(k_m L_1)}\right|^2 \approx \frac{\frac{\varepsilon_0 L}{am\pi} - \frac{1}{2}\sin(m\pi\frac{\triangle L}{L})}{\frac{\varepsilon_0 L}{am\pi} + \frac{1}{2}\sin(m\pi\frac{\triangle L}{L})}. \tag{B.3}$$

Substituting this into Eq. (B.2) we obtain

$$F_{\text{poynting}} = -\frac{\partial}{\partial t}\left(\frac{\epsilon_0 \left|\mathcal{E}_{Rm}\right|^2}{2c}\frac{\left(\frac{\varepsilon_0 L}{am\pi} - \frac{1}{2}\sin(m\pi\frac{\triangle L}{L})\right)\left(\frac{L+\Delta L}{2}\right) + \left(\frac{\varepsilon_0 L}{am\pi} + \frac{1}{2}\sin(m\pi\frac{\triangle L}{L})\right)\left(\frac{L-\Delta L}{2}\right)}{\frac{\varepsilon_0 L}{am\pi} - \frac{1}{2}\sin(m\pi\frac{\triangle L}{L})}\right). \tag{B.4}$$

This can be simplified by noting that the first term in the denominator dominates the second term for small a. This then yields

$$F_{\text{poynting}} = -\frac{\partial}{\partial t}\frac{\epsilon_0 \left|\mathcal{E}_{Rm}\right|^2}{2c}\left[L - \frac{am\pi\Delta L}{2\epsilon_0 L}\sin(m\pi\frac{\triangle L}{L})\right]. \tag{B.5}$$

The first term is simply the length of the cavity L and drops out since it is constant in time. At this point we make the approximation that the energy

$$\frac{\epsilon_0 \left|\mathcal{E}_{Rm} L\right|^2}{2}, \tag{B.6}$$

is approximately constant for small ΔL, and hence we can write it simply is E_{total}. By dividing by the total number of photons

$$n_{\text{photon}} = \frac{E_{\text{total}}}{\hbar c k_0}, \tag{B.7}$$

we obtain the force per unit area per photon due to the poynting term

$$F_{\text{poynting}} = \hbar k_0 \frac{\partial}{\partial t}\left[\frac{am\pi\Delta L}{2\epsilon_0 L^2}\sin(m\pi\frac{\triangle L}{L})\right]. \tag{B.8}$$

Expanding this to second order about $\Delta L = 0$ then yields the final result

$$F_{\text{poynting}} = \frac{\partial}{\partial t}\left(\hbar k_0 \frac{am^2\pi^2}{2\epsilon L^3}(\Delta L)^2\right). \tag{B.9}$$

B.2 Microscopic Investigations

Here, we connect the microscopic description of optical forces on atoms [65] with the classical derivation obtained in Section 5.4. This relationship will link the δ-function factor a in Eq. (5.1) with the polarizability of an atom. We begin by examining the force derived using the Maxwell stress tensor. Suppose we have a dielectric slab, which we approximate with a δ-function, interacting with two opposing plane waves. The stress-tensor force contribution is given by

$$F = \frac{\varepsilon_0}{2}\left(|\mathcal{E}_1|^2 + |\mathcal{E}_2|^2 - |\mathcal{E}_3|^2 - |\mathcal{E}_4|^2\right). \tag{B.10}$$

Let us rewrite the outgoing fields $\mathcal{E}_1$ and $\mathcal{E}_4$ as a linear combination of the incoming fields $\mathcal{E}_2 = \mathcal{E}_{\text{left}} e^{ikx+i\phi}$ and $\mathcal{E}_3 = \mathcal{E}_{\text{right}} e^{-ikx}$

$$\mathcal{E}_1 = r\mathcal{E}_2 + t\mathcal{E}_3, \tag{B.11}$$

$$\mathcal{E}_4 = t\mathcal{E}_2 + r\mathcal{E}_3, \tag{B.12}$$

where the reflectivity r and the transmission t for the δ-model are given by [88]

$$r = \frac{i\frac{ka}{2\varepsilon_0}}{1 - \frac{ika}{2\varepsilon_0}}, \tag{B.13}$$

$$t = \frac{1}{1 - \frac{ika}{2\varepsilon_0}}. \tag{B.14}$$

Substituting these equations into Eq. (B.10) yields

$$
\begin{aligned}
F &= \frac{\frac{\varepsilon_0}{2}\left|\frac{ka}{2\varepsilon_0}\right|^2}{\left|1-\frac{ika}{2\varepsilon_0}\right|^2}\left|\mathcal{E}_{\text{left}}\right|^2+\frac{\frac{\varepsilon_0}{2}}{\left|1-\frac{ika}{2\varepsilon_0}\right|^2}\left|\mathcal{E}_{\text{right}}\right|^2 \\
&+ \frac{i\frac{\varepsilon_0 ka}{4\varepsilon_0}}{\left|1-\frac{ika}{2\varepsilon_0}\right|^2}\mathcal{E}_{\text{left}}\mathcal{E}_{\text{left}}e^{2ikx+i\phi} \\
&- \frac{i\frac{ka^*}{4}}{\left|1-\frac{ika}{2\varepsilon_0}\right|^2}\mathcal{E}_{\text{left}}\mathcal{E}_{\text{right}}e^{-2ikx-i\phi} \\
&+ \frac{\varepsilon_0}{2}\left|\mathcal{E}_{\text{left}}\right|^2-\frac{\varepsilon_0}{2}\left|\mathcal{E}_{\text{right}}\right|^2-\frac{\frac{\varepsilon_0}{2}\left|\frac{ka}{2\varepsilon_0}\right|^2}{\left|1-\frac{ika}{2\varepsilon_0}\right|^2}\left|\mathcal{E}_{\text{right}}\right|^2 \\
&- \frac{\frac{\varepsilon_0}{2}}{\left|1-\frac{ika}{2\varepsilon_0}\right|^2}\left|\mathcal{E}_{\text{left}}\right|^2-\frac{i\frac{ka}{4}}{\left|1-\frac{ika}{2\varepsilon_0}\right|^2}\mathcal{E}_{\text{left}}\mathcal{E}_{\text{right}}e^{-2ikx-i\phi} \\
&+ \frac{i\frac{ka^*}{4}}{\left|1-\frac{ika}{2\varepsilon_0}\right|^2}\mathcal{E}_{\text{left}}\mathcal{E}_{\text{right}}e^{2ikx+i\phi}. \qquad \text{(B.15)}
\end{aligned}
$$

Here a is a complex parameter which we break up in its real and imaginary components $a = a_1 + ia_2$. Simplifying the expression above yields

$$
\begin{aligned}
F &= -\frac{ka_1\mathcal{E}_{\text{left}}\mathcal{E}_{\text{right}}\sin\left(2kx+\phi\right)}{\left|1-\frac{ika}{2\varepsilon_0}\right|^2} \\
&+ \frac{\frac{ka_2}{2}\left(\left|\mathcal{E}_{\text{left}}\right|^2-\left|\mathcal{E}_{\text{right}}\right|^2\right)}{\left|1-\frac{ika}{2\varepsilon_0}\right|^2} \\
&+ \frac{\varepsilon_0\left|\frac{ka}{2\varepsilon_0}\right|^2\left(\left|\mathcal{E}_{\text{left}}\right|^2-\left|\mathcal{E}_{\text{right}}\right|^2\right)}{\left|1-\frac{ika}{2\varepsilon_0}\right|^2}. \qquad \text{(B.16)}
\end{aligned}
$$

where ϕ is the phase difference between the two incoming waves at $x = 0$. Let us examine Eq. (B.16) term by term to gain a better understanding of what each term represents. The first term, which we label as F_1, is the reactive part of the force more commonly known as the dipole force. To see this let us consider the standard reactive force on an atom as given by Cohen-Tannoudji [65] for a field of the form $\mathcal{E}(x) = \mathcal{E}_{\text{left}}e^{ikx+i\phi} + \mathcal{E}_{\text{right}}e^{-ikx}$

$$F_{\text{reactive}} = -\frac{\hbar\Delta}{4}\frac{\vec{\nabla}\Omega^2}{\frac{\Gamma^2}{4}+\Delta^2+\frac{\Omega^2}{2}} = \frac{1}{4}\alpha_1\nabla\mathcal{E}^2. \tag{B.17}$$

Here Ω is the atomic Rabi frequency, Γ is the spontaneous decay rate, d is the dipole coherence, and Δ is the detuning. We also introduce α_1 as the real component of the atomic polarizibility given by

$$\alpha = \frac{-\Delta\left|d\right|^2}{\hbar\left[\frac{\Gamma^2}{4}+\Delta^2+\frac{\Omega^2}{2}\right]} \approx \frac{-\left|d\right|^2}{\hbar\Delta}. \tag{B.18}$$

One finds that for $\mathcal{E}(x) = \mathcal{E}_{\text{left}}e^{ikx+i\phi} + \mathcal{E}_{\text{right}}e^{-ikx}$

$$\nabla\mathcal{E}^2 = -4k\mathcal{E}_{\text{left}}\mathcal{E}_{\text{right}}\sin\left(2kx+\phi\right). \tag{B.19}$$

Substituting this back into Eq. (B.17) we get

$$F_{\text{reactive}} = -\alpha k\mathcal{E}_{\text{left}}\mathcal{E}_{\text{right}}\sin\left(2kx+\phi\right). \tag{B.20}$$

We now compare Eq. (B.20) to the first term F_1 of Eq. (B.16). If we are considering a single atom in the dispersive regime, then a may be assumed very small. We may therefore approximate F_1 to first order in a

$$F_1 \approx -a_1\mathcal{E}_{\text{left}}\mathcal{E}_{\text{right}}\sin\left(2kx+\phi\right). \tag{B.21}$$

Comparing Eq. (B.20) with Eq. (B.21) we see that for an atom, $\alpha_1 = a_1$, and that indeed F_1 is the reactive component of the optical force.

Let us now return to Eq. (B.16) and consider the second term F_2 in the equation. This term can be shown to be nothing more than the dispersive force. Following a similar scheme to that used above we have

$$F_2 = \frac{\frac{1}{2}ka_2\left(\left|\mathcal{E}_{\text{left}}\right|^2 - \left|\mathcal{E}_{\text{right}}\right|^2\right)}{\left|1-\frac{ik\alpha}{2}\right|^2}. \tag{B.22}$$

For small a we approximate F_2 to first order

$$F_2 \approx \frac{1}{2}ka_2\left(\left|\mathcal{E}_{\text{left}}\right|^2 - \left|\mathcal{E}_{\text{right}}\right|^2\right). \tag{B.23}$$

We now wish to compare this to the dispersive force as given by Cohen-Tannoudji [65]. The dispersive force felt by an atom under the influence of a field of the form $\mathcal{E}(x) = \mathcal{E}_{\text{left}}e^{ikx+i\phi} + \mathcal{E}_{\text{right}}e^{-ikx}$ is given by

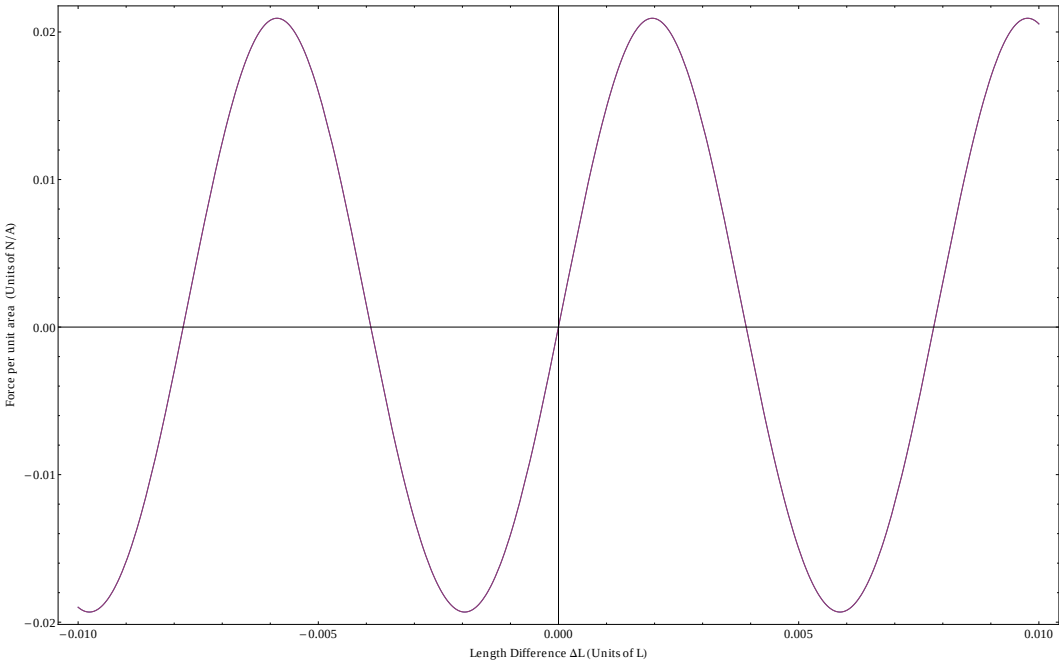

Figure B.1: This plot compares the complete force obtained using the Maxwell stress tensor (red) against the reactive component - the first term F_1 of Eq. (B.16) (blue). Here $\alpha = 10^{-8}$ was used. It is seen that for small α, the other two components of Eq. (B.16) may be neglected.

$$\begin{aligned} F_{\text{dispersivee}} &= -\hbar\Gamma\left(\overrightarrow{\nabla}\phi(\overrightarrow{r})\right)\frac{\Omega^2}{\Gamma^2+4\Delta^2+2\Omega^2} \\ &= \left(|\mathcal{E}_{\text{left}}|^2-|\mathcal{E}_{\text{right}}|^2\right)\frac{k\,|d|^2\,\Gamma}{4\hbar\Delta^2}. \end{aligned} \tag{B.24}$$

The imaginary component of the polarizibility of an atom is [65]

$$\alpha_2 = \frac{\frac{\Gamma}{2}\,|d|^2}{\hbar\left[\frac{\Gamma^2}{4}+\Delta^2+\frac{\Omega^2}{2}\right]} \approx \frac{\Gamma d^2}{2\hbar\Delta^2}. \tag{B.25}$$

Thus we can rewrite the dispersive force as

$$F_{\text{dispersive}} = \frac{\alpha_2 k}{2}\left(|\mathcal{E}_{\text{left}}|^2-|\mathcal{E}_{\text{right}}|^2\right). \tag{B.26}$$

Comparing Eq. (B.26) with Eq. (B.23) and see that $\alpha_2 = a_2$, consistent with what we found for the reactive component of the force. Now the third component F_3 of Eq. (B.16) is interpreted as the radiation pressure due to incoherent scattering. To see this we note that

$$R = |r|^2 = \frac{\left|\frac{ka}{2\varepsilon}\right|^2}{\left|1-\frac{ika}{2\varepsilon}\right|^2}. \tag{B.27}$$

Comparing the coefficient in Eq. (B.16) with Eq. (B.27) we see that indeed

$$F_3 = 2R\left(|\mathcal{E}_{\text{left}}|^2-|\mathcal{E}_{\text{right}}|^2\right). \tag{B.28}$$

This is a second order effect in a which is why it is neglected in the conventional optical force on an atom. For higher densities however, it dominates F_1 and F_2 which explains why the radiative pressure equation of classical electrodynamics [70] agrees well for high density objects such as mirrors.

Bibliography

[1] E. A. Hinds and S. M. Barnett, Phys. Rev. Lett. **102**, 050403 (2009).

[2] S. M. Barnett, Phys. Rev. Lett. **104**, 070401 (2010).

[3] M. Mansuripur and A. R. Zakharian, Phys. Rev. E **79**, 026608 (2009).

[4] M. Mansuripur and A. R. Zakharian, Phys. Rev. A **80**, 023823 (2009).

[5] M. Mansuripur, A. R. Zakharian, and E. M. Wright, Phys. Rev. A **88**, 023826 (2013).

[6] M. Mansuripur, Phys. Rev. Lett. **103**, 019301 (2009).

[7] C. J. Sheppard and B. A. Kemp, Phys. Rev. A **93**, 013855 (2016).

[8] J. S. O. Filho and P. L. Saldanha, Phys. Rev. A **92**, 052107 (2015).

[9] W. Sun, S. B. Wang, J. Ng, L. Zhou, and C. T. Chan, Phys. Rev. B **91**, 235439 (2015).

[10] C. Wang, Canadian Journal of Physics **93**, 1510 (2015).

[11] U. Leonhardt, Phys. Rev. A **90**, 033801 (2014).

[12] C. J. Sheppard and B. A. Kemp, Phys. Rev. A **89**, 013825 (2014).

[13] M. E. Crenshaw, Journal of Mathematical Physics **55**, 042901 (2014), http://dx.doi.org/10.1063/1.4869746.

[14] M. V. Gorkunov and A. V. Kondratov, Phys. Rev. A **88**, 011804 (2013).

[15] I. n. Liberal, I. n. Ederra, R. Gonzalo, and R. W. Ziolkowski, Phys. Rev. A **88**, 053808 (2013).

[16] M. E. Crenshaw, Annals of Physics **338**, 97 (2013).

[17] G. L. J. A. Rikken and B. A. van Tiggelen, Phys. Rev. Lett. **108**, 230402 (2012).

[18] I. Y. Dodin and N. J. Fisch, Phys. Rev. A **86**, 053834 (2012).

[19] W.-Z. Zhang, P. Zhang, R.-Q. Wang, and W.-M. Liu, Phys. Rev. A **85**, 053604 (2012).

[20] I. A. Pedrosa, A. Y. Petrov, and A. Rosas, The European Physical Journal D **66**, 1 (2012).

[21] T. Ramos, G. F. Rubilar, and Y. N. Obukhov, Physics Letters A **375**, 1703 (2011).

[22] B. A. Kemp, Journal of Applied Physics **109**, 111101 (2011), http://dx.doi.org/10.1063/1.3582151.

[23] M. Abraham, Rendiconti del Circolo Matematico di Palermo (1909).

[24] H. Minkowski, Nachrichten von der Gesellschaft der Wissenschaften, Mathematisch-Physikalische Klasse, Mathematisch-Physikalische Klasse (1908).

[25] N. L. Balazs, Phys. Rev. **91**, 408 (1953).

[26] O. Frisch, Contemp. Phys. **7** (1965), 10.1080/00107516508202135.

[27] R. V. Zee and J. Looney, *Cavity-Enhanced Spectroscopy*, 1st ed. (Academic Press, San Diego, 2002).

[28] P. Cladé, E. de Mirandes, M. Cadoret, S. Guellati-Khélifa, C. Schwob, F. m. c. Nez, L. Julien, and F. m. c. Biraben, Phys. Rev. A **74**, 052109 (2006).

[29] P. Cladé, E. de Mirandes, M. Cadoret, S. Guellati-Khélifa, C. Schwob, F. m. c. Nez, L. Julien, and F. m. c. Biraben, Phys. Rev. A **74**, 052109 (2006).

[30] R. V. Jones and J. C. S. Richards, Proceedings of the Royal Society of London A: Mathematical, Physical and Engineering Sciences **221**, 480 (1954), http://rspa.royalsocietypublishing.org/content/221/1147/480.full.pdf .

[31] A. Ashkin and J. M. Dziedzic, Phys. Rev. Lett. **30**, 139 (1973).

[32] R. P. James, Proc. Natl. Acad. Sci. USA **61** (1968).

[33] G. B. Walker and G. Walker, Can. J. Phys. **53** (1975).

[34] R. V. Jones and B. Leslie, Proceedings of the Royal Society of London A: Mathematical, Physical and Engineering Sciences **360**, 347 (1978), http://rspa.royalsocietypublishing.org/content/360/1702/347.full.pdf .

[35] G. K. Campbell, A. E. Leanhardt, J. Mun, M. Boyd, E. W. Streed, W. Ketterle, and D. E. Pritchard, Phys. Rev. Lett. **94**, 170403 (2005).

[36] L. Zhang, W. She, N. Peng, and U. Leonhardt, New Journal of Physics **17** (2015).

[37] M. Mansuripur and A. R. Zakharian, Proceedings of SPIE **7400** (2009).

[38] W. Pauli, *Theory of Relativity*, 1st ed. (Dover, New York, 1981).

[39] J. P. Gordon, Phys. Rev. A **8**, 14 (1973).

[40] R. Loudon, S. M. Barnett, and C. Baxter, Phys. Rev. A **71**, 063802 (2005).

[41] V. E. Lembessis, M. Babiker, C. Baxter, and R. Loudon, Phys. Rev. A **48**, 1594 (1993).

[42] M. V. Berry, Proceedings of the Royal Society of London A: Mathematical, Physical and Engineering Sciences **392**, 45 (1984), http://rspa.royalsocietypublishing.org/content/392/1802/45.full.pdf .

[43] A. Shapere and F. Wilczek, *Geometric Phases in Physics*, 5th ed. (World Scientific, Singapore, 1989).

[44] J. Dalibard, F. Gerbier, G. Juzeliūnas, and P. Öhberg, Rev. Mod. Phys. **83**, 1523 (2011).

[45] X.-G. He and B. H. J. McKellar, Phys. Rev. A **47**, 3424 (1993).

[46] M. Wilkens, Phys. Rev. Lett. **72**, 5 (1994).

[47] Y. Aharonov and D. Bohm, Phys. Rev. **115**, 485 (1959).

[48] Y. Aharonov and A. Casher, Phys. Rev. Lett. **53**, 319 (1984).

[49] J. P. Dowling, C. P. Williams, and J. D. Franson, Phys. Rev. Lett. **83**, 2486 (1999).

[50] L. Vaidman, Phys. Rev. A **86**, 040101 (2012).

[51] H. Wei, R. Han, and X. Wei, Phys. Rev. Lett. **75**, 2071 (1995).

[52] R. G. Chambers, Phys. Rev. Lett. **5**, 3 (1960).

[53] A. Tonomura, N. Osakabe, T. Matsuda, T. Kawasaki, J. Endo, S. Yano, and H. Yamada, Phys. Rev. Lett. **56**, 792 (1986).

[54] S. Olariu and I. I. Popescu, Rev. Mod. Phys. **57**, 339 (1985).

[55] M. Peshkin and A. Tonomura, (New York).

[56] A. Cimmino, G. I. Opat, A. G. Klein, H. Kaiser, S. A. Werner, M. Arif, and R. Clothier, Phys. Rev. Lett. **63**, 380 (1989).

[57] K. Sangster, E. A. Hinds, S. M. Barnett, E. Riis, and A. G. Sinclair, Phys. Rev. A **51**, 1776 (1995).

[58] K. Zeiske, G. Zinner, F. Riehle, and J. Helmcke, Applied Physics B **60**, 205.

[59] A. Görlitz, B. Schuh, and A. Weis, Phys. Rev. A **51**, R4305 (1995).

[60] S. Yanagimachi, M. Kajiro, M. Machiya, and A. Morinaga, Phys. Rev. A **65**, 042104 (2002).

[61] S. Lepoutre, A. Gauguet, G. Trénec, M. Büchner, and J. Vigué, Phys. Rev. Lett. **109**, 120404 (2012).

[62] J. Gillot, S. Lepoutre, A. Gauguet, M. Büchner, and J. Vigué, Phys. Rev. Lett. **111**, 030401 (2013).

[63] S. Lepoutre, A. Gauguet, M. Büchner, and J. Vigué, Phys. Rev. A **88**, 043627 (2013).

[64] S. Lepoutre, J. Gillot, A. Gauguet, M. Büchner, and J. Vigué, Phys. Rev. A **88**, 043628 (2013).

[65] C. Cohen-Tannoudji, G. Grynberg, and J. Dupont-Roc, *Atom-Photon Interactions: Basic Processes and Applications* (Wiley, New York, 1992).

[66] M. V. Berry and P. Shukla, Journal of Physics A: Mathematical and Theoretical **46**, 422001 (2013).

[67] S. M. Barnett and R. Loudon, Journal of Physics B: Atomic, Molecular and Optical Physics **39**, S671 (2006).

[68] G. B. Walker and D. G. Lahoz, Nature **253**, 339 (1975).

[69] M. Donaire and A. Lambrecht, Phys. Rev. A **93**, 022701 (2016).

[70] D. Griffiths, *Introduction to Electrodynamics*, 3rd ed. (Prentice-Hall Inc., New Jersey, 1999).

[71] I. Brevik, Physics Reports **52**, 133 (1979).

[72] P. Storey and C. Cohen-Tannoudji, Journal de Physique II, EDP Sciences **4** (1994).

[73] D. A. Steck, *Rubidium 87 D line Data*, Tech. Rep. (2001).

[74] A. Miffre, M. Jacquey, M. Büchner, G. Trénec, and J. Vigué, Phys. Rev. A **73**, 011603 (2006).

[75] D. A. Kokorowski, A. D. Cronin, T. D. Roberts, and D. E. Pritchard, Phys. Rev. Lett. **86**, 2191 (2001).

[76] W. F. Holmgren, I. Hromada, C. E. Klauss, and A. D. Cronin, New Journal of Physics **13**, 115007 (2011).

[77] S. Gupta, A. E. Leanhardt, A. D. Cronin, and D. E. Pritchard, Comptes Rendus de l'AcadÃľmie des Sciences - Series IV - Physics-Astrophysics **2**, 479 (2001).

[78] P. Meystre, *Atom Optics*, 5th ed. (Springer-Verlag, New York, 2001).

[79] M. Inguscio, S. Stringari, and C. Wieman, *Bose-Einstein Condensation in Atomic Gases*, 1st ed. (IOS Press, Amsterdam, 1998).

[80] T. Elsässer, B. Nagorny, and A. Hemmerich, Phys. Rev. A **69**, 033403 (2004).

[81] C. von Cube, S. Slama, D. Kruse, C. Zimmermann, P. W. Courteille, G. R. M. Robb, N. Piovella, Bonifacio, and R., Phys. Rev. Lett. **93**, 083601 (2004).

[82] S. Chiow, T. Kovachy, H.-C. Chien, and M. A. Kasevich, Phys. Rev. Lett. **107**, 130403 (2011).

[83] M. F. Andersen, C. Ryu, P. Cladé, V. Natarajan, A. Vaziri, K. Helmerson, and W. D. Phillips, Phys. Rev. Lett. **97**, 170406 (2006).

[84] C. Ryu, K. C. Henderson, and M. G. Boshier, New Journal of Physics **16**, 013046 (2014).

[85] B. Hester, G. K. Campbell, C. Lopez-Mariscal, C. L. Filgueira, R. Huschka, N. J. Halas, and K. Helmerson, Review of Scientific Instruments **83**, 043114 (2012), http://dx.doi.org/10.1063/1.4704373.

[86] L. Carbone, C. Bogan, P. Fulda, A. Freise, and B. Willke, Phys. Rev. Lett. **110**, 251101 (2013).

[87] K. Rzazewski and R. W. Boyd, Journal of Mod. Opt. **51**, 1137 (2004).

[88] N. Miladinovic, F. Hasan, N. Chisholm, I. E. Linnington, E. A. Hinds, and D. H. J. O'Dell, Phys. Rev. A **84**, 043822 (2011).

[89] R. Lang, M. O. Scully, and W. E. Lamb, Phys. Rev. A **7**, 1788 (1973).

[90] J. K. Asbóth, H. Ritsch, and P. Domokos, Phys. Rev. A **77**, 063424 (2008).

[91] D. P. Craig and T. Thirunamachandran, *Molecular Quantum Electrodynamics*, 1st ed. (Dover Publications, Inc, Mineola,New York, 1984).